Phonon-glass electron-crystal thermoelectric clathrates: Experiments and theory

Toshiro Takabatake* and Koichiro Suekuni

Graduate School of Advanced Sciences of Matter, Hiroshima University, Higashi-Hiroshima 739-8530, Japan

Tsuneyoshi Nakayama†

Max Planck Institute for the Physics of Complex Systems, Dresden 01187, Germany, Institute of Advanced Study, School of Physics Science and Engineering, Tongji University, 200092 Shanghai, People's Republic of China, and Hokkaido University, Sapporo 060-8628, Japan

Eiji Kaneshita

Sendai National College of Technology, Sendai 989-3128, Japan

(published 4 June 2014)

Type-I clathrate compounds have attracted a great deal of interest in connection with the search for efficient thermoelectric materials. These compounds constitute networked cages consisting of nanoscale tetrakaidecahedrons (14-hedrons) and dodecahedrons (12-hedrons), in which the group-1 or -2 elements in the periodic table are encaged as so-called "rattling" guest atoms. It is remarkable that, although these compounds have a crystalline cubic structure, they exhibit glasslike phonon thermal conductivity over the whole temperature range depending on the states of rattling guest atoms in the tetrakaidecahedron. In addition, these compounds show unusual glasslike specific heats and terahertz-frequency phonon dynamics, providing a remarkable broad peak almost identical to those observed in amorphous materials or structural glasses, the so-called boson peak. An efficient thermoelectric effect is realized in compounds showing these glasslike characteristics. In this decade, a number of experimental works dealing with type-I clathrate compounds have been published. These are diffraction, thermal, and spectroscopic experiments in addition to those based on heat and electronic transport. These form the raw materials for this review based on advances from this decade. The subject of this review involves interesting phenomena from the viewpoint not only of physics but also of the practical problem of elaborating efficient thermoelectric materials. This review presents a survey of a wide range of experimental investigations of type-I clathrate compounds, together with a review of theoretical interpretations of the peculiar thermal and dynamic properties observed in these materials.

DOI: 10.1103/RevModPhys.86.669 PACS numbers: 63.20.Ry, 72.15.Eb, 72.15.Jf, 82.75.−z

CONTENTS

*takaba@hiroshima-u.ac.jp
†tnaka@eng.hokudai.ac.jp

I. INTRODUCTION

A. History and motivation

Research on thermoelectricity has a long history. It started in the 1820s with the discovery of the Seebeck effect, i.e., the conversion of a temperature difference to electric current in metals (Seebeck, 1822, 1826). In 1821 Seebeck discovered that an electric current flows in a closed circuit made of two dissimilar metals when the two junctions are maintained at different temperatures. The reverse effect was found ten years later by Peltier (1834).

A. F. Ioffe made a breakthrough in the 1930s, noting that semiconductor thermoelements are more practical than the metals employed at that time (Vedernikov and Iordanishvili, 1998). In fact, modern thermoelectric devices contain many thermocouples consisting of *n*-type (electron carriers) and *p*-type (hole carriers) semiconductors wired electrically in series and thermally in parallel as shown in Fig. 1. Ioffe was the first to use the quantity *Z*, the "material's figure of merit," describing the efficiency of the thermal-to-electrical conversion (Ioffe, 1958a). The way to increase the conversion efficiency can be found from the definition,

$$Z = \frac{S^2\sigma}{\kappa_{\rm tot}} \quad [\mathrm{WK^{-2}\,m^{-1}}], \tag{1}$$

where $S(T)$ [V/K] is the Seebeck coefficient, $\sigma(T)$ $[1/(\Omega\,\mathrm{m})]$ is the electrical conductivity, and $\kappa_{\rm tot} = \kappa_{\rm el} + \kappa_{\rm ph}$ is the total thermal conductivity given by the sum of the electrical thermal conductivity $\kappa_{\rm el}$ and the phonon thermal conductivity $\kappa_{\rm ph}$. The physical meaning of Eq. (1) is explained in Sec. II.B.2.

The design concept proposed by Ioffe is to reduce the phonon thermal conductivity $\kappa_{\rm ph}(T)$ by forming semiconducting mixed crystals with *narrow* band gaps composed of heavy elements (Vedernikov and Iordanishvili, 1998). This approach has led to finding thermoelectric compounds based on Bi-Te and Pb-Te alloys (Goldsmid and Douglas, 1954; Ioffe, 1956; Ioffe and Ioffe, 1954, 1956; Sootsman, Chung, and Kanatzidis, 2009; Kanatzidis, 2010; LaLonde *et al.*, 2011), which are in practical use at present, although the elements on the lower right of the periodic table are toxic to humans. Increasing interest in recent years in the recovery of waste heat has focused attention on Earth- and human-friendly thermoelectric materials with improved efficiency.

Since *Z* of Eq. (1) contains the electrical conductivity σ in the numerator and the total thermal conductivity $\kappa_{\rm tot}$ in the denominator, high performance for thermoelectricity can be achieved for materials with the lowest possible thermal conductivity, the highest possible electrical conductivity, and the highest possible Seebeck coefficient. According to those ideas, efficient thermoelectric effects should be achieved by materials possessing both glasslike phonon thermal conductivity and crystalline electrical conductivity. In this framework, Slack (1995) proposed the important concept of a "phonon-glass electron-crystal" (PGEC) for designing efficient thermoelectric materials. This is really a controversial concept from the aspect of materials science. If such materials can be synthesized, it truly becomes one of the most significant innovations in alternative energy technologies. Ioffe (1958b) noted in an article entitled "The revival of thermoelectricity" that "Evidently we stand on the threshold of a new era in power engineering, heating and refrigeration. This prospect flows from the now-rapid advance of thermoelectricity." We have reached a new stage of

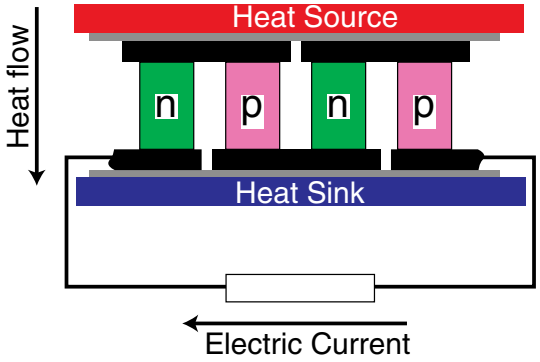

FIG. 1 (color online). Thermoelectric devices contain many couples of *n*-type and *p*-type thermoelectric elements wired electrically in series and thermally in parallel.

thermoelectricity since the concept of the phonon-glass electron-crystal was introduced (Slack, 1995).

General phenomena in thermoelectricity have been reviewed in a number of articles (Rowe, 1995, 2003; Slack, 1995; Mahan, Sales, and Sharp, 1997; Mahan, 1998; Sales, 1998, 2002; Dresselhaus and Thomas, 2001; Nolas, Sharp, and Goldsmid, 2001; Nolas, Slack, and Schujman, 2001; Tritt, 2001; Chen *et al.*, 2003; Koumoto, Terasaki, and Funahashi, 2006; Dresselhaus *et al.*, 2007; Snyder and Toberer, 2008; Goldsmid, 2010; LaLonde *et al.*, 2011; Gonçalves and Godart, 2013).

B. The concepts of phonon-glass electron-crystal: Exploring efficient thermoelectric materials

The concept of the phonon-glass electron-crystal coined by Slack (1995) is actually a summary of ideas discussed by Ioffe in the 1950s (Ioffe, 1958a; Vedernikov and Iordanishvili, 1998). In general, glasses and amorphous materials, having no periodic arrangement of atoms, show the lowest thermal conductivities.

The concept has stimulated numerous attempts to search for efficient thermoelectric materials, and the first achievement was for skutterudite compounds (Nolas *et al.*, 1995, 1996; Sales, Mandrus, and Williams, 1996). The filled skutterudites are described with a chemical formula $\mathcal{R}_yT_4X_{12}$ ($0 \leq y \leq 1$), where $\mathcal{R}$ is a positive element of the lanthanides or actinides, or a group-1 or -2 element. The element T is a transition metal, and X is a pnictogen belonging to the group-15 elements (P, As, Sb). The crystal structure of a skutterudite involves voids (or cages composed of T_8X_{12}) which are filled by $\mathcal{R}$ guests (Takabatake *et al.*, 2006). Because the radius of the $\mathcal{R}$ filler is significantly smaller than that of the voids, the fillers are trapped in highly anharmonic potentials and can vibrate with large amplitudes (Chakoumakos *et al.*, 1999).

Morelli *et al.* (1997) reported a significant reduction in the phonon thermal conductivity κ_{ph} of $Ce_yCo_4Sb_{12}$ relative to an unfilled skutterudite $CoSb_3$. It is remarkable that a small amount of Ce filler has a strong influence on the κ_{ph}. A similar outcome was observed in a La-filled skutterudite $La_yCo_4Sb_{12}$ (Nolas, Cohn, and Slack, 1998). Furthermore, it was revealed that all voids need not be occupied in order to achieve the maximum reduction in κ_{ph} (Tang *et al.*, 2001). For instance, the value of κ_{ph} of $Ce_yFe_{4-x}Co_xSb_{12}$ with $y = 0.7$ has a minimum value lower than 2 $W\,m^{-1}\,K^{-1}$ above room temperature (Uher, 2001).

The data strongly support the fact that low phonon thermal conductivities κ_{ph} are obtained when guest atoms fill voids at random. At the same time, since electrical conduction is mainly due to the pnictogen orbitals in the group-15 elements, the carrier mobility remains large enough to maintain its crystalline character. Thus, in general, materials like skutterudites with voids, cavities, cages, and empty sublattices are thought to be favorable candidates for realizing the phonon-glass electron-crystal concept.

Following these works, Nolas, Slack *et al.* (1998) and Nolas, Cohn *et al.* (1998) demonstrated that type-I clathrate compounds have the potential for use as high-efficiency thermoelectric materials. In fact, clathrate compounds belong to the category mentioned above. Highly efficient thermoelectric properties have been exhibited by these compounds encapsulating "rattlers." The terms rattler and rattling were introduced by Sales *et al.* (1997) for the atoms $\mathcal{R}$ = La, Ce, and Th in the filled skutterudite structure $\mathcal{R}_{1-y}Fe_{4-x}Co_xSb_{12}$ and by Tse *et al.* (1997) for Xe clathrate hydrates which are weakly bound in an oversized atomic cage. Sales *et al.* (1997) stated that rare-earth elements, undergoing incoherent rattling motion in cages, lower the phonon thermal conductivity at room temperature down to a value comparable to that of vitreous silica. Tse *et al.* (1997) noted that the coupling between guest modes and acoustic phonons arising from networked cages led to the glasslike behavior in the thermal conductivity of clathrate hydrates.

The type-I clathrate compounds constitute networked cages consisting of nanoscale tetrakaidecahedrons with 14 flat faces (14-hedrons) and dodecahedrons with 12 flat faces (12-hedrons), in which the group-1 or -2 element in the periodic table can fill in the cages as the so-called rattling guest atoms. We employ the term "guest" in this review, although some use "filler" instead. For $\mathcal{R}_8Ga_{16}Ge_{30}$ with the guest atom $\mathcal{R}$ = Ba, Sr, and Eu, Sales *et al.* (2001) found, by means of a neutron diffraction measurement, that the nuclear densities of guest atoms Sr and Eu are distributed in off-center positions away from the center of 14-hedrons, while Ba takes an on-center position in 14-hedrons. Glasslike low phonon thermal conductivity was realized in compounds with off-center guest atoms Sr and Eu, but not in those with on-center guest atom Ba. It is important that, although scaffold networks take a crystalline cubic structure, the emergence of glasslike phonon thermal conductivities *depends on* the state of the guest atoms in tetrakaidecahedrons.

II. BACKGROUND ON THERMOELECTRICITY

A. The Wiedemann-Franz law and the Lorenz number

Wiedemann and Franz (1853) found, when investigating the thermal conductivity κ $[W(Km)^{-1}]$ and the electrical conductivity σ $[(\Omega\,m)^{-1}]$ of several metals, that the two quantities are linearly proportional to each other at room temperature in the form

$$\kappa = \text{const} \times \sigma. \tag{2}$$

This relation indicates that electric and thermal conductions are definitely correlated. Twenty years later, Lorenz (1872) found, from data on the temperature dependence of Eq. (2), that the ratio is also proportional to the absolute temperature T:

$$\kappa = LT\sigma, \tag{3}$$

where L is a proportionality constant termed the Lorenz number. This relation is generally called the Wiedemann-Franz law or the Wiedemann-Franz-Lorenz law.

The first theoretical derivation of the Lorenz number was made by Sommerfeld (1927, 1928) using the Fermi-Dirac distribution function of degenerate metals, which provides

$$L_0 = \frac{\pi^2}{3}\left(\frac{k_B}{e}\right)^2 = 2.44 \times 10^{-8}\ [\mathrm{W\,\Omega\,K^{-2}}], \tag{4}$$

where k_B is the Boltzmann constant, and e is the electron charge. The L_0 defined via universal constants is called the Sommerfeld value of the Lorenz number. This relation can be simply derived from the free-electron model. The expression for the conductivity σ is

$$\sigma = \frac{ne^2\tau_{el}}{m_e^*}, \tag{5}$$

where τ_{el} is the average collision time of the electrons, n is the number of electrons per volume at the Fermi energy, and m_e^* is the effective mass of an electron. The electronic contribution to the thermal conductivity κ_{el} is expressed in the same way by

$$\kappa_{el} = \frac{1}{3}C_{el}v_F\ell_{el} = \frac{\pi^2 n k_B^2 T\tau_{el}}{3m_e^*}, \tag{6}$$

where C_{el} is the specific heat of the electrons, v_F is the Fermi velocity, and ℓ_{el} is the mean free path of the electrons.

The ratio of Eqs. (5) and (6) provides

$$\frac{\kappa_{el}}{\sigma} = \frac{\pi^2}{3}\left(\frac{k_B}{e}\right)^2 T = L_0 T, \tag{7}$$

where the collision time τ_{el} is canceled out. The mean free path ℓ_{el} is reduced by collisions with impurities and phonons in impure metals or in disordered alloys or semiconductors. Note that Eq. (7) has been obtained from the average collision-time approximation for free electrons in addition to the assumption that only electrons carry heat.

The Wiedemann-Franz law is valid for cases in which the elastic scattering of electrons dominates. The Wiedemann-Franz law holds, to a good approximation, at low temperatures where elastic scattering by impurities or defects is relevant and at high temperatures where the change in energy of each electron scattered by electron-electron or electron-phonon interactions is negligible compared with the energy scale k_BT. At intermediate temperatures 10–200 K, electronic energy loss becomes of the order of k_BT and Eq. (7) is no longer valid. See, for example, Ashcroft and Mermin (1976) for detailed arguments beyond the relaxation-time approximation for electron transport relevant to the Wiedemann-Franz law.

It was already pointed out by Lorenz (1881a, 1881b) that L is not a universal factor, but depends on the kind of metal. The actual values of the Lorenz number L are given, for example, by Kaye and Laby (1966) and Kumar, Prasad, and Pohl (1993) for elemental metals, semimetals, metallic alloys and compounds, and degenerate semiconductors. These provide $L = 2.3\text{–}2.6 \times 10^{-8}\,\mathrm{W\,\Omega\,K^{-2}}$ close to the Sommerfeld value L_0 for almost all elemental metals and smaller values $L = (1.7\text{–}2.5) \times 10^{-8}\ \mathrm{W\,\Omega\,K^{-2}}$ in degenerate semiconductors. In contrast, the Lorenz numbers of transition metals deviate considerably from the Sommerfeld value (Chari and Chari, 1989, 1990).

The experimental values for the thermal conductivity κ in Eq. (3) represent the total thermal conductivity κ_{tot} including the phonon contribution to heat transport. The phonon component of the thermal conductivity κ_{ph} can be estimated by subtracting the electric component κ_{el} from the measured total thermal conductivity κ_{tot}. Suppression of the electronic contribution to the thermal conductivity and hence the separation of the phonon and electronic parts of the conductivity can be achieved by applying a transverse magnetic field.

In the presence of a magnetic field, the Lorenz number varies with it. In this connection, we mention the Nernst-Ettingshausen effect (Ettingshausen and Nernst, 1886). This is a thermomagnetic phenomenon where an electric current is generated perpendicular to an applied magnetic field and a temperature gradient. This was discovered by Etttingshausen and his student Nernst in 1886 when heating one side of the sample during investigation of the Hall effect in bismuth. The reverse effect, in which a temperature gradient appears when a current and a magnetic field are applied, is called the Ettingshausen effect. There is a close correspondence between the expressions for cooling power and the coefficient of performance obtained by using the Ettingshausen and Peltier effects (O'Brien and Wallace, 1958). The Ettingshausen refrigerator requires only one material, so the issue of matching n-type and p-type transport does not arise. Detailed discussions about the Ettingshausen effect are given, for example, by Nolas, Sharp, and Goldsmid (2001).

B. Heat and electric transport as irreversible processes

1. Peltier and Seebeck coefficients

The Onsager reciprocal relations express the equality of certain ratios between generalized fluxes and forces based on the principle of detailed balance when a notion of local equilibrium is applicable. The thermoelectric effects discussed here deal with the relations between two kinds of flux (the heat flux density $\boldsymbol{Q}$ and the particle flux density $\boldsymbol{J}$), which are associated with two kinds of generalized forces [the gradient of the inverse of temperature $\nabla(1/T)$ and the gradient of electrochemical potential $\nabla\mu$]. Callen (1948, 1952) developed a general argument for the application of Onsager's theory to thermoelectric phenomena. The relations given by

Callen (1948) are expressed in the form of linear combinations among the generalized fluxes and forces,

$$-\boldsymbol{J} = L_{11}\frac{1}{T}\nabla\mu + L_{12}\nabla\left(\frac{1}{T}\right), \tag{8}$$

$$\boldsymbol{Q} = L_{21}\frac{1}{T}\nabla\mu + L_{22}\nabla\left(\frac{1}{T}\right), \tag{9}$$

where μ is the electrochemical potential composed of both a chemical potential μ_C and an electrical one μ_E with $\mu = \mu_C + \mu_E$. For the charge e of a particle $\mu_E = e\phi$, where ϕ is the electrostatic potential. The chemical potential μ_C is a function of the temperature T and the particle density n, and the $\nabla\mu_C$ plays a minor role in electrical conductors. The Onsager reciprocal relation (Onsager, 1931) states that

$$L_{12} = L_{21}. \tag{10}$$

Provided that an applied magnetic field $\boldsymbol{H}$ exists, this relation becomes $L_{ij}(\boldsymbol{H}) = L_{ji}(-\boldsymbol{H})$.

The kinetic coefficients L_{ij} are closely related to the electrical $\sigma[(\Omega\mathrm{m})^{-1}]$ and thermal conductivity $\kappa[\mathrm{W(Km)}^{-1}]$ as can be seen by expressing Eqs. (8) and (9) in terms of σ and κ. Here σ is defined as the electrical current density $\boldsymbol{j} = e\boldsymbol{J}$ per unit electric field $\boldsymbol{E} = -\nabla\mu_E/e$ in an isothermal system, which provides

$$\sigma = \frac{\boldsymbol{j}}{\boldsymbol{E}} = -\frac{\boldsymbol{j}}{\nabla\mu_E/e}, \quad \text{for} \quad \nabla T = 0. \tag{11}$$

Substituting Eq. (11) into Eq. (8), we have

$$\sigma = \frac{e^2 L_{11}}{T}. \tag{12}$$

The thermal conductivity κ is the heat current $\boldsymbol{Q}$ per unit temperature gradient, given by

$$\kappa = -\frac{\boldsymbol{Q}}{\nabla T}, \quad \text{for} \quad \boldsymbol{j} = 0. \tag{13}$$

The above can be related to the kinetic coefficient L_{ij} using Eqs. (8) and (9), and this is written as

$$\kappa = \frac{L_{11}L_{22} - L_{12}^2}{T^2 L_{11}}. \tag{14}$$

The Seebeck effect implies that the temperature gradient ∇T yields the electric field $\boldsymbol{E}'$ in a system. This is expressed as $\boldsymbol{E}' = -S\nabla T$, where S [V/K] is called the Seebeck coefficient or the thermoelectric power of a medium. The use of S enables us to rewrite Eqs. (8) and (9) in terms of the electric field $\boldsymbol{E}$ [V/m] and the temperature gradient ∇T [K/m] as

$$\boldsymbol{j} = \sigma(\boldsymbol{E} - S\nabla T), \tag{15}$$

$$\boldsymbol{Q} = \sigma ST\boldsymbol{E} - \kappa\nabla T, \tag{16}$$

where $S = -eL_{12}/\sigma T^2$.

Equations (15) and (16) recover the Onsager reciprocal relation $L_{12} = L_{21} = -T^2\sigma S/e$. From Eqs. (15) and (16) with $\nabla T = 0$, the Peltier coefficient Π is defined by

$$\boldsymbol{Q} = TS\boldsymbol{j} \rightarrow S = \frac{\Pi}{T}. \tag{17}$$

Thus, the Peltier and Seebeck effects are essentially the same in thermoelectrics. The Peltier coefficient has a simple physical meaning of the energy carried by charged particles per unit charge.

The Seebeck coefficient S becomes negative for electron carriers as in n-type semiconductors and positive for hole carriers in p-type semiconductors.

2. Figure of merit

The direct expression for the heat current $\boldsymbol{Q}$ driven by an electrical current $\boldsymbol{j}$ and the temperature gradient ∇T is obtained from Eqs. (15) and (16). This yields

$$\boldsymbol{Q} = ST\boldsymbol{j} - \kappa_{\mathrm{tot}}\nabla T, \quad \text{with } \kappa_{\mathrm{tot}} \equiv \kappa(1 - Z'T), \tag{18}$$

where $Z' \equiv \sigma S^2/\kappa$. Since κ_{tot} is a positive quantity, Z' is bounded by the inequality $Z'T < 1$ as can be seen from Eq. (18).

Instead of Z', we introduce the quantity called the material's figure of merit defined by (Mahan and Sofo, 1996; Mahan, 1998)

$$Z = \frac{\sigma S^2}{\kappa_{\mathrm{tot}}} = \frac{Z'}{1 - Z'T}, \tag{19}$$

where Z has the dimension of inverse temperature. Thus the efficiency of the thermoelectric conversion is alternatively defined by the dimensionless parameter ZT termed the "dimensionless figure of merit," which is given by

$$ZT = \frac{S^2\sigma T}{\kappa_{\mathrm{eh}} + \kappa_{\mathrm{ph}}}. \tag{20}$$

Here $\kappa_{\mathrm{tot}} = \kappa_{\mathrm{ph}} + \kappa_{\mathrm{eh}}$ is the total thermal conductivity composed of the phonon part κ_{ph} and the electronic part κ_{eh}. We use the notation of κ_{eh} to indicate hole or electron carriers in semiconductors. When electron-hole pairs are present at temperatures comparable to the gap energy, a bipolar term contributing to the electric thermal conductivity should be taken into account; see, for example, Yang (2004).

The Carnot limit (also known as the Carnot efficiency) specifies limits on the maximum efficiency that any heat engine can obtain. The Carnot limit solely depends on the temperature difference between the hot (T_H) and cold (T_C) temperature reservoirs. It is clear that the hotter the heat source, the higher the possible efficiency. The maximum efficiency η_{Carnot} is given by the dimensionless ratio between the temperature difference $\Delta T = T_H - T_C$ and T_H. The formula for the actual efficiency η of a thermoelectric generator is expressed by using η_{Carnot} as (Goldsmid, 2010)

$$\eta = \eta_{\text{Carnot}} \frac{\sqrt{1+ZT}-1}{\sqrt{1+ZT}+T_C/T_H}. \tag{21}$$

Thus the performance of thermoelectric materials is characterized by ZT, determined by three parameters: the Seebeck coefficient S [V/K], the electrical conductivity σ $[(\Omega\,\text{m})^{-1}]$, and the thermal conductivity κ $[\text{W}\,(\text{K}\,\text{m})^{-1}]$. Since for efficiency it is required for η to take values above around 10% at the temperature difference of 300 K, thermoelectric materials satisfying the relation $ZT > 1$ are thought to be especially efficient in practical applications.

3. The Mott formula for the Seebeck coefficient

In three-dimensional systems, the x component of the electric current density j_x and the electric heat flux density Q_x under the electric field F_x can be expressed in terms of the electron mobility $\mu(E)$ of the charge $-e < 0$ as

$$j_x = eF_x \int \mu(E) f(1-f) N(E) dE, \tag{22}$$

$$Q_x = -F_x \int \mu(E)(E-\zeta) f(1-f) N(E) dE, \tag{23}$$

where $N(E)$ is the electron density of states, ζ is the chemical potential, and $f(E)$ is the Fermi-Dirac distribution function. Equation (22) provides the conductivity expressed by an integral over the single-electron states (Fritzsche, 1971)

$$\sigma = e \int \mu(E) f(1-f) N(E) dE \equiv \int \sigma(E) dE, \tag{24}$$

where $\sigma(E)dE$ is the conductivity in the energy interval between E and $E+dE$.

The product of the Peltier coefficient Π and the conductivity σ is obtained by differentiating Eq. (23) with respect to the electric field F_x. The Seebeck coefficient is obtained from Eqs. (16) and (23) in comparison,

$$S(T) = -\frac{k_B}{e} \int \left(\frac{E-\zeta}{k_B T}\right) \frac{\sigma(E)}{\sigma} dE. \tag{25}$$

This yields $S < 0$ for electrons, and $S > 0$ for holes, taking account of the sign of $-e$.

We can set $f(1-f) = -k_B T \partial f/dE$ when only states near the Fermi energy E_F contribute to the conductivity. By expanding $\sigma(E)$ defined in Eq. (24) around $E = E_F$ up to the order $(k_B T/E_F)^2$, we have the convenient expression for the Seebeck coefficient from Eq. (25) of the form

$$S(T) \cong -\frac{\pi^2 k_B^2 T}{3e} \left[\frac{\partial \ln \sigma(E)}{\partial E}\right]_{E=E_F}. \tag{26}$$

This is the Mott formula (Mott and Jones, 1936), showing that the Seebeck coefficient S is proportional to the logarithmic derivative of $\sigma(E)$ or $\mu(E)N(E)$ with respect to the energy at $E = E_F$.

The Mott formula can be applied not only to monovalent metals, but also to other metals or degenerate semiconductors. It is valid even for alloys at temperatures above the Debye temperature θ_D, and at low temperatures, as long as the residual resistivity is large compared with the resistivity due to phonon scattering, in addition to doped semiconductors exhibiting the metal-insulator Anderson transition (Cutler and Mott, 1969). Since the Mott relation is correct only to second order in $k_B T/\zeta$, it is not applicable to transition metals with narrow bands and at high temperatures (Chari and Chari, 1989, 1990). Kirchner, Zamani, and Muñoz (2013) theoretically discussed the effect of a nonlinear thermoelectric response for systems with narrow band structures.

Equation (25) shows that the Seebeck coefficient $|S|$ is proportional to the resistivity $\rho = 1/\sigma$ and the energy difference $E-\zeta$ from the chemical potential. This indicates that heavily doped degenerate semiconductors are suitable for increasing $|S|$. Equation (26) in the degenerate limit yields, for example, from the definitions $\mu(E) \propto E^\alpha$, with α characterizing the scattering mechanisms, and the energy dependence of the electron density of states $N(E) \propto E^{3/2}$,

$$S \cong -\frac{\pi^2 k_B^2 T}{3eE_F}(\alpha + 1.5), \tag{27}$$

where $\alpha = -0.5$ for scattering by acoustic phonons and $\alpha = 1.5$ for ionized impurity scattering. The actual evaluation of the above equation gives $S \cong -2.44 \times 10^{-2} T(\alpha+1.5)/E_F$ [eV] in units of $[\mu\text{V/K}]$. This is a measure of the Fermi energy E_F.

The discussion above focused on degenerate electrons. In semiconductors, the Fermi level lies in the gap and positively charged holes exist. These positive carriers contribute to the transport in addition to negatively charged electrons. One needs to assign different time scales to electrons and holes depending on the band index (Nolas, Slack, and Schujman, 2001; Yang, 2004).

III. CRYSTAL STRUCTURES OF TYPE-I CLATHRATE COMPOUNDS

A. Various types of clathrate compounds

1. Classification of clathrate compounds

Clathrates or clathrate compounds consist of regular lattices of cages in which guest atoms or molecules are encapsulated. Cages with restricted geometry form the basic framework of a lattice with translational invariance. Clathrates are also called host-guest complexes. Typical examples of host-guest complexes are inclusion compounds and intercalation compounds. A gas hydrate is a special type of clathrate compound consisting of water molecules and gas molecules. The history of gas hydrates can be traced back to the work of 200 years ago by Davy (1811a, 1811b), who discovered chlorine hydrate in the combination of a water host molecule (H_2O) and a guest chlorine molecule (Cl_2) when pressurizing water with chlorine gas below 9 °C. Davy and his assistant Michael Faraday continued the research on chlorine hydrate at the Royal Institution of London from 1813. Faraday (1823) determined the composition of chlorine clathrate hydrate as nearly 1 part of Cl_2 and 10 parts of H_2O molecules.

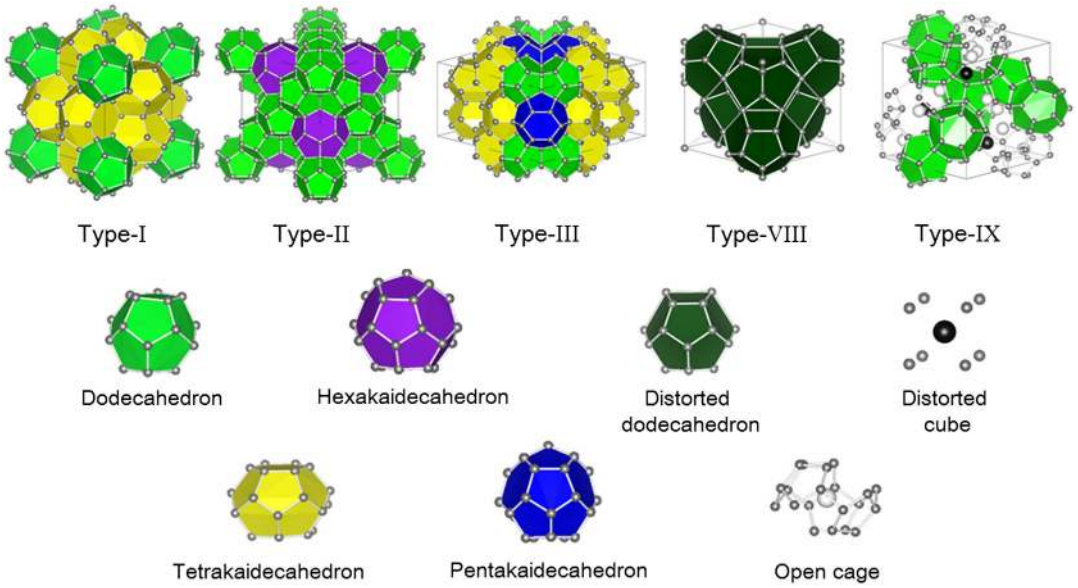

FIG. 2 (color online). Crystal structures of type-I, type-II, type-III, type-VIII, and type-IX intermetallic clathrates.

The water molecule H_2O forms a variety of cages different in size and in geometrical structure. Typical examples of hydrate-forming substances include CH, CO, and HS molecules. The terms "gas hydrate" and "clathrate hydrates" have been used for these solids (Davidson, 1973). Oxygen atoms forming a cage are tetrahedrally connected by hydrogen bonds, which make cages with open space for guest atoms and molecules. In the early stages of this research, the vast majority of clathrate hydrates were classified into two types, type I and type II, belonging to the cubic space groups $Pm\bar{3}n$ and $Fd\bar{3}m$, respectively (Claussen, 1951a, 1951b, 1951c; von Stackelberg and Müller, 1951a, 1951b; Müller and von Stackelberg, 1952; Pauling and Marsh, 1952). Jeffrey (1984) classified clathrate hydrates into seven types by introducing five further types in addition to type-I and type-II structures. Crystal structures of type III, type VIII, and type IX in addition to type I and type II are shown in Fig. 2.

The unit cell of the type-I structure consists of 46 water molecules which form two types of cages, small and large. There are two small cages in the unit cell and six large ones. The small cage has the shape of a pentagonal dodecahedron (5^{12}), and the large one that of a tetrakaidecahedron ($5^{12}6^2$), as given in Fig. 2. Typical guests in type-I clathrate hydrates are CO_2 in carbon dioxide hydrate and CH_4 in methane hydrate. Methane hydrates attracted much interest as a possible new energy source, in which large amounts of methane gas are contained both in permafrost formations and under the ocean seabed (Englezos, 1993; Hester and Brewer, 2009). Hydrogen storage in clathrates is also expected to have potentially important energy applications (Struzhkin *et al.*, 2007).

The unit cell of type-II clathrate hydrates consists of 136 water molecules, forming also small and large cages. There are 16 small cages in the unit cell and 8 large ones. The small cage is again a pentagonal dodecahedron (5^{12}), but the large one is a hexakaidecahedron ($5^{12}6^4$). Type-II hydrates contain larger molecules like CCl_4 and SF_6 than type-I hydrates.

The compositions of the type-I and type-II hydrates are expressed as $2D \cdot 6T \cdot 46H_2O$ and $16D \cdot 8H \cdot 136H_2O$, respectively, where D, T, and H represent, respectively, the guest atoms or molecules in a cage of a pentagonal dodecahedron, tetrakaidecahedron, and hexakaidecahedron composed of water molecules.

2. Intermetallic clathrate compounds

Intermetallic clathrates are inorganic inclusion compounds structurally related to the hydrates (Rogl, 2006). The clathrates composed of the group-14 elements were discovered as prospective thermoelectric materials that realize the phonon-glass electron-crystal concept (Slack, 1995; Nolas, Cohn *et al.*, 1998; Blake *et al.*, 1999; Iversen *et al.*, 2000). The group-14 clathrates have been intensively investigated because of their great potential for converting temperature differences to electric energy (Kuznetsov *et al.*, 2000; Christensen, Snyder, and Iversen, 2006; Saramat *et al.*, 2006; Sootsman, Chung, and Kanatzidis, 2009; Kleinke, 2010).

The frameworks of the group-14 clathrate compounds are constructed from face-sharing polyhedron. The five structures given in Fig. 2 are known as type-I $(2D \cdot 6T \cdot 46F)$, type-II $(16D \cdot 8H \cdot 136F)$, type-III $(10D \cdot 16T \cdot 4P \cdot 172F)$, type-VIII $(8D' \cdot 46F)$, and type-IX $(8D \cdot 12O \cdot 4C \cdot 100F)$ clathrates (Mudryk *et al.*, 2002; Rogl, 2006; Karttunen and Fässler, 2011). Here P, D', O, and C express guests in the pentakaidecahedron, distorted dodecahedron, open cage, and distorted cube, respectively, and F means a framework (cage) atom. D, T, and H are defined previously. Type VIII and type IX have no representatives among hydrate structures.

A silicon clathrate, for example, is formed by covalently bonded Si atoms. Thereby, Si atoms and sp^3 hybridized orbital electrons play the roles of O atoms and H atoms in clathrate hydrates due to their tetrahedral coordination and hydrogen bonding by "ice rules" (Bernal and Fowler, 1933; Pauling, 1948). Kasper *et al.* (1965) discovered the first silicon clathrates, type-I Na_8Si_{46} and type-II Na_xSi_{136}, where

cationic Na guests are enclosed in the silicon framework. The synthesis of Ge-based and Sn-based type-I clathrates with alkali metal atoms as guests was reported by Gallmeier, Schäfer, and Weiss (1969).

Ternary type-I clathrates $\mathcal{R}_8M_{16}Z_{30}$, where $\mathcal{R}$ belongs to the group-2, M belongs to the group-13, and Z belongs to the group-14 elements, respectively, were first synthesized by Eisenmann, Schäfer, and Zagler (1986). The $\mathcal{R}$ guest atom is encapsulated by the cage formed by M and Z elements. The combination of M and Z elements makes it possible to tune the size of the cages. When the cage has a large open space, the encapsulated guest atoms are weakly bound to the cage. Such a loosely bound guest is referred to as a rattler (Sales *et al.*, 1997). This review is concerned with a type-I $\mathcal{R}_8M_{16}Z_{30}$ clathrate with potential application to efficient thermoelectric materials.

Structural and thermoelectric properties for various types of intermetallic clathrates, including type-II and type-III clathrates, have been treated in the following works: type I $\mathcal{R}'_8M_8Z_{38}$ with an alkali metal guest $\mathcal{R}'_8$ (Bobev and Sevov, 2000; Nolas, Chakoumakos *et al.*, 2000; Myles, Dong, and Sankey, 2001; Hayashi *et al.*, 2010; Tanaka *et al.*, 2010); type-I with a transition metal element as a cage atom (Anno *et al.*, 2003; Akai *et al.*, 2005; Johnsen *et al.*, 2007; Christensen *et al.*, 2009; Melnychenko-Koblyuk *et al.*, 2009; Christensen, Johnsen, and Iversen, 2010; Nasir *et al.*, 2010; Nguyen *et al.*, 2010; Zhang *et al.*, 2011; Xu *et al.*, 2012); type-I mainly constructed from the group-15 elements (As and Sb) (Liu *et al.*, 2009; He *et al.*, 2012); type-II (Kasper *et al.*, 1965; Beekman and Nolas, 2008; Beekman *et al.*, 2010), type-III (Bobev and Sevov, 2001; Zaikina *et al.*, 2008, 2010), and type-IX clathrates (Kröner, Nesper, and von Schnering, 1988; Carrillo-Cabrera *et al.*, 2000; Fukuoka *et al.*, 2000; Kim *et al.*, 2000, 2007a, 2007b; Paschen *et al.*, 2002; Rachi *et al.*, 2005); "inverse clathrates" with halogen or tellurium guests (Menke and von Schnering, 1973; Kishimoto, Arimura, and Koyanagi, 2006; Kishimoto *et al.*, 2007; Zaikina *et al.*, 2010; Falmbigl and Rogl, 2012).

3. Crystal chemistry of a type-I clathrate

Among various types of intermetallic clathrate compounds, the type-I structure of $\mathcal{R}_8M_{16}Z_{30}$ and $\mathcal{R}'_8M_8Z_{38}$ stoichiometry has been most often adopted, where $\mathcal{R}$ is a guest atom of group 2 (Ba, Sr) or a divalent rare-earth element (Eu), and $\mathcal{R}'$ a group-1 element (Na, K, Rb, and Cs). The cage constituents M and Z are the elements of group 13 (Al, Ga, and In) and group 14 (Si, Ge, and Sn), respectively (Eisenmann, Schäfer, and Zagler, 1986; Bobev and Sevov, 2000). It should be noted that only $Ba_8Ga_{16}Sn_{30}$ and $Eu_8Ga_{16}Ge_{30}$ are known to form the type-VIII structure with the same composition as the type-I (Eisenmann, Schäfer, and Zagler, 1986; von Schnering *et al.*, 1998; Paschen *et al.*, 2001; Carrillo-Cabrera *et al.*, 2002; Leoni, Carrillo-Cabrera, and Grin, 2003). Large single crystals of type-I and type-VIII $Ba_8Ga_{16}Sn_{30}$, which are shown in Fig. 3, were grown by a flux method using excess amounts of Ga and Sn (Suekuni, Avila *et al.*, 2008). The type-VIII structure can be formed in the alloyed compounds $Sr_8Al_xGa_{16-x}Si_{30}$ ($8 \le x \le 13$) and $Sr_8Al_xGa_yGe_{46-x-y}$ ($6 \le x \le 7$ and $10 \le y \le 11$) (Kishimoto *et al.*, 2008; Sasaki *et al.*, 2009; Shimizu *et al.*, 2009). This structure is cubic (space group number 217; $I\bar{4}3m$) and the unit cell consists of eight distorted dodecahedra, as shown in Fig. 2. Aspects of the chemistry and synthesis of intermetallic clathrates have been reported (Kovnir and Shevelkov, 2004; Shevelkov and Kovnir, 2011).

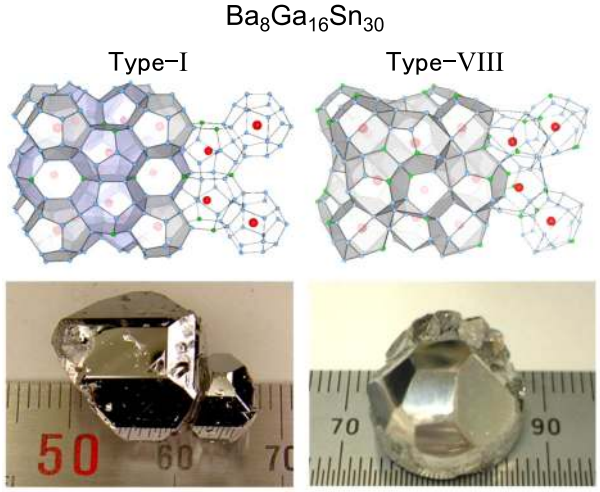

FIG. 3 (color online). Crystal structures and single crystals of type-I and type-VIII $Ba_8Ga_{16}Sn_{30}$. The units of rulers are given in millimeters. From Suekuni, Avila *et al.*, 2008.

Most of the type-I and type-VIII clathrates follow the so-called Zintl concept (Paschen *et al.*, 2003; Rodriguez, Saribaev, and Ross, Jr., 2010; Toberer, May, and Snyder, 2010; Shevelkov and Kovnir, 2011). In a Zintl compound, each constituent attains a closed valence shell by combining a formal charge transfer with covalent bonds. In intermetallic clathrate compounds, the cage atom Z is partially substituted by the acceptor atoms M for charge compensation between the guest and the cage. Consequently, the cage atoms are tetrahedrally bonded by an sp^3 hybridized orbital as shown in Fig. 4.

In the type-I structure the guests occupy two sites as shown in Fig. 4(b): the 2*a* site in the dodecahedron and the 6*d* site in the tetrakaidecahedron. The cage atoms M and Z in type-I $\mathcal{R}_8M_{16}Z_{30}$ and $\mathcal{R}'_8M_8Z_{38}$ occupy three crystallographic sites 6*c*, 16*i*, and 24*k*. The 6*c* site is bound to four 24*k* sites; the 16*i* site, to three 24*k* sites and one 16*i* site; the 24*k* sites, to one 6*c* site, two 16*i* sites, and one 24*k* site. Note that there are no equivalent positions around the 6*c* site. The M and Z atoms do not order in the host framework, but are distributed by a certain rule (see below). First-principles calculations by Blake *et al.* (1999, 2001) and Gatti *et al.* (2003) suggested that the M atoms in $\mathcal{R}_8M_{16}Z_{30}$ preferentially occupy the 6*c* site which does not have adjoining equivalent sites. This is because the bonds between M atoms are energetically unfavorable. In fact, as described in Sec. III.B, the preferential occupation of the M atom at 6*c* sites was experimentally proved from the analysis of x-ray and neutron diffraction experiments (Eisenmann, Schäfer, and Zagler, 1986; Zhang *et al.*, 2002; Bentien *et al.*, 2005; Christensen *et al.*, 2006; Christensen and Iversen, 2007; Christensen, Johnsen, and Iversen, 2010). For type-I $Ba_8Ga_{16}Sn_{30}$, extended x-ray absorption fine-structure (EXAFS) analyses have shown that the Ga-Ga bond is

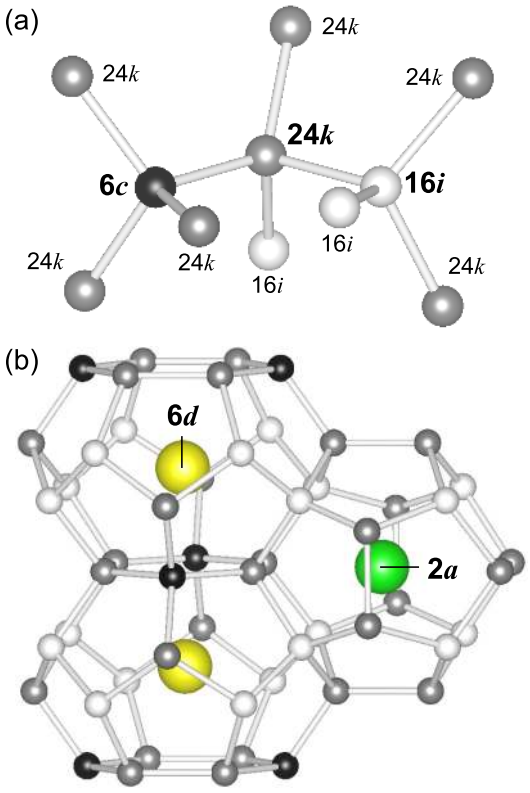

FIG. 4 (color online). (a) Tetrahedral bonds of framework atoms, and (b) guests in dodecahedral and tetrakaidecahedral cages for type-I clathrates.

unfavorable; only 15% of the Ga nearest neighbors are Ga (Kozina *et al.*, 2009).

First-principles calculations pointed out that type-I clathrates with $\mathcal{R}_8M_{16}Z_{30}$ stoichiometry have a semiconducting electronic structure (Blake *et al.*, 1999, 2001; Madsen *et al.*, 2003; Nenghabi and Myles, 2008a; Uemura *et al.*, 2008; Akai *et al.*, 2009; Kono *et al.*, 2010). Despite the balanced electron count $[\mathcal{R}^{2+}]_8[M^{1-}]_{16}[Z^0]_{30}$, these compounds often behave like a metal or a doped semiconductor in their electrical conduction. This is attributed to a minor off-stoichiometry $[\mathcal{R}^{2+}]_8[M^{1-}]_{16+x}[Z^0]_{30-x}$ and/or vacancy formation on the cage sites. It is crucial for efficient thermoelectric materials that the carrier type and the carrier density can be tuned by adjusting x in $\mathcal{R}_8M_{16+x}Z_{30-x}$. For instance, in type-I $Ba_8Ga_{16+x}Ge_{30-x}$, a positive value of x yields p-type conduction and negative x leads to n-type (Anno *et al.*, 2002, 2003; Avila, Suekuni, Umeo, and Takabatake, 2006, Avila, Suekuni, Umeo, Fukuoka *et al.*, 2006; Tang *et al.*, 2010). A tunable carrier type in one compound has the advantage of the possibility of constructing a thermoelectric module using p- and n-type legs.

B. On-center and off-center positions of guest atoms in type-I clathrate compounds

1. X-ray and neutron diffraction and EXAFS

This section describes the atomic configuration in type-I clathrate compounds determined by means of x-ray diffraction (Nolas, Weakley *et al.*, 2000; Bentien *et al.*, 2005; Christensen *et al.*, 2006; Christensen, Johnsen, and Iversen, 2010), neutron diffraction (Chakoumakos *et al.*, 2000; Chakoumakos, Sales, and Mandrus, 2001; Sales *et al.*, 2001; Christensen *et al.*, 2006; Christensen, Johnsen, and Iversen, 2010), and EXAFS (Baumbach *et al.*, 2005; Jiang *et al.*, 2008; Kozina *et al.*, 2009; Mansour *et al.*, 2012).

In type-I clathrates, the guest sites in the dodecahedron and tetrakaidecahedron are denoted by guest (1) and (2) sites, respectively. Chakoumakos *et al.* (2000) investigated the vibrational characteristics of a Sr(2) guest atom encaged in type-I $Sr_8Ga_{16}Ge_{30}$ in terms of neutron diffraction at room temperature, claiming that the isotropic atomic displacement parameter (ADP) for Sr(2) is enormous. Taking into account the anisotropic displacement, the vibrations of Sr(2) show a large ADP in the plane parallel to the six-member ring cage. These results suggest that the site of Sr(2) could be equally described by a fractionally occupied fourfold split site. In fact, the differential Fourier map around the cage center 6d site shows a residual nuclear density with lobes in the directions of the split positions 24k. Following the above work, Sales *et al.* (2001) and Chakoumakos, Sales, and Mandrus (2001) performed a neutron diffraction study on single crystals of type-I $\mathcal{R}_8Ga_{16}Ge_{30}$ ($\mathcal{R}$ = Ba, Sr, Eu). Difference Fourier maps suggest that the nuclear density of Ba(2) is centered at the cage center, while those of Sr(2) and Eu(2) move off to one of four off-center sites 24k, 0.3 Å and 0.4 Å away from the cage center, respectively. Refinements result in similar residual

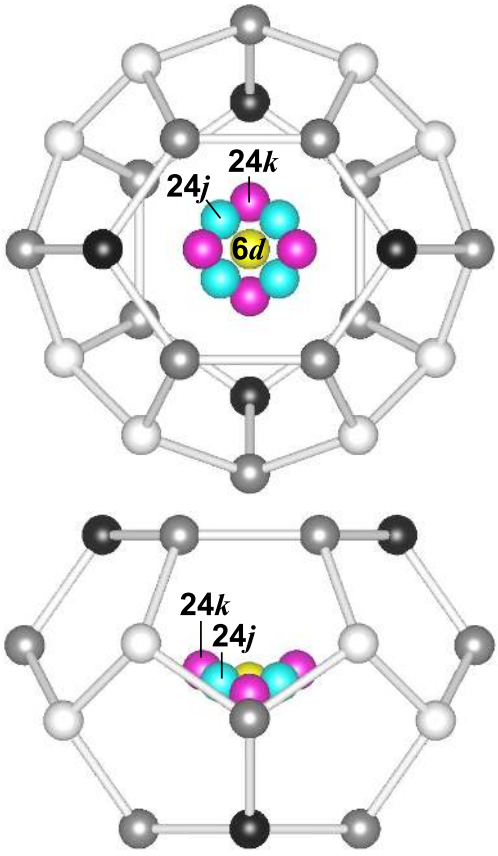

FIG. 5 (color online). Split 24j and 24k sites for guest (2) atoms around 6d sites in tetrakaidecahedral cages for a type-I clathrate.

TABLE I. Key properties of type-I and type-VIII clathrates $\mathcal{R}_8M_{16}Z_{30}$. The samples are in the forms of polycrystallines, powders, or single crystals. Listed are carrier types n or p, $\kappa_{ph}(T)$, on-center or off-center states of the guest atom $\mathcal{R}(2)$, and two characteristic temperatures θ of $\mathcal{R}(2)$. Features of $\kappa_{ph}(T)$ are denoted by C (crystalline) or G (glasslike). The exponents of the temperature dependence of $\kappa_{ph}(T)$ below 1 K are given for single crystals. The states of guest atom $\mathcal{R}(2)$, on center or off center, have been judged by various experiments: x-ray diffraction (XRD), neutron diffraction (ND), resonant x-ray diffraction (RXD), extended x-ray absorption fine-structure spectroscopy (EXAFS), resonant ultrasound spectroscopy (RUS), Mössbauer spectroscopy (Mössbauer), microwave absorption spectroscopy (MW), specific heat (SH), electrical resistivity (ER), Raman scattering (Raman), THz spectroscopy (THz), inelastic neutron diffraction (INS), and nuclear inelastic scattering (NIS). Two characteristic temperatures θ on $\mathcal{R}(2)$ correspond to vibrational modes in out of the plane or on the plane perpendicular to the fourfold axis of the tetrakaidecahedron. Single or nonseparated values denote the cases not distinguished or assumed off-center $24k$ or $24j$ sites. The values in parentheses may include the components of $\mathcal{R}(1)$ in the dodecahedron in addition to $\mathcal{R}(2)$. For type-VIII clathrates, the characteristic temperature θ is for the guest atom in a distorted dodecahedron. RT indicates room temperature.

Compounds type of $\mathcal{R}_8M_{16}Z_{30}$	Sample form	Carrier types	$\kappa_{ph}(T)$	Experiments (temperature)	Rattling states of $\mathcal{R}(2)$	θ [K] for $\mathcal{R}(2)$	References
I-$Ba_8Al_{16}Si_{30}$	Poly	n	C				Mudryk *et al.* (2002)
	Single			XRD	On center	92,100/68,74	Christensen, Johnsen, and Iversen (2010)
($Ba_8Al_{14}Si_{31}$)	Single	n	C	ND (298 K)	On		Condron *et al.* (2006)
I-$Sr_8Al_{10}Si_{36}$	Single			XRD (90 K)	On		Roudebush *et al.* (2012)
I-$Sr_8Al_{11}Si_{35}$	Single	n	C	SH		125/67	Our data, unpublished
I-$Ba_8Ga_{16}Si_{30}$	Single			ND	On	98/69	Bentien *et al.* (2002)
	Powder	n	C	ND	Off center	85	Qiu *et al.* (2004)
	Single			ND	Off		Bentien *et al.* (2005)
	Powder			XRD	On	101/77	Bentien *et al.* (2005)
	Single			XRD	On	92–95/66–69	Christensen, Johnsen, and Iversen (2010)
($Ba_8Ga_{12}Si_{33}$)	Powder			XRD (RT)	On		Mudryk *et al.* (2002)
($Ba_8Ga_{15-16}Si_{31-30}$)	Powder			XRD (RT)	On	88–96/53–57	Anno *et al.* (2012)
	Single			Raman (4 K)	Off	−/59	Takasu *et al.* (2008)
I-$Sr_8Ga_{16}Si_{30}$	Single	n	C	SH		120/59	Suekuni *et al.* (2007)
	Single	n	C	Raman (50 K)	Off	−/56	Takasu *et al.* (2008)
I-$Ba_8Al_{16}Ge_{30}$	Single			XRD	On	81–85/61–69	Christensen and Iversen (2007)
	Single			XRD	Off	81–84	Christensen and Iversen (2007)
	Single			ND (20 K)	Off		Christensen and Iversen (2007)
	Poly	n	C				Christensen and Iversen (2007)
I-$Ba_8Ga_{16}Ge_{30}$				XRD (RT?)	On	(51)	Eisenmann, Schäfer, and Zagler (1986)
							Sales *et al.* (1999)
	Single		C	ND (15 K)	?		Keppens *et al.* (2000)
	Single			ND	On		Chakoumakos, Sales, and Mandrus (2001)
	Single	n		ND	On	64	Sales *et al.* (2001)
		n		XRD (293 K)	Off	72	Paschen *et al.* (2001)
	Powder			XRD	On	101/73	Bentien *et al.* (2005)
	Single	p		ND	On	90/62	Christensen *et al.* (2006)
	Single	p		XRD	On	87/60	Christensen *et al.* (2006)
	Single	n		ND	On	89/59	Christensen *et al.* (2006)
	Single	n		XRD	On	84/60	Christensen *et al.* (2006)
	Single	p		ND	Off	88	Christensen *et al.* (2006)
	Single	p		XRD	Off	82	Christensen *et al.* (2006)
	Single	n		ND	Off	88	Christensen *et al.* (2006)
	Single	n		XRD	Off	81	Christensen *et al.* (2006)
	Single	p		XRD (20 K)	Off: 65%, on: 33%		Fujiwara *et al.* (2012)
	Single	n		XRD (20 K)	On		Fujiwara *et al.* (2012)
	Powder	n, p		EXAFS	Off	86	Jiang *et al.* (2008)
	Poly	n	C				Uher, Yang, and Hu (1998)
	Single	n	C	SH		(60)	Sales *et al.* (2001)
		n		SH		(80)	Paschen *et al.* (2001)
	Single		G:$T^{\sim 1.8}$				Paschen *et al.* (2003)
	Single	p	G:$T^{1.5}$	SH		38	Bentien *et al.* (2004)
				SH		80	Bentien *et al.* (2005)
	Single	p	G:T^2	SH		42	Umeo *et al.* (2005)

(Table continued)

TABLE I. (*Continued*)

Compounds type of $\mathcal{R}_8M_{16}Z_{30}$	Sample form	Carrier types	$\kappa_{ph}(T)$	Experiments (temperature)	Rattling states of $\mathcal{R}(2)$	θ [K] for $\mathcal{R}(2)$	References
	Single	p	G:T^2	SH		87/49	Avila, Suekuni, Umeo, and Takabatake (2006) and Avila, Suekuni, Umeo, Fukuoka *et al.* (2006)
	Single	n	C:T^2	SH		87/49	Avila, Suekuni, Umeo, and Takabatake (2006) and Avila, Suekuni, Umeo, Fukuoka *et al.* (2006)
	Single	n		SH		74	Xu *et al.* (2011)
	Single	n, p		Raman (2 K)	Off	92/47, 45–47[a]	Takasu *et al.* (2006, 2010)
	Single	p		THz (6.6 K)		86/55	Mori *et al.* (2009)
	Poly			INS (295 K)		55	Hermann *et al.* (2005)
	Powder	p		INS		−/50	Christensen, Juranyi, and Iversen (2006)
	Powder	n		INS		65/52	Christensen, Juranyi, and Iversen (2006)
	Single	n		INS (RT)		−/52	Lee *et al.* (2007)
	Single	n		INS		87/53	Christensen *et al.* (2008)
I-$Ba_8In_{16}Ge_{30}$	Powder			XRD	On	65/65	Bentien *et al.* (2005)
	Single	n	C				Bentien, Johnsen, and Iversen (2006)
(With vacancy)	Poly	n	G				Bentien, Johnsen, and Iversen (2006)
	Single	n	C	SH		99/38	Suekuni, Yamamoto *et al.* (2008)
I-$Sr_8Ga_{16}Ge_{30}$	Powder			XRD (RT)	On	85/39	Schujman *et al.* (2000)
	Powder, single			ND	Off		Chakoumakos *et al.* (2000)
	Powder, single			ND	Off or on	85	Chakoumakos *et al.* (2000)
	Single			XRD (RT)	On	74	Nolas, Weakley *et al.* (2000)
	Single		G	ND (15 K)	Off		Keppens *et al.* (2000)
	Powder			XRD		90/29	Iversen *et al.* (2000)
	Single	n	G	ND	Off		Sales *et al.* (2001)
	Single	n	G	ND	On	80	Sales *et al.* (2001)
	Powder			RXD (RT)	Off		Zhang *et al.* (2002)
	Powder	n	G	ND	Off	76	Qiu *et al.* (2004)
	Powder			XRD	On	104/163	Bentien *et al.* (2005)
	Single	n		XRD (20 K)	Off: 98%, on: 2%		Fujiwara *et al.* (2012)
	Poly	n	G:T^2				Nolas, Slack *et al.* (1998) Cohn *et al.* (1999)
	Poly	n	G/C				Uher, Yang, and Hu (1998)
	Poly	n	G				Nolas, Cohn *et al.* (1998)
			G				Nolas, Weakley *et al.* (2000)
	Powder	n		EXAFS	Off	126–128	Baumbach *et al.* (2005)
	Powder	n		EXAFS	Off: 75%, on: 25%	147–156	Baumbach *et al.* (2005)
				SH		(50)	Chakoumakos *et al.* (2000)
	Single	n	G	SH		(53)	Sales *et al.* (2001)
				SH		(79)	Paschen *et al.* (2001)
				SH		80	Bentien *et al.* (2005)
	Single	n	G	SH		34	Umeo *et al.* (2005)
	Single	n	G	SH		90/35	Suekuni *et al.* (2007)
	Single	n		SH		80	Xu *et al.* (2011)
	Single			RUS		45	Keppens *et al.* (2002)
	Poly			Raman (300 K)		−/46	Nolas and Kendziora (2000)
	Single	n		Raman (2 K)	Off	95/42, 42[a]	Takasu *et al.* (2006)
	Poly			INS (295 K)		49	Hermann *et al.* (2005)
	Powder	n		INS		62/48	Christensen, Juranyi, and Iversen (2006)
	Single	n		INS		−/46	Lee *et al.* (2008)
I-$Eu_8Ga_{16}Ge_{30}$	Single			XRD (RT)	On	53	Nolas, Weakley *et al.* (2000)
	Single			ND	Off		Chakoumakos, Sales, and Mandrus (2001)
	Single	n	G	ND	Off		Sales *et al.* (2001)

(Table continued)

TABLE I. (*Continued*)

Compounds type of $\mathcal{R}_8M_{16}Z_{30}$	Sample form	Carrier types	$\kappa_{ph}(T)$	Experiments (temperature)	Rattling states of $\mathcal{R}(2)$	θ [K] for $\mathcal{R}(2)$	References
	Single	*n*		XRD (293 K)	Off	45	Paschen *et al.* (2001)
	Powder	*n*		EXAFS	Off	93–96	Baumbach *et al.* (2005)
			G				Nolas, Weakley *et al.* (2000)
	Single	*n*	G	SH		(30)	Sales *et al.* (2001)
	Poly	*n*	G				Paschen *et al.* (2001)
	Poly	*n*	G				Bentien *et al.* (2005)
	Single			RUS		22	Zerec *et al.* (2004)
	Poly			Mössbauer, MW	Off	−/31	Hermann *et al.* (2006)
	Poly			Raman (300 K)		−/33	Nolas and Kendziora (2000)
	Single	*n*		Raman (2 K)	Off	69/26, 26[a]	Takasu *et al.* (2006)
	Powder			NIS (25 K)		87, 57, 35	Hermann *et al.* (2005)
VIII-$Eu_8Ga_{16}Ge_{30}$	Single	*n*		XRD (293 K)		45	Paschen *et al.* (2001)
	Poly	*n*	C	SH		72	Paschen *et al.* (2001)
I-$Ba_8Ga_{16}Sn_{30}$	Single	*p*	G:$T^{\sim 2}$	XRD	Off		Suekuni, Avila *et al.* (2008)
	Single	*n*	G:$T^{\sim 2}$	XRD	Off	60	Suekuni, Avila *et al.* (2008)
	Single	*n*	G:$T^{\sim 2}$	SH	Off	−/20	Avila *et al.* (2008)
	Single	*p*	G:$T^{\sim 2}$	SH	Off	−/20	Suekuni, Avila *et al.* (2008)
		p?		SH		55, 14	Zheng *et al.* (2012)
		p?		ER		54	Zheng *et al.* (2012)
	Single	*n*		Raman (4 K)	Off	68/27, 20[a]	Suekuni *et al.* (2010)
	Single	*p*		Raman (4 K)	Off	−/27, 21[a]	Suekuni *et al.* (2010)
	Single	*n*		THz (7 K)		64/34	Mori *et al.* (2011)
				NMR	Off	−/20	Zheng, Rodriguez, and Ross, Jr. (2011)
VIII-$Ba_8Ga_{16}Sn_{30}$	Single, Powder	*n*		XRD		64	Huo *et al.* (2005)
	Single	*n*	C	SH		50	Huo *et al.* (2005)
							Avila, Suekuni, Umeo, Fukuoka *et al.* (2006)
	Single	*p*	G	SH		50	Avila, Suekuni, Umeo, Fukuoka *et al.* (2006)

[a] $E_g(1)/E_g(A)$, $T_{2g}(1)$ modes in the tetrakaidecahadron.

factors for two models with a four-split site on 24*k* and 24*j*, as shown in Fig. 5. Therefore, the disorder of the guest position is more complex than in the case of just four sites. In fact, Fujiwara *et al.* (2012) reported that the Sr(2) are widely distributed onto 24*k* and 24*j* sites.

By combining x-ray and neutron diffraction methods, Christensen *et al.* (2006) and Christensen, Johnsen, and Iversen (2010) revealed that the Ba(2) guests in *n*-type and *p*-type $Ba_8Ga_{16}Ge_{30}$ also occupy slightly off-center sites 24*k* or 24*j*. A more definite off-center 24*k* site for Ba(2) situated 0.43 Å away from the center was found in type-I $Ba_8Ga_{16}Sn_{30}$ (β-BGS), where the cage size is larger by 8% than that of $Ba_8Ga_{16}Ge_{30}$. The off-center displacement of 0.43 Å is comparable to that of Eu(2) (Avila *et al.*, 2008; Suekuni, Avila *et al.*, 2008).

EXAFS has also been employed to investigate the rattling sites of the guests in $\mathcal{R}_8Ga_{16}Ge_{30}$ ($\mathcal{R}$ = Ba, Sr, Eu) (Baumbach *et al.*, 2005; Jiang *et al.*, 2008; Mansour *et al.*, 2012). The analysis has confirmed that Eu(1) is located at the center 2*a* sites, but Eu(2) is located at an off-center site 0.445 Å away from the center of the cage. For $\mathcal{R}$ = Sr, ~75% of Sr(2) atoms take off-center sites 0.40 Å away from the center and the rest reside at the center. The results of EXAFS were in reasonable agreement with those of x-ray and neutron diffraction. Furthermore, the analysis for $\mathcal{R}$ = Ba indicates a somewhat off-center site for Ba(2).

To summarize, it was revealed that the degree of off-center displacement of the guest (2) atoms primarily depends on the relative size of the cage to that of the guest atom. Actually, neutron diffraction experiments have shown that the guest (2) atoms occupy four off-center positions away from the centers of the cages when the size of the cage is large enough, or, equivalently, the ionic radius of the guest atom is small enough (Sales *et al.*, 2001).

Table I gives the sets of the data obtained from various types of experimental methods on characteristic properties of type-I and type-VIII $\mathcal{R}_8M_{16}Z_{30}$. This is useful for the purpose of overviewing the characteristics of actual clathrate compounds.

IV. SPECIFIC HEATS OF TYPE-I CLATHRATE COMPOUNDS

It is common to use an appropriate energy scale in each experiment. These are joules (J) or kelvins (K) for thermal measurements, cm^{-1} or terahertz for optical spectroscopies, and eV for inelastic neutron or x-ray scattering. The conversion relation is 1 THz = 47.99 K = 33.36 cm^{-1} = 4.136 meV. This relation will be helpful for readers in connection

with the following descriptions of the dynamical behaviors of type-I clathrate compounds.

A. Observed characteristics of specific heats

The heat capacity provides fundamental information about the thermal properties of materials. It represents the amount of energy needed to raise the temperature of a given material by 1 K. The heat capacity per unit mass is called the specific heat. The molar specific heat is referred to as specific heat C_V in this review. The temperature dependences of specific heat reflect the phonon density of states, the electronic density of states at E_F, the magnetic degree of freedom, superconducting properties, etc.

Three characteristic temperature regions are manifested in the observed specific heats of type-I clathrate compounds after subtraction of the electronic contribution. These are temperature regions below 1 K, around several kelvin, and above several 10 K. We describe in detail these characteristics in the following sections.

1. Low-temperature specific heats below 1 K

A series of specific-heat experiments on type-I clathrate compounds have made it clear that the characteristics critically depend on the states of the guest atoms in cages (Nolas *et al.*, 1995, 1996; Sales, Mandrus, and Williams, 1996; Nolas, Slack *et al.*, 1998; Nolas, Cohn *et al.*, 1998; Nolas, Cohn, and Slack, 1998; Sales, 1998, 2001; Cohn *et al.*, 1999; Nolas, Weakley *et al.*, 2000; Nolas, Sharp, and Goldsmid, 2001; Bentien *et al.*, 2004, 2005; Avila, Suekuni, Umeo, and Takabatake, 2006; Avila, Suekuni, Umeo, Fukuoka *et al.*, 2006; Suekuni *et al.*, 2007, 2010; Suekuni, Avila *et al.*, 2008; Suekuni, Yamamoto *et al.*, 2008; Xu *et al.*, 2010). The most intriguing findings in the regime below about 1 K are that the temperature dependences and the magnitude are almost identical to those of glasses for type-I clathrate compounds with off-center guest atoms.

The specific heats of type-I clathrates with off-center guest atoms scale in the following form:

$$C_V(T) \cong \alpha T^{1+\delta} + \beta T^3. \tag{28}$$

The first term proportional to $T^{1+\delta}$ is not exactly linear in T at temperatures below 1 K with the positive small factor δ, a dependence that is identical to that of structural glasses (Zeller and Pohl, 1971; Stephens, 1973; Freeman and Anderson, 1986). This term has no connection with the conduction-electron specific heat proportional to γT.

From careful measurements of specific heats of type-I β-BGS, it has been estimated that $\alpha \cong 30\ \mathrm{mJ\,mol^{-1}K^{-2}}$ and $\beta \cong 50\ \mathrm{mJ\,mol^{-1}\,K^{-2}}$ with $\delta = 0.2$ (Suekuni, Avila *et al.*, 2008; Suekuni, Yamamoto *et al.*, 2008). In silica glass (Zeller and Pohl, 1971), $\alpha \cong 0.072\ \mathrm{mJ\,mol^{-1}\,K^{-2}}$ and $\beta \cong 0.108\ \mathrm{mJmol^{-1}K^{-4}}$ with the positive small factor $\delta \cong 0.2$. The most carefully measured silica glass (Lasjaunias *et al.*, 1975) gives $\delta = 0.22$–0.30 between $T = 25$ mK and 0.9 K.

The coefficient of the second term β should be separated into β_D and β_B, where β_D is the coefficient from the Debye phonon specific heat and β_B is that of the excess specific heat originating from the tail of the hump observed at around $T \simeq 4$ K in β-BGS.

2. Excess specific heats over Debye phonons at temperatures of several kelvin

Atomic vibrations of type-I clathrates containing off-center guest atoms display glasslike low-lying modes. Actually, the excess densities of states in type-I clathrate compounds have been observed as a hump in specific-heat experiments in the temperature range around several kelvin, i.e., broad peaks observed in a temperature range 10–100 times smaller than the Debye temperature $\theta_D = \hbar\omega_D/k_B$. The characteristics are almost identical to those of structural glasses observed by a variety of measurements such as optical spectroscopies, inelastic neutron scattering, and specific heats in the THz-frequency range [see, for example, Nakayama (2002)]. The Debye frequency ω_D is related to the velocities of transverse v_t and longitudinal v_ℓ acoustic phonons by

$$\omega_D^3 = \frac{18\pi^2 N}{V}\left(\frac{2}{v_t^3} + \frac{1}{v_\ell^3}\right)^{-1}. \tag{29}$$

Here N is the number of atoms in the volume V. The experimental values of velocities of silica glass are $v_t = 3.767 \times 10^5\ \mathrm{cm\,s^{-1}}$ and $v_\ell = 5.970 \times 10^5\ \mathrm{cm\,s^{-1}}$. These give a Debye frequency $\omega_D/2\pi$ of 10.40 THz corresponding to the Debye temperature $\theta_D = 500$ K from $\theta_D = \hbar\omega_D/k_B$. The specific heat of the Debye phonons is expressed by

$$C_{ph}(T) \cong \frac{12\pi^4 N k_B}{5V}\left(\frac{T}{\theta_D}\right)^3. \tag{30}$$

This formula for the phonon specific heat holds in the temperature regime $T \ll \theta_D$. However, the observed specific heats of structural glasses do not show the temperature dependence of Eq. (30) at low temperatures but manifest excess humps in the temperature range around several kelvin.

Anderson (1959) and Flubacher *et al.* (1959) observed the excess specific heat of silica glass at around 10 K over the Debye contribution of Eq. (30). This is clearly realized by plotting $C_V(T)/T^3$ vs T (Zeller and Pohl, 1971; Pohl, 1981; Buchenau *et al.*, 1986). These observations have been ascribed to the presence of excess vibrational states over the Debye density of states $D(\omega) \propto \omega^2$. The term "boson peak" refers to this excess contribution to the conventional Debye density of states. The issue in structural glasses has been revitalized along with the advent of various experimental techniques. However, the nature of these vibrational states in glasses has been the subject of an intensive and controversial debate for decades.

The humps in C_V/T^3 of type-I β-BGS and type-I $Sr_8Ga_{16}Ge_{30}$ appear around $T \simeq 5$ K (Umeo *et al.*, 2005; Suekuni *et al.*, 2007; Avila *et al.*, 2008; Suekuni, Avila *et al.*, 2008; Suekuni, Yamamoto *et al.*, 2008; Xu *et al.*, 2011); see Fig. 7. This excess hump possesses almost identical characteristics to the boson peak.

3. Characteristic temperatures of excess specific heats

The data on specific heats have been used to characterize the vibrational properties of type-I clathrate compounds. An analysis based on the Einstein model has been carried out on type-I $Eu_8Ga_{16}Ge_{30}$ (EGG), $Sr_8Ga_{16}Ge_{30}$ (SGG), and $Ba_8Ga_{16}Ge_{30}$ (BGG) single crystals by Sales *et al.* (2001), where the cages and the guests were assumed to behave as Debye phonons and Einstein oscillators, respectively. At temperatures above 80 K, the specific-heat data were the same among the three samples to within the experimental error and well described by the Debye specific heat with a θ_D of about 300 K. At low temperatures, however, the Einstein oscillators predicted significantly different behaviors to the three samples. The Einstein temperatures θ_E corresponding to the vibrations of Ba, Sr, and Eu guest atoms were estimated to be 60, 53, and 30 K, respectively.

Paschen *et al.* (2001) reported a different analysis for these three compounds. The data of C_V vs T were fitted by including the phonon and electronic contributions given by C_{ph} and C_{el}. The fitting parameters are θ_D, θ_E, and the numbers of atoms N_D and N_E contributing to the Debye and Einstein specific heats, respectively, where their sum $N_D + N_E$ is taken as 54. For BGG, the obtained parameters were $\theta_D = 355$ K, $\theta_E = 80$ K, $N_D = 39$, and $N_E = 15$. Similar results were obtained for SGG. The fits to the data for BGG and SGG yield $N_E = 15$ and 16, respectively, instead of the number of guests equal to 8. For β-EGG, θ_E was not evaluated due to the large magnetic contribution of Eu^{2+} at temperatures up to 50 K. The value of θ_D was estimated to be 302 K using θ_E obtained from room-temperature isotropic ADP and $C_V(T)$ data at temperatures above the Curie temperature of 36 K.

Bentien *et al.* (2004) analyzed C_V for BGG using two kinds of Einstein oscillators. The obtained characteristic temperatures are $\theta_D = 324(4)$ K, $\theta_{E1} = 78(2)$ K, and $\theta_{E2} = 38(1)$ K with $N_D = 2.8(6)$, $N_{E1} = 9.7(5)$, and $N_{E2} = 1.5(5)$, respectively. A linear fit to the data of C_V/T vs T^2 between 1.5 and 4 K^2 gave $\theta_D = 311(10)$ K , in agreement with the result from the fitting of the data C_V vs T above 5 K. The Sommerfeld coefficient γ was estimated to be 14 mJ/K^2 mol.

In this analysis on BGG, N_D and N_E are free fitting parameters. Bentien *et al.* (2005) then imposed the constraints $N_D = 46$ and $N_{E1} + N_{E2} = 8$. By using $\theta_D = 312$ K obtained from the temperature dependence of the ADP of the cage atoms, the parameters were evaluated to be $\gamma = 35$ mJ/K^2 mol, $\theta_{E1} = 80$ K, $N_{E1} = 6.5$, $\theta_{E2} = 42$ K and $N_{E2} = 1.5$, respectively. For SGG, the evaluated parameters were $\gamma = 40$ mJ/K^2 mol, $\theta_{E1} = 80$ K, and $\theta_{E2} = 33$ K. They argued that N_{E1} and N_{E2} almost correspond to the numbers of the large and small cages. However, the result disagrees with the fact that the guest in a small cage has a higher vibrational energy (Christensen, Johnsen, and Iversen, 2010).

Avila, Suekuni, Umeo, Fukuoka *et al.* (2006) analyzed the specific-heat data for BGG by plotting C_V/T^3 vs T. The contributions of the guest atoms from these systems appear as broad peaks over electronic and Debye backgrounds originating from the stiff cage. This treatment reproduced the specific-heat data for type-VIII $Ba_8Ga_{16}Sn_{30}$ (Huo *et al.*, 2005). Recall that six Ba(2) atoms at the 6*d* site in the tetrakaidecahedra show strongly anisotropic vibration with larger amplitudes within the plane perpendicular to the fourfold axis. So, at least two characteristic temperatures are required to describe the vibrations of Ba(2) when applying the Einstein model: in-plane $\theta_{E2}^{\parallel}$ and out-of-plane $\theta_{E2}^{\perp}$. Furthermore, the characteristic temperature of a Ba(1) atom at a 2*a* site in the dodecahedra was assumed to be the single parameter θ_{E1} because of the isotropic shape of the cage. The dimensionality and the numbers of oscillators were predefined: $D \times N_{E1} = 3 \times 2$, $D \times N_{E2}^{\parallel} = 2 \times 6$, and $D \times N_{E2}^{\perp} = 1 \times 6$. Additional constraints $\theta_{E2}^{\parallel} < \theta_{E2}^{\perp}$ and $\theta_{E2}^{\parallel} < \theta_{E1}$ were imposed. The values of γ and θ_D determined from the plot of C/T vs T^2 were fixed, together with the number N_E. Therefore, only three fitting parameters were left, which characterize the vibrational energies of the Ba guests. The best fits give the values $\theta_{E1} = 87.2$ K, $\theta_{E2}^{\perp} = 87.1$ K, and $\theta_{E2}^{\parallel} = 49.4$ K.

Specific-heat experiments on cage-size-tuned $Sr_8Ga_{16}Si_{30-x}Ge_x$ were performed by Suekuni *et al.* (2007). With increased x from 0 to 30, the cage size was expanded by 8%. The data in Fig. 6 plotted as C_V/T^3 vs T show that the peak temperatures of the boson-peak-like hump shift lower from 10.5 to 7 K with increasing hump heights. These observations do not depend on the carrier density, whose contribution becomes vanishingly small at temperatures above 4 K. In the analysis based on the Einstein

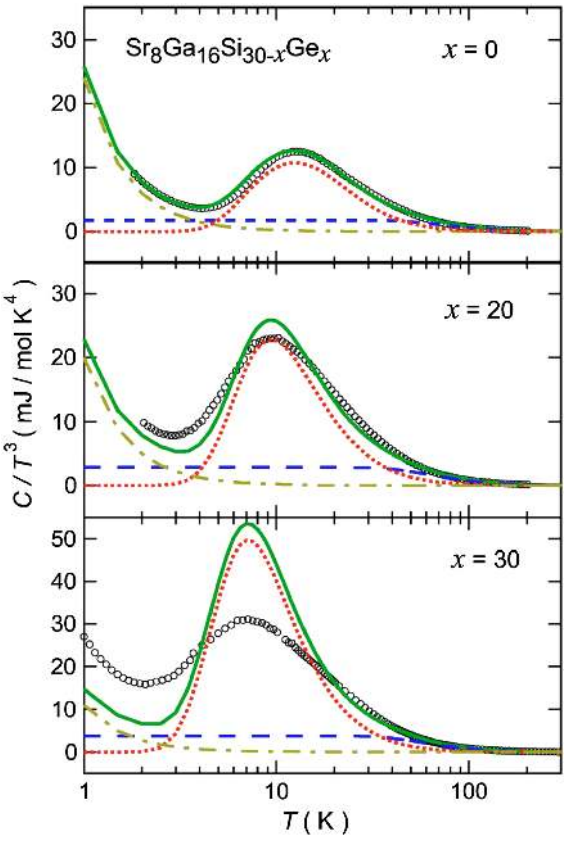

FIG. 6 (color online). The specific-heat data plotted as $C_V(T)/T^3$ vs T (open circles) for type-I $Sr_8Ga_{16}Si_{30-x}Ge_x$. The dotted, dashed, and dash-dotted lines are from the Einstein model, the Debye model, and the electronic components, respectively. From Suekuni *et al.*, 2007.

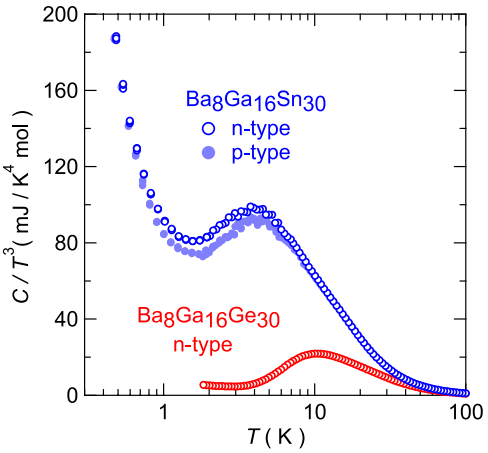

FIG. 7 (color online). The specific-heat data plotted as C_V/T^3 vs T for n-type type-I $Ba_8Ga_{16}Ge_{30}$ and n-type and p-type type-I $Ba_8Ga_{16}Sn_{30}$ single crystals. Adapted from Avila, Suekuni, Umeo, Fukuoka *et al.*, 2006, Avila *et al.*, 2008, and Suekuni, Avila *et al.*, 2008.

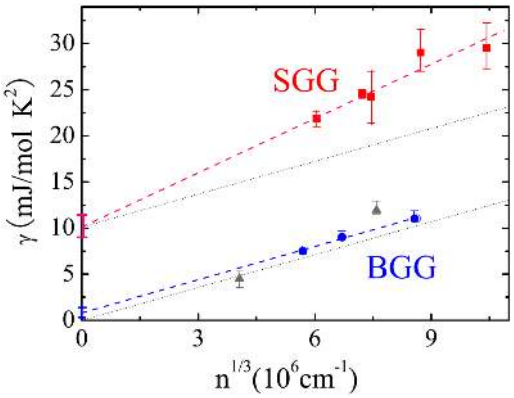

FIG. 8 (color online). The temperature-linear factor γ of low-temperature specific heat for type-I $\mathcal{R}_8Ga_{16}Ge_{30}$ ($\mathcal{R}$ = Sr and Ba) plotted as a function of the carrier concentration $n^{1/3}$. Adapted from Xu *et al.*, 2010.

model, the constraints $\theta_{E2}^{\parallel} = \theta_{\rm EL}$ and $\theta_{E2}^{\perp} = \theta_{E1} = \theta_{\rm EH}$ were imposed, and the rest of the fitting parameters were taken as the lower and higher characteristic temperatures $\theta_{\rm EL}$ and $\theta_{\rm EH}$. For $x = 0$, a good fit was obtained with $\theta_{\rm EL} = 59$ K and $\theta_{\rm EH} = 120$ K, indicating the validity of the Einstein model for Sr guests in $Sr_8Ga_{16}Si_{30}$. However, for $x = 20$ and 30, the Einstein model apparently did not yield an adequate fitting to the observed data, as seen in Fig. 6. These discrepancies indicate the relevance of the anharmonic potential for the Sr(2) sites on increasing the cage size for $x = 20$ and 30.

Avila *et al.* (2008) and Suekuni, Avila *et al.* (2008) reported specific-heat measurements on type-I BGS, which has a larger cage and a larger off-center displacement of Ba(2) than does BGG. The C/T^3 vs T plot for β-BGS shows a larger boson-peak-like hump around 4 K than that around 10 K; see Fig. 7. The temperature of 4 K is the lowest among type-I clathrates and corresponds to a vibrational energy equivalent to 20 K for Ba(2) in the plane perpendicular to the fourfold axis. The height of the hump for β-BGS was not reproduced by the Einstein model, unlike that for BGG, which indicates a strong anharmonicity of Ba(2) vibrations. The low-temperature T-linear coefficient for n-type β-BGS was estimated to be 29 $\rm mJ/K^2\,mol$, which is about 5 times larger than 6 $\rm mJ/K^2\,mol$ for n-type BGG, regardless of the lower carrier density in β-BGS. It was argued that the larger coefficient in β-BGS can be attributed to a tunneling contribution of Ba(2) among the off-center sites. The boson-peak-like hump at low temperature and the anomalously large temperature-linear coefficient in β-BGS are almost identical to those in vitreous silica.

Xu *et al.* (2010) made an analysis of the data for low-temperature specific heats of type-I BGG and SGG. By using the relation $\gamma = \alpha + \gamma_e = \alpha + cm_e^* n^{1/3}$ (c is a known constant) together with the measured values of γ and the carrier density n, they obtained α and the carrier effective mass m_e^*. The relationships between γ and $n^{1/3}$ are shown in Fig. 8. The α value of 10.1 ± 1.5 $\rm mJ/K^2\,mol$ for type-I SGG is larger than that of 0.8 ± 0.4 $\rm mJ/K^2\,mol$ for BGG. It was suggested that the finite α value in these clathrates presumably results from the random displacement of Ga and Ge in the host framework. The larger α value in type-I SGG indicates large disorder. The m_e^* was obtained from the slope of the γ vs $n^{1/3}$ plot to be $1.68m_0$ for type-I SGG and $1.01m_0$ for BGG, where m_0 is the free-electron mass. The enhancement of m_e^* was interpreted in terms of electron-phonon interactions. The value of m_e^* is described as $m_e^* = m_0(1 + \lambda_{e\text{-ph}} + \lambda_s)$, where $\lambda_{e\text{-ph}}$ is the electron-phonon term and λ_s is the spin fluctuation one. The last term is not important in SGG and BGG, and the values of $\lambda_{e\text{-ph}}$ were estimated to be 0.68 for SGG and 0.01 for BGG. For BGG, the low value of $\lambda_{e\text{-ph}}$ indicates a weak interaction between electrons and vibrations of guest atoms. In contrast, $\lambda_{e\text{-ph}}$ is enhanced for SGG.

V. TRANSPORTS PROPERTIES OF TYPE-I CLATHRATE COMPOUNDS

A. Electrical resistivity and Seebeck coefficient

The type-I clathrates exhibit semiconducting or metallic behaviors in their electrical transport and thermoelectric properties depending on the magnitude of the gap energy and doping level. Semiconducting behaviors are characterized by an exponential decrease of ρ and a $1/T$ dependence of $|S|$ with increasing temperature, which can be attributed to the thermal excitations of electrons over the intrinsic energy gap between the valence and conduction bands, or hopping excitations between impurity states and the band edge. Metallic behaviors are characterized by increase of ρ and $|S|$ with increasing temperature, which are caused by heavily doped electrons or holes. The self-doping is due to off-stoichiometry and/or vacancy in the cage structure. Binary and ternary type-I clathrates have gained much attention because of their high thermoelectric performance.

Among type-I Si clathrates, $Na_2Ba_6Si_{46}$ and Ba_8Si_{46} are superconductors with the transition temperatures $T_{\rm sc}$ of 4 and 8 K, respectively (Yamanaka *et al.*, 1995, 2000). The superconductivity in these compounds based on the covalent sp^3 network has attracted much attention. It was followed by the discovery of superconductivity in diamond (Ekimov *et al.*, 2004) and diamond-structured Si (Bustarret *et al.*, 2006).

False superconductivity in BGG was observed for a polycrystalline sample of $Ba_{7.62}Ga_{17.30}Ge_{28.70}$ (Bryan *et al.*, 1999). Magnetic measurements for the finely ground sample showed a diamagnetic signal below $T_{sc} = 7.5$ K. The diamagnetic signal was approximately 40% of the shielding expected for a perfect diamagnet. An ac resistance measurement on the pelletized sample showed a resistive transition below 4.8 K. The higher T_{sc} in the diamagnetic signal was attributed to surface oxidation and nonstoichiometric surface states in the polycrystalline grains.

Sales *et al.* (2001) carefully examined the superconducting properties using single crystals. The crystal of BGG was grown by slowly cooling molten mixtures of the stoichiometric elements. The crystal with a carrier density $n \simeq 10^{21}$ cm^{-3} provided no evidence of superconductivity down to 2 K in either C_V, ρ, or ac susceptibility. Thus, the superconductivity observed by Bryan *et al.* (1999) may be due to small amounts of impurity phases such as Ga and Ba-Ge alloys with $T_{sc} =$ 1–10 K (Cohen, Abeles, and Weisbarth, 1967; Li and Ross, Jr., 2003; Li *et al.*, 2004).

Good electrical transport and thermoelectric properties have been observed in the type-I clathrates $\mathcal{R}_8Ga_{16}Ge_{30}$ ($\mathcal{R}$ = Ba, Sr, and Eu). The replacement of Ge by Ga produces a charge compensation for the divalent alkaline-earth ion $\mathcal{R}^{2+}$. Adjusting the Ga:Ge ratio can tune the carrier density and improve the thermoelectric power factor S^2/ρ and the dimensionless figure of merit ZT. Electrical transport and thermoelectric properties for single crystals of SGG and β-EGG were examined by Sales *et al.* (2001). Both ρ and S showed metallic behavior because of the heavily doped level of electrons at $n \simeq 10^{21}$ cm^{-3}. The sharp drop in ρ for β-EGG below 35 K is characteristic of the loss of spin disorder scattering due to the long-range magnetic order of the Eu^{2+} magnetic moments. The room-temperature S of -50 μV/K is typical for heavily doped n-type semiconductors; see Fig. 9. The Hall mobility μ_H of the carriers increases with decreasing temperature, which suggests that the scattering of carriers is dominated by acoustic phonons. Woods *et al.* (2006) investigated magnetic and electric properties of type-I $Eu_4Sr_4Ga_{16}Ge_{30}$. They found the ferrromagnetic ordering of these Eu-containing clathrates substantially altered by incorporating Sr compared to β-EGG.

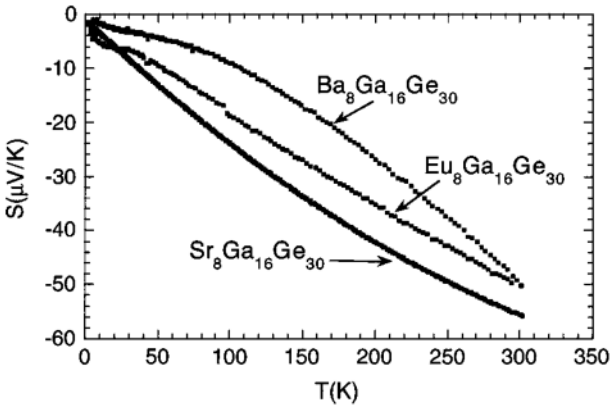

FIG. 9. Temperature dependences of the thermopower S [μV/K] for $\mathcal{R}_8Ga_{16}Ge_{30}$ ($\mathcal{R}$ = Ba, Sr, Eu) single crystals. From Sales *et al.*, 2001.

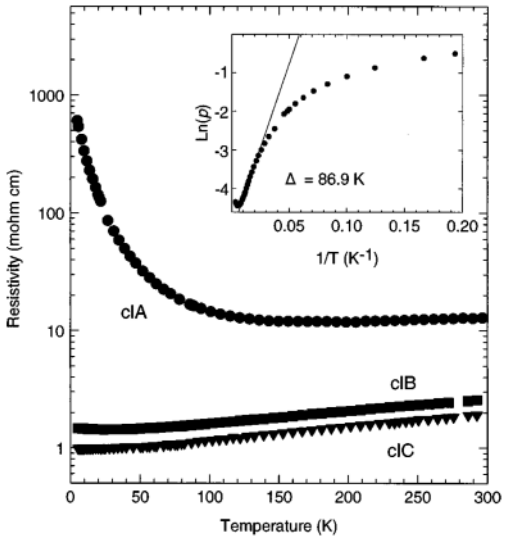

FIG. 10. Temperature dependences of electrical resistivity ρ for $Sr_8Ga_{16}Ge_{30}$ polycrystalline samples with various carrier densities (see text). From Nolas, Cohn *et al.*, 1998.

The thermoelectric properties for hot-pressed polycrystals of SGG were reported by Nolas, Cohn *et al.* (1998) and Nolas (2003). The values of n in the article in 1998 were corrected in the review in 2003. The sample with $n \simeq 10^{19}$ cm^{-3} allowed the measurement of the semiconducting ρ contribution below 100 K, as shown in Fig. 10. The negative S decreases with increasing temperature and reaches a value of -320 μV/K at 300 K, as shown in Fig. 11. The sample with $n \simeq 10^{20}$ cm^{-3} exhibited metallic behaviors in both ρ and S in the temperature range from 5 to 300 K. The thermal conductivity κ is approximately 1 W/K m and the value of ZT reaches 0.25 at 300 K.

The value of the carrier density n in type-I SGG was tuned by adjusting the nominal composition in polycrystalline samples. Fujita *et al.* (2006) prepared the samples by arc melting the elements with the nominal ratio of

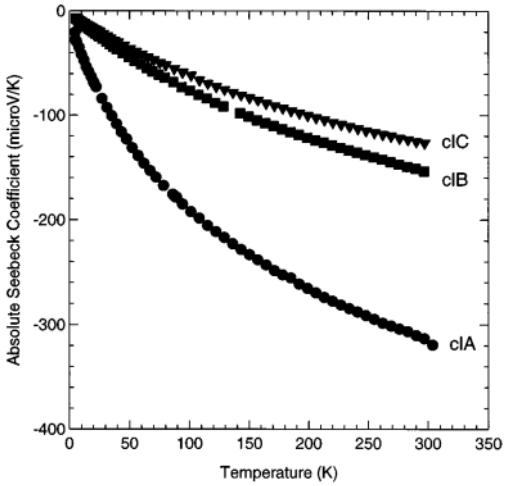

FIG. 11. Temperature dependences of the thermopower S [μV/K] for type-I $Sr_8Ga_{16}Ge_{30}$ polycrystalline samples with various carrier densities (see text). From Nolas, Cohn *et al.*, 1998.

Sr:Ga:Ge $= 8:x:46-x$ ($x = 13$–20). The ingot was powdered and sintered by the spark-plasma-sintering (SPS) technique. With increasing x, the actual Ga composition tended to increase, and the carrier density n decreased from 11.1×10^{20} to 1.8×10^{20} cm^{-3}. The effective mass m_e^* was almost constant at $3.1m_0$, and μ_H was 8–13 cm^2/V s, at room temperature. The electrical conductivity σ and the negative S exhibited metallic behavior from 300 up to 700 K; the metallic behavior turned into an intrinsic semidonducting one above 700–800 K . The tuning of the carrier density n to 5.6×10^{20} cm^{-3} maximized ZT of 0.62 at 800 K.

Wang *et al.* (2009) started with the nominal composition of Sr:Ga:Ge $= 9.6:x:30$ ($x = 18$–23). The ground polycrystalline sample was ultrasonically washed with diluted hydrochloric acid to remove the excess Ga. Dense samples were obtained by sintering the ground samples. The carrier density n decreased from 2.81×10^{20} to 0.33×10^{20} cm^{-3} as the Ga:Ge ratio increased from 0.481 to 0.517. The samples with $n < 10^{20}$ cm^{-3} showed a high S of 350–400 μV/K at 450 K and intrinsic semiconducting behavior above 450 K while those with higher n exhibited a metallic behavior up to 700 K. The value of ZT reached 0.85 at 650 K for the sample with the lowest Ga:Ge ratio of 0.481.

For β-$Eu_8Ga_{16+x}Ge_{30-x}$ (EGG), the carrier density n was controlled by changing the annealing temperature between 823 and 970 K (Bentien *et al.*, 2005; Pacheco *et al.*, 2005). The samples for $-1.01 < x < -0.47$ had n between $0.43e^-$ and $1.53e^-$ per unit cell. All samples showed a metallic behavior in ρ with a hump around 35 K attributable to the ferromagnetic transition. S exhibited metallic behavior and reached $-(75$–$160)$ μV/K at 400 K.

For SGG and β-EGG, no p-type conduction has been observed yet. In contrast, the carrier types and density have been tuned in BGG (Anno *et al.*, 2002, 2003; Avila, Suekuni, Umeo, and Takabatake, 2006; Avila, Suekuni, Umeo, Fukuoka *et al.*, 2006; Cederkrantz *et al.*, 2009; Tang *et al.*, 2010). Anno *et al.* (2002) tuned the carrier type by adjusting the initial composition of Ba:Ga:Ge$=8:x:46-x$($x=12$–20). Polycrystalline samples were synthesized by arc melting and SPS. The carrier type changed from n type ($x = 12$–16) to p type ($x = 17$–20), which was confirmed by the change in the signs of S and R_H. The thermoelectric power factor S^2/ρ at high temperatures had a maximum of 22 μW/K^2 cm at $x = 14$ for n type and that of 15 μW/K^2 cm at $x = 19$ for p type; see Fig. 12. κ was less than 2.5 W/Km. The estimated ZT value for n type ($x = 15$) and p type ($x = 18$) reached approximately 1.0 at 900 K. The tunable carrier type in BGG is advantageous for constructing a thermoelectric module using p-type and n-type legs.

Martin *et al.* (2006, 2007) performed transport experiments on polycrystalline Si-Ge type-I clathrates with the nominal composition $Ba_8Ga_{16}Si_xGe_{30-x}$ such that a constant ratio of Ga to group-IV element is maintained but with increasing Si substitution $4 < x < 14$. Electrical transport measurements on n-type specimens show a modest increase in the absolute Seebeck coefficient and a decrease in electrical resistivity with increasing Si content. Substitution of 20 at.% Si within the Ga-Ge lattice framework of the type-I clathrate BGG results in thermoelectric performance

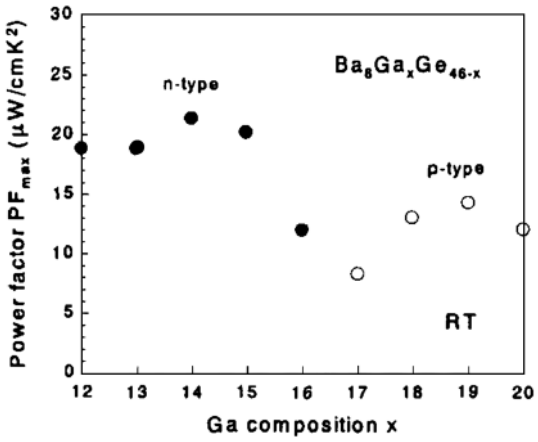

FIG. 12. Thermoelectric power factor at room temperature as a function of Ga composition x for n-type and p-type $Ba_8Ga_xGe_{46-x}$ polycrystalline samples. Adapted from Anno *et al.*, 2002.

enhancement. They interpreted these observations as a modification in the band structure with Si substitution. The band modification has been confirmed by the x-ray absorption fine-structure (XAFS) spectroscopy study by Mansour *et al.* (2012).

Martin, Wang, and Nolas (2008) identified the optimal carrier density n for n-type BGG. A polycrystalline sample with $n = 9.86 \times 10^{20}$ cm^{-3} exhibited high $ZT = 0.8$ at 953 K. The ZT value was comparable to the values for n-type BGG reported by Kuznetsov *et al.* (2000) ($ZT = 0.7$ for a polycrystalline sample at 700 K), by Christensen, Snyder, and Iversen (2006) ($ZT = 0.9$ for a Czochralski-grown single crystal at 1000 K) by Toberer *et al.* (2008) ($ZT = 0.8$ for a flux-grown single crystal and $ZT = 0.74$ for a polycrystalline sample at 1000 K), and by Hou *et al.* (2009) ($ZT \sim 0.8$ for a Czochralski-grown crystal at 850 K). The highest ZT of 1.35 at 900 K was reported for an n-type crystal synthesized by the Czochralski method (Saramat *et al.*, 2006), but it has not been confirmed.

We mention the band calculations and x-ray photoemission spectroscopy studies on $\mathcal{R}_8M_{16}Z_{30}$ ($\mathcal{R}$ = Sr, Ba) (Blake *et al.*, 2001; Madsen *et al.*, 2003; Nenghabi and Myles, 2008a, 2008b; Tang *et al.*, 2009, 2011; Kono *et al.*, 2010). Madsen *et al.* (2003) pointed out that undoped SGG and BGG are semiconductors with band gaps of 0.71 and 0.89 eV, respectively. Tang *et al.* (2009) revealed that the valence band is constructed mainly from the Ga and Ge 4s and 4p wave functions with little contribution of the Sr and Ba atomic orbitals. However, the conduction band hybridizes with the unoccupied d states of the guest atom. These results indicate that electrical transport and thermoelectric properties of the n-type sample are expected to depend strongly on the guest atom while those of p-type clathrate compounds are relatively unaffected. Kono *et al.* (2010) calculated the electronic structures and the thermoelectric properties for type-I and type-VIII $Ba_8Ga_{16}Sn_{30}$ (β-BGS and α-BGS). The calculation showed that these compounds are indirect semiconductors with band gaps of 0.51 and 0.32 eV, respectively. The Seebeck coefficient of n-type β-BGS is higher than that of n-type α-BGS.

B. Phonon thermal conductivity

As mentioned in Sec. III, ternary type-I clathrates have received much attention as potential high-performance thermoelectric materials because of not only the good electronic properties but also the low κ_{ph} of $\simeq 1$ W/Km. Nolas, Cohn *et al.* (1998) and Nolas, Slack *et al.* (1998) reported glasslike temperature dependences of κ_{ph} for SGG polycrystalline samples. It was then regarded as satisfying the true PGEC concept. The nature of the THz-frequency vibrational states in structural glasses has been the subject of an intensive and controversial debate for decades. This is due to the difficulty in identifying the microscopic structure of glasses. The microscopic structures of clathrate compounds are well defined, and this makes it possible to interpret the origin of glasslike thermal and dynamic properties generally observed in type-I clathrates containing off-center guest atoms.

Nolas, Slack *et al.* (1998) and Cohn *et al.* (1999) investigated the temperature dependence of κ_{ph} down to 60 mK for a SGG polycrystalline sample. κ_{ph} varies as T^2 below 1 K and has a plateau around 10 K, which is quite similar to the behavior of vitreous SiO_2 in its temperature dependence in addition to its magnitude, as shown in Fig. 13. The glasslike plateau in $\kappa_{ph}(T)$ has also been observed for a single crystal of SGG. However, BGG showed a crystalline peak due to the umklapp process (Keppens *et al.*, 2000), which indicates the existence of translational symmetry in the sample. We mention that the plateau in $\kappa_{ph}(T)$ was observed in gas hydrates in the same temperature region (Krivchikov *et al.*, 2005; English and Tse, 2010).

Sales *et al.* (2001) reported a temperature dependence of heat transport for BGG, SGG, and β-EGG using single crystals with *n*-type carriers. The crystals were grown by slowly cooling molten stoichiometric mixtures of the elements. For SGG and β-EGG crystals, κ_{ph} exhibits a glasslike plateau in the temperature range 10–20 K; see Fig. 14. The room-temperature values of κ_{ph} for SGG and β-EGG are 1.0 and 0.6 W/Km, respectively. In contrast, κ_{ph} for BGG shows a typical crystalline umklapp peak at around 10 K.

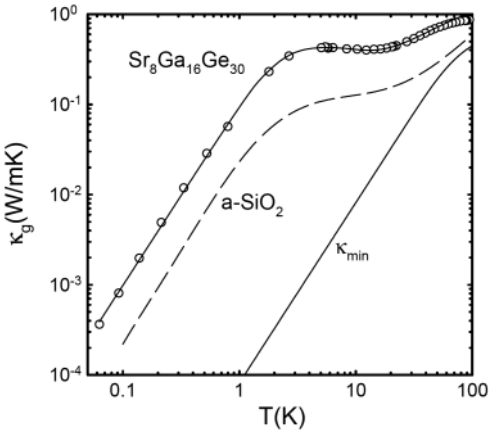

FIG. 13. Temperature dependences of phonon thermal conductivity κ_{ph} for polycrystalline samples of type-I $Sr_8Ga_{16}Ge_{30}$. The dashed line represents κ_{ph} for vitreous SiO_2. From Cohn *et al.*, 1999.

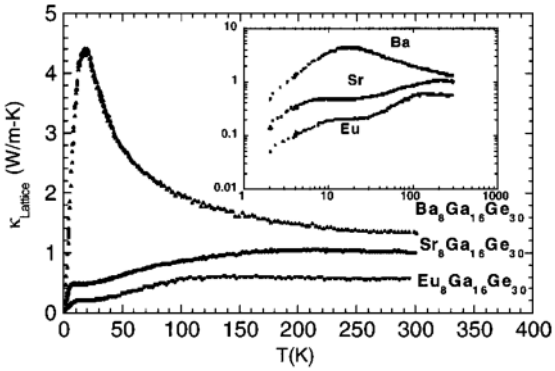

FIG. 14. Temperature dependences of phonon thermal conductivity $\kappa_{ph}(T)$ for type-I $\mathcal{R}_8Ga_{16}Ge_{30}$ ($\mathcal{R}$ = Ba, Sr, Eu) single crystals. Adapted from Sales *et al.*, 2001.

Nevertheless, the room-temperature κ_{ph} value is no more than 1.3 W/Km.

The data for κ_{ph} on type-I (β phase) and type-VIII (α phase) EGG by Paschen *et al.* (2001) are given in Fig. 15. In contrast to the plateau for the β-EGG sample, the crystalline umklapp peak was observed around 5 K for a type-VIII sample. Type-I and type-VIII samples of EGG possess magnetic moments realizing ferromagnetic orderings at 36 and 10.5 K, respectively.

Martin *et al.* (2006, 2007) reported on the temperature dependence of $\kappa_{ph}(T)$ of polycrystalline Si-Ge type-I clathrates with nominal composition of $Ba_8Ga_{16}Si_xGe_{30-x}$ in the temperature range 10–400 K with increasing Si substitution $4 < x < 14$.

Suekuni *et al.* (2007) reported the variations of κ_{ph} in type-I $Sr_8Ga_{16}Si_{30-x}Ge_x$ ($0 \le x \le 30$) (SGSG) of single crystals. In this alloy series, the cage size is enlarged by the substitution of Ge for Si. The cage size expands by 8% and the guest vibrational energy decreases as x increases from 0 to 30. Thereby, the height of the peak in κ_{ph} at around 10–20 K is reduced and the temperature dependence of $\kappa_{ph}(T)$ changed from crystal-like to glasslike as illustrated in Fig. 16. The drastic reduction in κ_{ph} suggests a strong interaction between acoustic phonons of cages and vibrational modes of Sr guests.

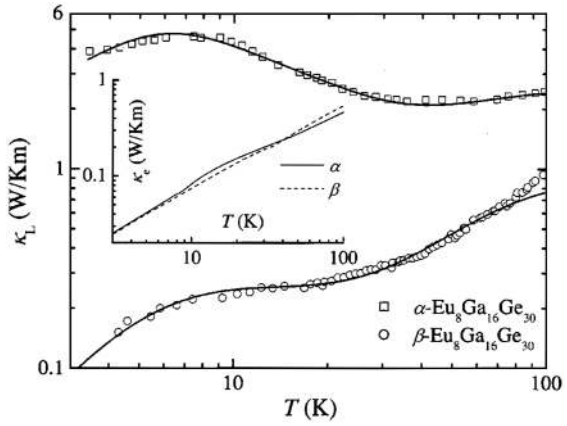

FIG. 15. Temperature dependences of phonon thermal conductivity κ_{ph} for type-I and type-VIII $Eu_8Ga_{16}Ge_{30}$ polycrystalline samples. From Paschen *et al.*, 2001.

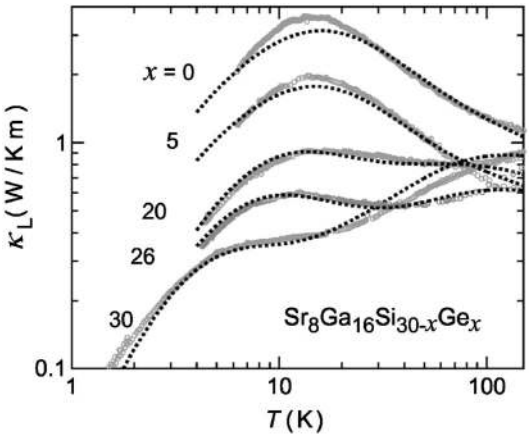

FIG. 16. Temperature dependences of phonon thermal conductivity $\kappa_{ph}(T)$ vs T on a log-log scale for type-I $Sr_8Ga_{16}Si_{30-x}Ge_x$ single crystals. From Suekuni *et al.*, 2007.

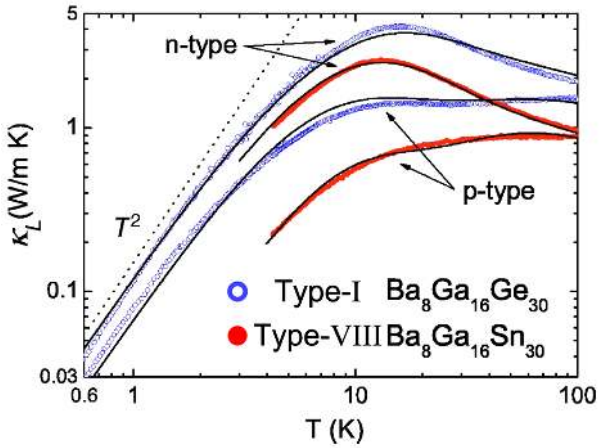

FIG. 17. (color online). Temperature dependences of phonon thermal conductivity κ_{ph} for n-type and p-type $Ba_8Ga_{16}Ge_{30}$ and type-VIII $Ba_8Ga_{16}Sn_{30}$ single crystals on a log-log scale. From Avila, Suekuni, Umeo, Fukuoka *et al.*, 2006.

A detailed theoretical interpretation of the above is given in Sec. VII. $\kappa_{ph}(T)$ for $x = 30$ varies as $T^{2-\delta}$ with a small factor of $\delta < 1$ below 1 K (Umeo *et al.*, 2005), which confirms the data for the polycrystalline samples (Cohn *et al.*, 1999).

Some data for the thermal conductivity in polycrystalline SGG samples displayed crystal-like peaks at 4–10 K (Uher, Yang, and Hu, 1998). These peaks may be due to metallic impurities. The samples were synthesized in a quartz tube or in a pyrolytic boron nitride (pBN) crucible placed inside a quartz tube, which were referred to as as-grown samples. The sample synthesized in the pBN crucible was then crushed and sintered in a carbon die. For the as-grown samples, κ_{ph} shows crystalline behavior: $\kappa_{ph} \propto 1/T$ and a large peak at around 4–10 K. On the other hand, for the sintered sample, κ_{ph} shows a glasslike temperature dependence. Despite the similar value of the carrier density $n = 10^{21}$ cm^{-3}, the behaviors of ρ and S seem to strongly depend on the crucible material. For samples synthesized in the quartz tube, ρ decreases to zero at liquid-helium temperatures. This is totally different from the data for single crystals with a similar carrier density of 10^{21} cm^{-3} (Sales *et al.*, 2001). The quite low ρ can be ascribed to the presence of highly conducting metallic impurities, e.g., gallium. In fact, the S goes to zero at low temperatures, which is a result of a short circuit. Therefore, the crystal-like behavior in κ reported for some SGG polycrystalline samples is not intrinsic but is attributable to the metallic impurities.

For type-I BGG, a large difference in $\kappa_{ph}(T)$ between the n-type and p-type samples was reported by different groups (Bentien *et al.*, 2004; Avila, Suekuni, Umeo, and Takabatake, 2006; Avila, Suekuni, Umeo, Fukuoka *et al.*, 2006; Tang *et al.*, 2009). The single crystals were synthesized by the flux method using excess Ga. Avila, Suekuni, Umeo, and Takabatake (2006) and Avila, Suekuni, Umeo, Fukuoka *et al.* (2006) grew crystals with both p-type and n-type carriers from nominal compositions of Ba:Ga:Ge = 8:38:x, where $x = 30$ for p-type and $x = 34$ for n-type carriers. κ_{ph} for the n-type samples showed a typical crystalline peak at 15 K, which is totally suppressed for p-type samples, as shown in Fig. 17. κ_{ph} below 1 K for the p-type single crystal follows $\sim T^2$ (Avila, Suekuni, Umeo, Fukuoka *et al.*, 2006) or $\sim T^{1.5}$ (Bentien, Johnsen, and Iversen, 2006); that for n type follows $\sim T^2$ (Avila, Suekuni, Umeo, Fukuoka *et al.*, 2006). However, no difference was observed in either the crystal structure or the specific heat $C_V(T \gtrsim 4$ K) for these compounds. A similar difference in κ_{ph} between p-type and n-type samples was observed also in type-I $Ba_8Ni_{6-x}Ge_{40-x}$, $Ba_8Au_xSi_{46-x}$, and type-VIII $Ba_8Ga_{16}Sn_{30}$ (Avila, Suekuni, Umeo, Fukuoka *et al.*, 2006; Bentien, Johnsen, and Iversen, 2006; Aydemir *et al.*, 2011).

The Ba guest in type-I $Ba_8Ga_{16}Sn_{30}$ (β-BGS) has larger off-center displacement and lower guest vibration energy than those of BGG (Avila *et al.*, 2008; Suekuni, Avila *et al.*, 2008). The carrier types of β-BGS are tunable as in BGG. κ_{ph} varies as $T^{2-\delta}$ below 1 K and exhibits a plateau around 4 K irrespective of the carrier type; see Fig. 18. The value of κ_{ph} below 10 K is the lowest among intermetallic clathrates. Because of the glasslike κ_{ph} and the boson-peak-like structure in the specific heat C_V, β-BGS is regarded as a true phonon-glass material.

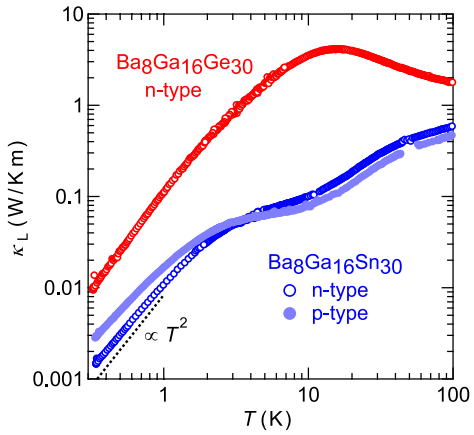

FIG. 18. (color online). Temperature dependences of phonon thermal conductivity $\kappa_{ph}(T)$ of n-type and p-type type-I $Ba_8Ga_{16}Ge_{30}$ and $Ba_8Ga_{16}Sn_{30}$ single crystals on a log-log scale. From Avila, Suekuni, Umeo, Fukuoka *et al.*, 2006, Avila *et al.*, 2008, and Suekuni, Avila *et al.*, 2008.

VI. SPECTROSCOPIES IN THE TERAHERTZ-FREQUENCY REGION

The excess densities of states realized as a hump in specific heats at around 10 K for type-I clathrate compounds have also been observed by various types of spectroscopy such as Raman scattering, infrared absorption, and inelastic neutron scattering measurements. This section describes these observations in detail.

A. Optical spectroscopies

1. Raman spectra and assignments

The reflected light from crystals yields small shifts in initial frequency. This shift is called the Raman shift or scattering, which enables us to investigate characteristic frequencies relevant to optical phonons in the vicinity of the Γ point ($\boldsymbol{q} = \boldsymbol{0}$) in the Brillouin zone. This is due to the fact that the wave vector $\boldsymbol{k}$ of photons is negligibly small compared to that $\boldsymbol{q}$ of an optical phonon. It is known that Raman spectroscopy is a powerful method to access the dynamics relevant to the excess density of states.

Krishnan (1953) found during his Raman scattering experiments on silica glass a broad band in the vicinity of 30–120 cm^{-1}, which markedly differs from the behavior of crystal quartz. Note that 1 THz = 33.35 cm^{-1}. This band has its maximum intensity at the low-frequency end and the intensity falls off continuously. The broad and intense band has also been observed in various types of amorphous materials or structural glasses by Raman scattering, inelastic neutron scattering, and infrared absorption. Note that Helen *et al.* (2000) performed hyper-Raman scattering experiments to investigate the broadband in the THz region in silica glass. The relevant mode obtained by hyper-Raman scattering principally involves rotational motion of SiO_4 tetrahedra. This mode corresponds to the mode suggested by Buchenau, Nücker, and Dianoux (1984) and Buchenau *et al.* 1986)) from analysis of their inelastic neutron scattering data.

Type-I clathrates have three distinct cage sites 6*c*, 16*i*, and 24*k*. The guest (1) occupies the 2*a* sites in the dodecahedra, and the guest (2) occupies the 6*d* sites in the tetrakaidecahedra. There are 54 atoms per unit cell and thus 162 (3×54) phonon modes at the Γ point. Group theory of lattice vibrations for type-I clathrates with a cubic primitive structure $Pm\bar{3}n$ indicates the number of Raman-active vibrational modes $3A_{1g} + 7E_g + 8T_{2g}$ relevant to the cage atoms. The group theory also ensures the existence of two guest (2) modes E_g and T_{2g} under the assumption that the guest (2) occupies the on-center 6*d* site. Because the vibrations of the guest (1) at the 2*a* site are not Raman active, all observed guest modes are attributed to the guest (2) atoms.

Raman scattering from a polycrystalline sample provides all active modes. The study of β-$\mathcal{R}_8Ga_{16}Ge_{30}$ ($\mathcal{R}$ = Sr and Eu) provided assignments of the guest (2) and cage modes (Nolas and Kendziora, 2000). However, they were unable to identify all of the modes due to the numerous Raman-active modes.

Takasu *et al.* (2006) gave full assignments to the Raman-active modes observed for type-I $\mathcal{R}_8Ga_{16}Ge_{30}$ ($\mathcal{R}$ = Ba, Sr, and Eu) by combining polarized Raman scattering measurements on single crystals with first-principles calculations. The vibrational modes in each irreducible representation have been determined by polarization dependence measurements. The polarization geometry is represented by the notation (α, β), where α and β denote the polarization directions of incident and scattered light, respectively. Three geometries, (x, x), (x, y), and $(x + y, x - y)$, were employed, where x and y correspond to the [100] and [010] crystal axes, respectively. The phonon with A_{1g} symmetry appears in (x, x), E_g in both (x, x) and $(x + y, x - y)$, and T_{2g} in (x, y). The A_{1g} spectra were obtained by subtracting the E_g spectra from the $A_{1g} + E_g$.

The Raman spectra of the $A_{1g} + E_g$, E_g, and T_{2g} modes are shown in Fig. 19 for the three compounds at room temperature (Takasu *et al.*, 2006). The modes above 70 cm^{-1} are fully assigned as cage modes in comparison with the energies obtained by experiments and calculations. For $\mathcal{R}$ = Ba, the $E_g(1)$ mode at 64 cm^{-1} and $T_{2g}(1)$ mode at 34 cm^{-1}, marked by G in Fig. 19, are assigned to the modes for Ba(2). The $E_g(1)$ mode concerns guest vibrations along the fourfold axis; and the $T_{2g}(1)$ concerns the vibrations in the plane perpendicular to the fourfold axis and along the [100] axis. The modes for Sr(2) and Eu(2) have been assigned by

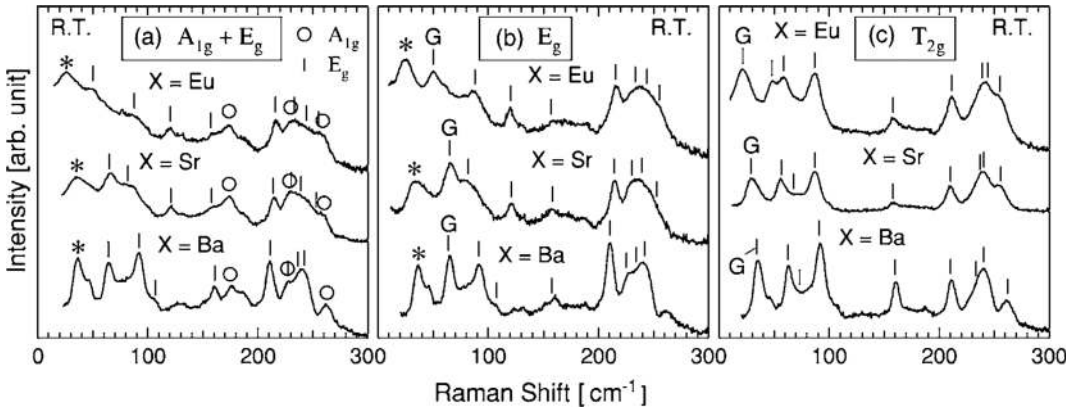

FIG. 19. Polarization dependence of Raman spectra for type-I $\mathcal{R}_8Ga_{16}Ge_{30}$ ($\mathcal{R}$ = Ba, Sr, Eu) at room temperature. "G" are the symmetry-allowed Raman-active phonons, and the bars and open circles denote the assigned peak. The peaks marked by ∗ are additional modes. From Takasu *et al.*, 2006.

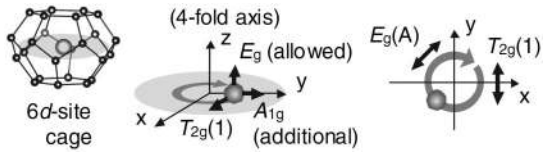

FIG. 20. Illustration of fundamental modes of the guest atom $\mathcal{R}(2)$. See the text for the notations for the additional A_{1g}, E_g(A), and $T_{2g}(1)$ modes. Adapted from Takasu *et al.*, 2008.

comparing the analogous spectral shape between $\mathcal{R}$ = Ba, Sr, and Eu. The energy of the $T_{2g}(1)$ mode at room temperature decreased on going from Ba(2) (34 cm^{-1}), to Sr(2) (30 cm^{-1}), and to Eu(2) (21 cm^{-1}). The energies for Ba(2) and Sr(2) agreed with those obtained from the analysis of specific-heat data (Avila, Suekuni, Umeo, Fukuoka *et al.*, 2006; Suekuni *et al.*, 2007).

Besides the assigned peaks, there are two additional modes, marked by asterisks in Fig. 19, in the low-energy regions of the $A_{1g} + E_g$ and E_g spectra (Takasu *et al.*, 2006). Particularly for $\mathcal{R}$ = Eu, subtraction of the E_g from the $A_{1g} + E_g$ spectra allowed us to assign the additional modes to one A_{1g} and one E_g mode. These modes were identified as the vibrations of the guest (2).

Neutron diffraction experiments have provided evidence that the nuclear density of the guest atom Eu(2) departs from the 6*d* site at the cage center to one of four off-center 24*k* sites along the [1,0,0] direction (Chakoumakos, Sales, and Mandrus, 2001; Sales *et al.*, 2001). This deviation lowers the site symmetry from $4\bar{2}m$ (6*d*) to *m* (24*k*). The lowered symmetry does not affect the $E_g(1)$ and $T_{2g}(1)$ modes, but the displacement along the [1,0,0] direction, corresponding to the A_{1g}(A) mode, becomes Raman active, as shown in Fig. 20, in which the arrows provide the relative displacements between cage and guest atom (Takasu *et al.*, 2008). The additional E_g(A) mode has been identified as the tangential fluctuation to [1,1,0]. Thus, the vibrations of the guest (2) have been described as rotational or librational modes, together with an additional A_{1g} mode.

2. Temperature, carrier-type, and pressure dependences of Raman spectra

The temperature dependences of the Raman spectra for the guest atom $\mathcal{R}$ = Eu are shown in Figs. 21 and 22 (Takasu *et al.*, 2006, 2007). The modes related to cages show no anomalous dependence on cooling from 500 to 2 K, in which temperature range their energy increases due to the thermal shrinkage effect. This is the same tendency for $\mathcal{R}$ = Ba and Sr. However, it should be emphasized that the vibrational energies of the $T_{2g}(1)$ and E_g(A) modes on the guest (2) *decrease* upon cooling. This anomalous softening can be primarily explained by the anharmonic potential such as $V(u) = k_2 u^2/2 + k_4 u^4/4$, from which the mode frequency ω can be expressed by $\omega^2 = \omega_0^2 + k_4\langle u^2\rangle/2m$ taking the thermal average of the anharmonic term, where ω_0 is the eigenfrequency of the harmonic term, k_4 is the coefficient of the quartic anharmonic potential, *m* is the mass of guest atom, and $\langle u^2\rangle \propto T$ is the mean-square atomic displacement of the guest (2), respectively. The quantity $\langle u^2\rangle$ explains the temperature dependence of ω^2 and Raman spectra relevant to the guest (2) upon cooling. More details will be discussed in Sec. VII.A.

For $\mathcal{R}$ = Ba, the energy of $T_{2g}(1)$ coincides with that of E_g(A) at temperatures between 300 and 2 K, as shown in Fig. 22 (Takasu *et al.*, 2006). For $\mathcal{R}$ = Sr and Eu, the energy of $T_{2g}(1)$ is lower than that of E_g(A) at 300 K. This means that the potential minima are located toward the [100] direction which points from the high-symmetry 6*d* site to the off-center 24*k* sites.

Vibrational properties of the pseudoternary systems $\mathcal{R}_8Ga_{16}Si_{30-x}Ge_x$ ($\mathcal{R}$ = Ba and Sr) have also been investigated in terms of the Raman spectroscopy (Takasu *et al.*, 2008). The vibrational energies of the guest (2) clearly decreased with increasing Ge content *x* and cage size. For Ba samples of the end compositions $x = 0$ and $x = 30$ and the Sr compound with $x = 0$, the energy difference between $T_{2g}(1)$ and E_g(A) was small, indicating an isotropic potential at the guest (2) site for these samples. For the Sr samples with $x = 20$ and $x = 30$, the difference becomes larger with increasing cage size, and thereby the energy of the $T_{2g}(1)$

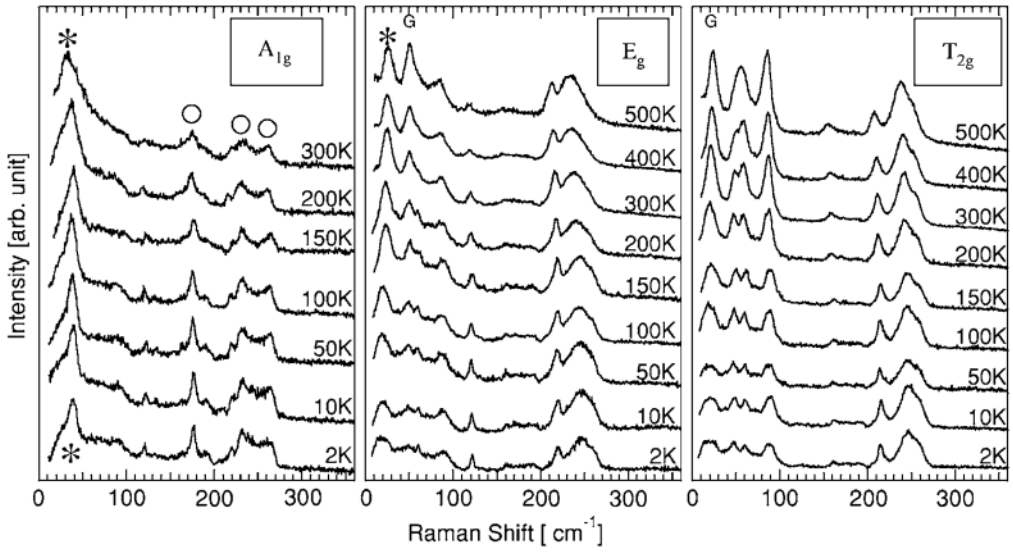

FIG. 21. Temperature dependences of Raman spectra for type-I $Eu_8Ga_{16}Ge_{30}$. From Takasu *et al.*, 2006.

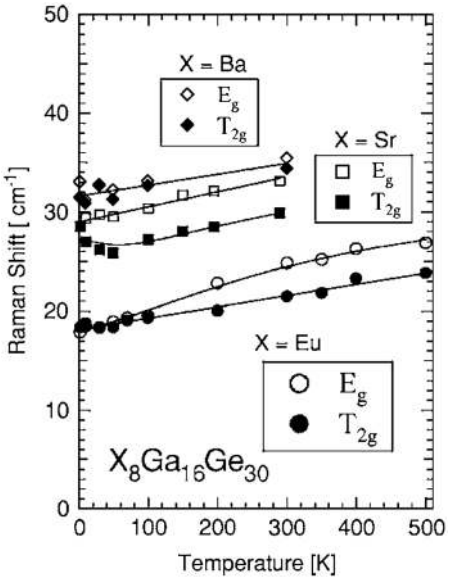

FIG. 22. Temperature dependences of mode energies of guest atoms, $T_{2g}(1)$ and $E_g(\mathrm{A})$, for type-I $\mathcal{R}_8Ga_{16}Ge_{30}$ ($\mathcal{R}$ = Ba, Sr, Eu). From Takasu *et al.*, 2006.

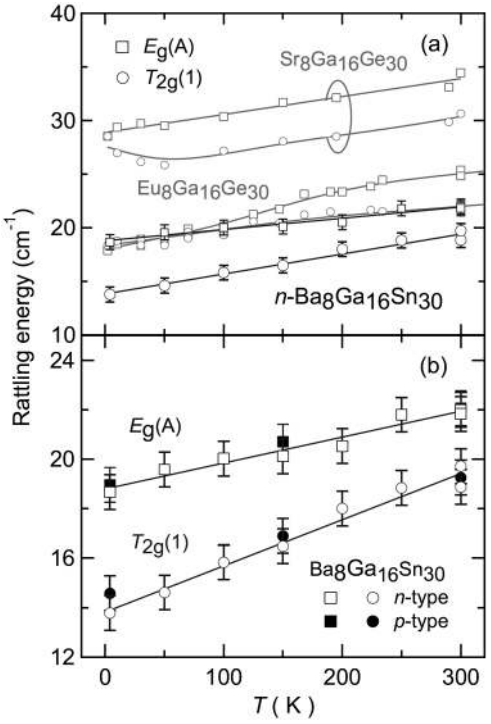

FIG. 23. Temperature dependences of the mode energies $T_{2g}(1)$ and $E_g(\mathrm{A})$ for n-type and p-type type-I $Ba_8Ga_{16}Sn_{30}$ and $\mathcal{R}_8Ga_{16}Ge_{30}$ ($\mathcal{R}$ = Sr, Eu). Adapted from Takasu *et al.*, 2006, and Suekuni *et al.*, 2010.

mode was lower than that of $E_g(\mathrm{A})$. The results indicate that potential anisotropy for Sr(2) between the [100] and [110] directions emerges with increasing the cage size.

Compared with BGG, type-I $Ba_8Ga_{16}Sn_{30}$ has a larger cage, which results in a larger off-center deviation of Ba(2). The energy of $T_{2g}(1)$ is lower than that of $E_g(\mathrm{A})$ at temperatures between 300 and 4 K (Suekuni *et al.*, 2010), indicating the strong anisotropy of the potential at the Ba(2) site. The energy of $T_{2g}(1)$ at 4 K in Fig. 23 is 14 cm^{-1}, which is lower than that in $\mathcal{R}_8Ga_{16}Ge_{30}$ for $\mathcal{R}$ = Ba (31 cm^{-1}), Sr (29 cm^{-1}), and Eu (18 cm^{-1}).

For BGG, the carrier-type (n-type and p-type) dependences of Raman spectra were studied by Takasu *et al.* (2010). They observed the additional $E_g(\mathrm{A})$ mode independent of carrier types. For both n and p types, the decrease in the energies of $T_{2g}(1)$ and $E_g(\mathrm{A})$ modes upon cooling provides information concerning the anharmonic potential for the guest Ba(2). The energy difference between $T_{2g}(1)$ and $E_g(\mathrm{A})$ was larger in the p-type sample, and the energy of $T_{2g}(1)$ was clearly lower than that of $E_g(\mathrm{A})$. Therefore, the potential anisotropy at the Ba(2) site is stronger in the p-type sample. Furthermore, it was clarified that the potential energy difference between the [100] and [110] directions is proportional to the off-center deviation of the guest (2) from the cage center in a series of type-I clathrates. The Raman intensity of cage vibrations at the 6c site for the p type is weaker than that for the n type, indicating that the vibration amplitude at the 6c site is smaller in the case of p type. These experimental findings suggest that the 6c site in the p type provides the guests with a larger space.

Raman scattering experiments under high pressure provided important information on the structural stability of type-I clathrate compounds (Shimizu *et al.*, 2009, 2009; Kume *et al.*, 2010). The phase transition and the vibrational properties of BGG have been investigated at pressures up to 40 GPa at room temperature by Kume *et al.* (2010). They demonstrated the occurrence of a first-order phase transition at 33 GPa by combining Raman scattering and synchrotron x-ray powder diffraction experiments at high pressures. The Raman spectra showed anomalies at around 17 GPa. They investigated the shift of vibrational frequency of the guest Ba as a function of the cage size. The results indicated a linear relation between the vibrational frequency and the cage size.

The deviation of nearest-neighboring Ba(2) atoms creates electric dipole fields (Takasu *et al.*, 2010). The T_{1u} and T_{2g} modes are correlated with the motion of the neighboring Ba(2) guests, and the corresponding dipole moment lies along its direction. The dipole fields of the T_{1u} and T_{2g} modes are directed opposite. In fact, the dipole interaction yields the energy shift: the energy of T_{1u} is larger by about 6 cm^{-1} than that of T_{2g}, indicating the existence of interacting dipoles between the neighboring terakaidecahedra.

3. Infrared spectroscopy in the terahertz-frequency range

Terahertz-frequency spectroscopy plays an important role in the investigation of the characteristics of vibrational modes not accessible by other optical spectroscopies such as Raman scattering. For this method, input and propagated electromagnetic pulse shapes are measured. Fourier analysis of both pulses enables us to obtain the frequency-dependent absorption and dispersion of the observed spectra. Infrared-active phonon modes can be investigated in terms of this spectroscopy. THz time-domain spectroscopy (THz-TDS) has been successfully adopted for investigating vibrational properties of various kinds of clathrates. Ultrafast laser pulses generate short pulses of broadband THz radiation, which provide both high sensitivity and time-resolved phase information for the

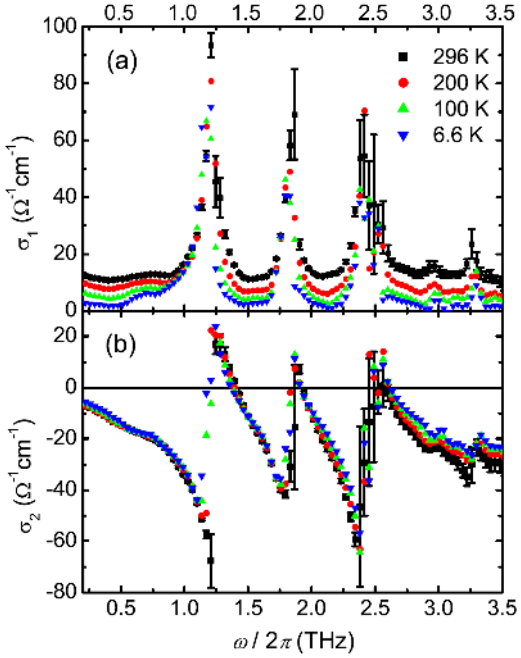

FIG. 24. (color online). Temperature dependences of conductivity $\sigma(\omega) = \sigma_1(\omega) + i\sigma_2(\omega)$ for type-I $Ba_8Ga_{16}Ge_{30}$. From Mori *et al.*, 2009.

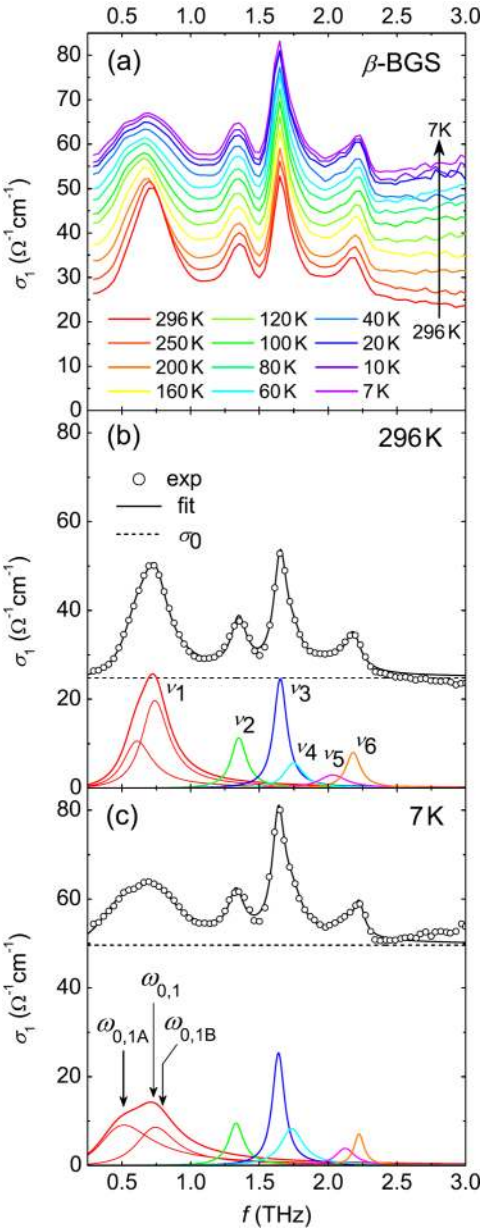

FIG. 25. (color online). (a) Temperature dependences of the real part of the conductivities σ_1 for type-I $Ba_8Ga_{16}Sn_{30}$. (b), (c) Experimental data (open circles) and fitting results (solid lines) at 296 and 7 K, respectively (see text). From Mori *et al.*, 2011.

transmitted THz electric fields. Group theory of the lattice vibrations of type-I clathrates with cubic primitive structure $Pm\bar{3}n$ gives the infrared-active vibrational modes of ten T_{1u} modes for the cage atoms, one T_{1u} mode for the guest (1), and two T_{1u} modes for the guest (2) when the guest (2) occupies the on-center 6*d* site.

THz-TDS studies on *p*-type $Ba_8Ga_{16}Ge_{30}$ single crystals with on-center guest atoms have been performed in the frequency range between 0.2 and 3.5 THz (Mori *et al.*, 2009). As shown in Fig. 24, peaks in conductivity spectra at $\nu_1 = 1.15$ and $\nu_2 = 1.80$ THz are identified with the guest (2) modes. They have assigned these modes as the vibrational mode of Ba(2) in the plane perpendicular to the fourfold axis and that along the [100] axis, respectively. The broad peak around 2.4 THz (ν_3 and ν_4) results from a hybridization between the cage mode and Ba(1) vibrations. Two peaks at higher frequencies are the cage modes.

The energies of ν_1 and ν_2 decrease by 4.2% with decreasing temperature from 300 to 6.6 K. The decrease is attributed to the anharmonic potential at the Ba(2) site, as theoretically discussed in Sec. VII.A. For other modes, however, the mode energies slightly increased with decreasing temperature as a result of the effect of thermal shrinkage. The temperature dependence of each mode was consistent with the results of Raman scattering (Takasu *et al.*, 2006).

The vibrational modes for a type-I $Ba_8Ga_{16}Sn_{30}$ single crystal with off-center guest atoms have been investigated in the frequency range between 0.3 and 3.0 THz (Mori *et al.*, 2011). As shown in Fig. 25, the mode with the lowest energy $\nu_1 = 0.72$ THz at 296 K is assigned as the vibrations relevant to the off-center Ba(2) guest in the plane perpendicular to the fourfold axis. The observed peak was fitted by superposing two Lorentzian curves. The peak energy, defined as the peak position of the superposed curves, decreases by 7% with decreasing temperature down to 100 K, and then *increases* with further decreasing temperature. Such anomalous peak-shape and temperature dependence were not observed for type-I $Ba_8Ga_{16}Ge_{30}$ containing on-center guest atoms. They tried to explain the peak splitting at low temperatures by assuming a one-dimensional double-well potential. The energy levels with quantum numbers $n = 0$ and 1 are quasidegenerate, whereas the $n = 2$ and 3 levels are well separated due to the moderately deep potential well. At sufficiently low temperatures, the optical transitions occur mainly from $n = 0$ to 3 and from $n = 1$ to 2 owing to the parity requirement of the wave functions. As a result, these two transitions result in double peaks. However, significant

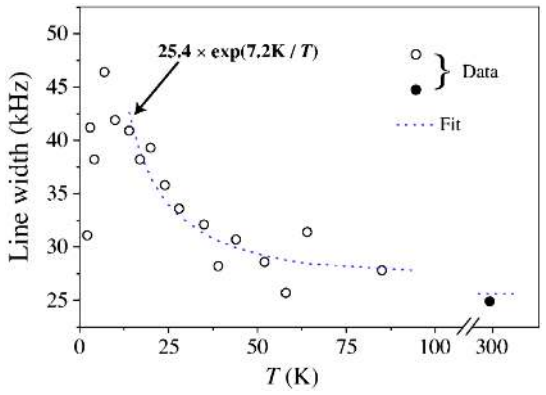

FIG. 26 (color online). ^{71}Ga NMR linewidth (square root of the second moment) vs temperature for type-I $Sr_8Ga_{16}Ge_{30}$. Adapted from Gou *et al.*, 2005.

broadening of the spectra for the guest (2) toward low temperature was not reproduced by assuming this type of one-dimensional potential. The mechanism of this broadening at low temperatures is discussed in Sec. VII.C.2.

A nuclear magnetic resonance (NMR) study provides important information on the motion of encaged guest atoms depending on temperature. Gou *et al.* (2005) performed NMR studies for $Sr_8Ga_{16}Ge_{30}$ which is in the category of an off-center system. They measured ^{71}Ga NMR down to 1.9 K. The values of the Knight shift and T_1 showed low-density metallic behavior. There is a significant increase in the linewidth above 4 K attributed to atomic motion, as shown in Fig. 26. They estimated the relevant time scale of roughly $\tau \sim 10^{-5}$ s from the inverse of the linewidth. From the time scale of the narrowing of the NMR line, they concluded that the reduced high-temperature width is due to motional narrowing. The point is that this is very slow compared with relevant vibrational frequencies of $\omega_{\rm ph}/2\pi \simeq 1$ THz, and the relation $\omega_{\rm ph}\tau \gg 1$ holds. This indicates very slow hopping rates of Sr atoms between sites within the same cage. Another point is that the motion of guest atoms can be treated as vibrational.

Arcon *et al.* (2013) performed ^{71}Ga NMR experiments on type-I SGG and BGG in order to extract the contributions from different Ga sites at randomly occupied Ga/Ge sites. They claimed that the effect of weak covalent bonding should be taken into account in addition to ionic interactions.

B. Inelastic neutron scattering

Time-of-flight inelastic neutron scattering (INS) is a powerful technique for the investigation of vibrational states in clathrate compounds. In INS experiments, the energy $\hbar\omega$ and wavelength λ of incident neutrons can be taken as comparable to those of excited phonon energies and the length scale of lattice spacing, respectively. From this wavelength-energy relation, INS experiments have been proven to be unique for the study of the dynamic properties of materials on the atomic scale (Squires, 1978; Lovesey, 1984).

The quantity obtained by INS experiments is the dynamic structure factor $S(\boldsymbol{Q},\omega)$, which provides information projected onto plane-wave states since it is defined through the spatiotemporal Fourier transformation. When one projects exact eigenstates onto plane-wave states, a lifetime is obtained in frequency or wave vector space, where the width arises from what a plane wave experiences. Thus, it is necessary to take into account this point for the interpretation of the energy width of local modes associated with $\mathcal{R}(2)$ guest atoms in cages.

1. Dynamic structure factor and the flat dispersion relation of phonons

Vibrational dynamics in the THz-frequency range is the most important aspect for clarifying the glasslike phonon thermal conductivity $\kappa_{\rm ph}(T)$ in type-I clathrate compounds, because the upper limits of frequencies of acoustic branches appear in this frequency range. The THz-frequency dynamics concerns the lowest two bands: the acoustic and the lowest optical modes originating from networked cages and $\mathcal{R}(2)$ guest atoms.

The deformed vibrations of cages themselves manifest higher-energy states than those in the THz-frequency region. For this reason, it is sufficient to treat the rigid cage as having a mass M and an effective charge $-e_C^*$, and the $\mathcal{R}(2)$ guest atom as having mass m and charge e_G^*. We define the position vector of the ℓth cage at time t as $\boldsymbol{R}_\ell + \boldsymbol{r}_\ell(t)$, where $\boldsymbol{R}_\ell$ is the equilibrium position of the ℓth cage center. The vector $\boldsymbol{r}_\ell(t)$ represents a small deviation from $\boldsymbol{R}_\ell$. The position of the $\mathcal{R}(2)$ guest atom from the center of the ℓth cage $\boldsymbol{R}_\ell$ is defined by the vector $\boldsymbol{U}_\ell + \boldsymbol{u}_\ell(t)$, where $\boldsymbol{U}_\ell$ is the equilibrium position of the $\mathcal{R}(2)$ guest atom with respect to $\boldsymbol{R}_\ell$, and $\boldsymbol{u}_\ell(t)$ is a small deviation from $\boldsymbol{U}_\ell$ at time t. Note that $\boldsymbol{U}_\ell \neq 0$ corresponds to the case of an *off-center* guest atom, while the *on-center* case becomes $\boldsymbol{U}_\ell = 0$. Figure 27 gives the definitions of the vectors $\boldsymbol{R}$, $\boldsymbol{r}_\ell(t)$, $\boldsymbol{U}_\ell$, and $\boldsymbol{u}_\ell(t)$.

The dynamic structure factor $S(\boldsymbol{Q},\omega)$ is proportional to the spatiotemporal Fourier transform of the density-density correlation function defined by

$$G(|\boldsymbol{r}-\boldsymbol{r}'|,t) = \langle \rho(\boldsymbol{r},t)\rho(\boldsymbol{r}',0)\rangle, \tag{31}$$

where $\rho(\boldsymbol{r},t)$ is the atomic number density at time t, and the angular brackets denote an ensemble average at an equilibrium state. The variation of the atomic number density, e.g., induced by vibrations of the $\mathcal{R}(2)$ guest atom, is defined as

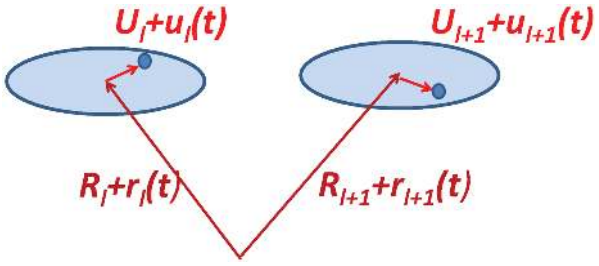

FIG. 27. (color online). The definition of the position vector of the ℓth cage at time t as $\boldsymbol{R}_\ell + \boldsymbol{r}_\ell(t)$, where $\boldsymbol{R}_\ell$ is the equilibrium position of the ℓth cage center. The vector $\boldsymbol{r}_\ell(t)$ represents a small deviation from $\boldsymbol{R}_\ell$. The position of the $\mathcal{R}(2)$ guest atom from the center of the ℓth cage $\boldsymbol{R}_\ell$ is defined by the vector $\boldsymbol{U}_\ell + \boldsymbol{u}_\ell(t)$, where $\boldsymbol{U}_\ell$ is the equilibrium position of the $\mathcal{R}(2)$ guest atom from $\boldsymbol{R}_\ell$, and $\boldsymbol{u}_\ell(t)$ is a small deviation from $\boldsymbol{U}_\ell$ at time t.

$$\rho(\boldsymbol{r},t)=\sum_{\ell}\delta(\boldsymbol{D}_{\ell}+\boldsymbol{d}_{\ell}(t)-\boldsymbol{r}), \tag{32}$$

where the definitions $\boldsymbol{D}_{\ell}=\boldsymbol{R}_{\ell}+\boldsymbol{U}_{\ell}$ and $\boldsymbol{d}_{\ell}(t)=\boldsymbol{r}_{\ell}(t)+\boldsymbol{u}_{\ell}(t)$ apply. The $\boldsymbol{Q}$ component of the spatial Fourier transform of Eq. (32) becomes

$$\rho_{\boldsymbol{Q}}(t)=\sum_{\ell}e^{-i\boldsymbol{Q}\cdot[\boldsymbol{D}_{\ell}+\boldsymbol{d}_{\ell}(t)]}. \tag{33}$$

The dynamic structure factor $S(\boldsymbol{Q},\omega)$ is proportional to the differential cross section for incident neutrons through

$$\frac{d^2\sigma}{d\Omega dE}=\frac{k_f}{k_i}\frac{\bar{\sigma}}{4\pi}\,e^{-\beta\hbar\omega/2}S(\boldsymbol{Q},\omega), \tag{34}$$

where k_i and k_f are the strengths of the initial and final momenta of the neutrons. The change of momentum is given by $\hbar\boldsymbol{Q}=\hbar(\boldsymbol{k}_f-\boldsymbol{k}_i)$, and $\hbar\omega=(\hbar^2/2m)(k_f^2-k_i^2)$ is the change of energy of the incident neutron. $\bar{\sigma}$ is an arbitrarily chosen microscopic scattering cross section. The dynamic structure factor $S(\boldsymbol{Q},\omega)$ is expressed by the Fourier transform of Eq. (31) as

$$S(\boldsymbol{Q},\omega)=\frac{1}{2\pi\hbar N}\int_{-\infty}^{\infty}dt e^{-i\omega t}\times\sum_{\ell,\ell'}^{N}\bar{b}_{\ell}\bar{b}_{\ell'}\langle e^{i\boldsymbol{Q}\cdot[\boldsymbol{D}_{\ell}+\boldsymbol{d}_{\ell}(t)]}e^{-i\boldsymbol{Q}\cdot[\boldsymbol{D}_{\ell'}+\boldsymbol{d}_{\ell'}(0)]}\rangle, \tag{35}$$

where $\bar{b}_{\ell}$ is the neutron scattering length of atom ℓ, and N is its total number. The sum is taken over all atoms ℓ,ℓ' ($\ell\neq\ell'$) of the system. The expansion of Eq. (33) in terms of the small deviation $\boldsymbol{d}_{\ell}(t)$ yields the first-order density fluctuation,

$$\Delta\rho_{\boldsymbol{Q}}(t)=\sum_{\lambda}\Delta\rho_{\lambda}(\boldsymbol{Q},t)+O(d^2), \tag{36}$$

where the first term is expressed by

$$\Delta\rho_{\lambda}(\boldsymbol{Q},t)=-i\hbar\sum_{\lambda,\ell}\frac{\boldsymbol{Q}\cdot\boldsymbol{e}_{\lambda}}{\sqrt{2M_{\ell}\omega_{\lambda}}}\times e^{-i\boldsymbol{Q}\cdot\boldsymbol{D}_{\ell}}[\phi_{\lambda}(\boldsymbol{D}_{\ell})a_{\lambda}^{\dagger}(t)+\text{H.c.}]. \tag{37}$$

Here H.c. stands for the Hermitian conjugate, $\boldsymbol{e}_{\lambda}$ is the polarization vector of the λ mode, and ϕ_{λ} is the associated eigenfunction. $a_{\lambda}^{\dagger}$ (a_{λ}) is the creation (annihilation) operator of the phonon mode λ. M_{ℓ} indicates the mass of atoms in the ℓth cell. The substitution of Eq. (37) into Eq. (35) expanded up to the first order in $\boldsymbol{d}_{\ell}(t)$ yields the coherent inelastic term for the dynamic structure factor given by

$$S(\boldsymbol{Q},\omega)=\frac{n(\beta\omega+1)}{N\bar{\sigma}}\sum_{\lambda}4\pi\delta(\omega-\omega_{\lambda})\times\left|\sum_{\ell}\bar{b}_{\ell}\frac{(\boldsymbol{Q}\cdot\boldsymbol{e}_{\lambda})\phi_{\lambda}(\boldsymbol{D}_{\ell})}{\sqrt{2M_{\ell}\omega_{\lambda}}}\,e^{-i\boldsymbol{Q}\cdot\boldsymbol{D}_{\ell}}\right|^2, \tag{38}$$

where $n(\beta\omega+1)$ is the Bose-Einstein distribution function with the definition $\beta=1/k_{\mathrm{B}}T$.

Equation (38) indicates that $S(\boldsymbol{Q},\omega)$ becomes a flat dispersion relation independent of $\boldsymbol{Q}$ for a spatially localized mode ϕ_{λ}. This point is realized in the results of INS experiments on type-I clathrate compounds as given in Secs. VI.B.2 and VI.B.3. The phonon densities of states (PDOSs) can be obtained from the INS measurements, although caution is needed in the case of multicomponent systems because of the different scattering lengths $\bar{b}_{\ell}$ for different atomic species.

2. Inelastic neutron scattering experiments for on-center systems

INS measurements on polycrystalline powder samples of type-I $\mathcal{R}_8Ga_{16}Ge_{30}$ ($\mathcal{R}$ = Ba and Sr) were performed by Hermann *et al.* (2005) and Christensen, Juranyi, and Iversen (2006). Hermann *et al.* (2005) investigated the PDOS in the THz-frequency range associated with $\mathcal{R}(2)$ guest atoms in both $\mathcal{R}$ = Ba and Sr compounds. The case $\mathcal{R}$ = Ba is in the category of a quasi-on-center system showing the crystalline umklapp process of the phonon thermal conductivity $\kappa_{\mathrm{ph}}(T)$, while the $\mathcal{R}$ = Sr belongs to the off-center system yielding the glasslike plateau in thermal conductivity at around 10 K, as shown in Figs. 14 and 16. Christensen, Juranyi, and Iversen (2006) observed the PDOSs of three powder samples with $\mathcal{R}$ = Sr, and *n*- and *p*-type $\mathcal{R}$ = Ba; see Fig. 28. These results (Hermann *et al.*, 2005; Christensen, Juranyi, and Iversen, 2006) involved information about both quasi-on-center and off-center systems, so we discuss them in detail in Sec. VI.B.3, by focusing on the essential difference between the dynamics of on-center and off-center systems.

Lee *et al.* (2007) carried out coherent INS experiments on a single crystal of $Ba_8Ga_{16}Ge_{30}$, a quasi-on-center system, using a triple-axis spectrometer. They obtained the phonon dispersion relations along the [100] direction in the THz-frequency range. The results close to the Γ point showed the optical mode with T_u symmetry associated with the Ba(2) guest atom at $E=4.5$ meV. It is remarkable that the anticrossing between the optical mode and the acoustic mode in the THz region was observed at around $\boldsymbol{q}=(0.45,0,0)$ in the

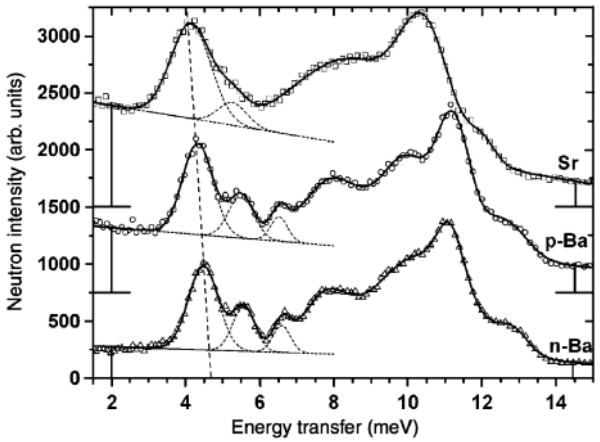

FIG. 28. Neutron scattering intensity corresponding to PDOSs for type-I *n*-$Sr_8Ga_{16}Ge_{30}$, *p*-$Ba_8Ga_{16}Ge_{30}$, and *n*-$Ba_8Ga_{16}Ge_{30}$. Gaussian fits are shown for the first curves. From Christensen, Juranyi, and Iversen, 2006.

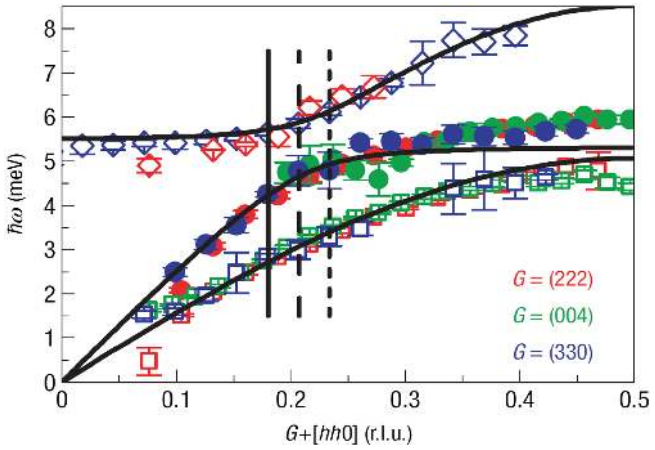

FIG. 29. (color online). Phonon dispersion curves for quasi-on-center $Ba_8Ga_{16}Ge_{30}$ along $[hh0]$ around the positions $G = (222)$, $G = (004)$, and $G = (330)$. The error bars represent the standard deviation of the fitted energies. From Christensen *et al.*, 2008.

Brillouin zone, which indicates that the Ba(2) guest atoms play a crucial role for splitting out the acoustic modes attributable to the vibrations of networked cages.

Christensen *et al.* (2008) observed the avoided crossing in $Ba_8Ga_{16}Ge_{30}$ containing a quasi-on-center Ba(2) guest atom by using a 13 g single crystal. The dispersion curve of a (330) reflection along the [110] direction exhibits the avoided crossing between the longitudinal acoustic phonon and the optical mode attributed to the Ba(2) guest atom at $h = 0.225$ of $(3, 3, 0) + [h, h, 0]$; see Fig. 29. They estimated the phonon lifetime τ from the data for the scattered intensity of the incident neutron. The τ of the phonons around the avoided crossing area is about 2 ps, which is much longer than 0.2 ps obtained from the simple relation $\kappa_{ph}(T) = C_{ph}(T)v^2\tau/3$ using known values of κ_{ph}, the specific heat $C_{ph}(T)$ of acoustic phonons, and the average phonon velocity v. This discrepancy indicates that this simple relation for $\kappa_{ph}(T)$ is not applicable in the region of flattened dispersion relations of acoustic phonons.

Christensen *et al.* (2009) carried out INS experiments for powder samples of type-I $Ba_8\mathcal{Y}_xGe_{46-x}$ ($\mathcal{Y}_x = Ni_6$, Cu_6, Zn_8, and Ga_{16}) under pressure of 9 kbars. The phonon thermal conductivities of these samples show the crystalline umklapp peak at around 10 K except for p-type $Ba_8Ga_{16}Ge_{30}$ (Bentien, Johnsen, and Iversen, 2006). Christensen *et al.* (2009) imposed chemical pressure by atomic substitution, and the physical pressure of 9 kbars was applied using a clamp cell. The volume reduction induced by the physical pressure increases the energy of the modes associated with the guest atom. A softening of the mode energies was observed upon cooling the sample. Both p-type and n-type BGG showed a similar temperature dependence.

Koza *et al.* (2010) performed INS experiments for $Ba_8Zn_xGe_{46-x-y}Ø_y$ with $x = 0$, 2, 4, 6, 8 and $y = 3 - 6x/8$, where Ø denotes a vacancy. They studied the modulation of the eigenfrequency distribution of these compounds by progressively substituting Ge with Zn in addition to probing its dependence on temperature between 2 and 300 K. A number of peaks were shifted toward higher energies by about 1–2 meV as a result of the substitution. Measurements on temperature dependence demonstrated a hardening of the overall frequency distribution upon cooling. They observed a softening upon cooling of the lowest peak energy at 4.5–4.8 meV with a relative shift of 5% from 300 to 2 K; this peak is attributable to the Ba(2) guest atom.

Euchner *et al.* (2012) made a high-resolution INS study of the PDOS and the phonon dispersion relation of $Ba_8Ni_{6-x}Ge_{40+x}$. They obtained evidence of spectral weight transfer between acoustic and optical phonons due to the strong hybridization. These data exclude an interpretation in terms of independent oscillators, e.g., the Einstein model or the soft potential model, since the relevance of hybridized modes between the Ba(2) guest atom and network cages is evident. The phonon lifetimes are at least an order of magnitude larger than those estimated from $\kappa_{ph}(T)$.

3. Inelastic neutron scattering experiments on off-center systems

Hermann *et al.* (2005) carried out INS measurements on the PDOSs at room temperature on 2.81 and 1.34 g samples of

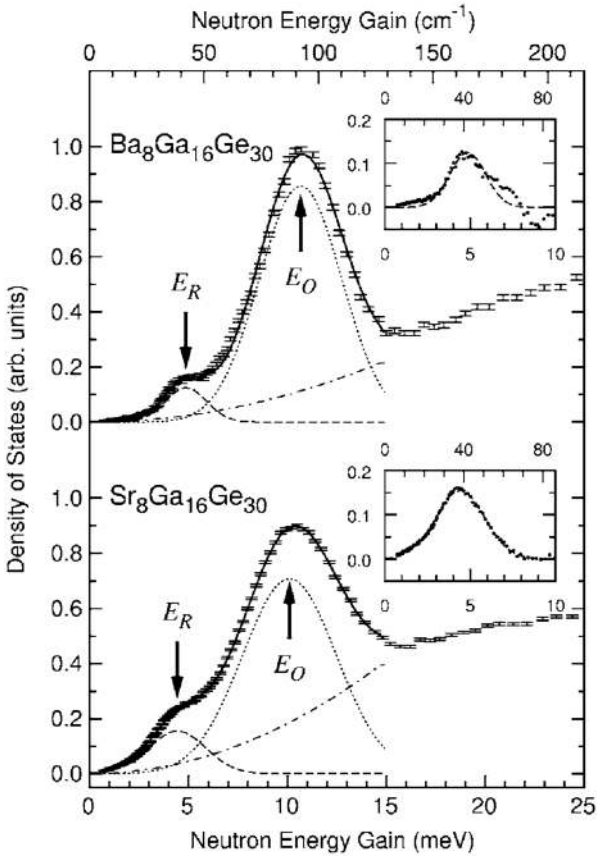

FIG. 30. The PDOSs of type-I $Ba_8Ga_{16}Ge_{30}$ and $Sr_8Ga_{16}Ge_{30}$ obtained from INS measurements. The dashed line is the contribution of the modes associated with Ba(2) guest atoms and Sr(2), the dot-dashed line is the parabolic Debye contribution, and the dotted line is a Gaussian fit to the optical phonon density of states below 15 meV. Because the neutron scattering lengths of Ba and Sr are different, the measured PDOSs have been arbitrarily scaled. Insets: The Gaussian peaks at E_R associated with Ba(2) and Sr(2). Deviations in the inset for type-I $Ba_8Ga_{16}Ge_{30}$ are related to the Ba(1) mode. From Hermann *et al.*, 2005.

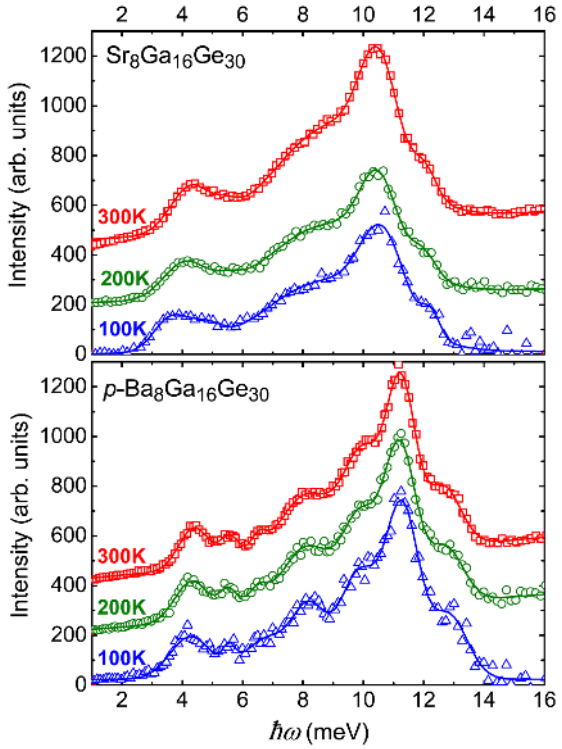

FIG. 31. (color online). INS data as a function of temperature 300, 200, and 100 K for type-I $Sr_8Ga_{16}Ge_{30}$ and p-type $Ba_8Ga_{16}Ge_{30}$. These are given by the squares, circles, and triangles, respectively. From Christensen *et al.*, 2009.

polycrystalline samples of type-I BGG and SGG. Figure 30 shows weighted PDOSs for BGG and SGG, which were extracted from the INS data by integrating the scattering over a 6θ range of 30°–130° and with a subsequent subtraction of the background (Hermann *et al.*, 2005). The observation confirmed that the local mode due to the $\mathcal{R}(2)$ guest atom is independent of the integration range. The local modes of both Ba(2) and Sr(2) guest atoms exhibited a linewidth that exceeds the instrumental resolution. These results indicated a damping of these local modes due to the interactions with network cages. The observed linewidth for Sr(2) local modes is larger than that for the Ba(2) local mode, which indicates a more pronounced interaction of the Sr guests with network cages.

Type-I $Eu_8Ga_{16}Ge_{30}$ (β-EGG) belongs to the category of off-center systems, showing a plateau in $\kappa_{ph}(T)$ as in the case of SGG. However, INS experiments on β-EGG were not possible because Eu(2) has a very large neutron absorption cross section (Hermann *et al.*, 2005). But nuclear inelastic scattering (NIS) measurements are available to obtain the PDOS associated with the Eu(2) guest atom. This technique utilizes the high brilliance of synchrotron radiation to obtain an element-specific PDOS as in Mössbauer absorption spectroscopy (Hermann *et al.*, 2006). NIS has the advantage over INS experiments that the nuclear fluorescence yields an ideal averaging over the entire Brillouin zone. Because of the resonant nature of the NIS technique, the determination of the PDOS in β-EGG provides clear evidence that the Eu(2) guest atom neither interacts with nor participates in any high-energy vibrational modes. Furthermore, the microscopic determination of the PDOS in terms of NIS measurements suggests the presence of low-lying local modes associated with Eu(2) guest atoms in β-EGG (Hermann *et al.*, 2005).

Lee *et al.* (2008) performed coherent INS experiments to investigate phonon dispersion relations for SGG, an off-center system. They observed that the optical T_u mode of Sr(2) appears around 4.0 meV. Compared with the results of the low-lying modes in BGG containing on-center Ba(2) guest atoms by Lee *et al.* (2007), the avoided crossing due to the Sr(2) guest atom is less clear (Lee *et al.*, 2008).

Christensen *et al.* (2009) carried out INS experiments on powder samples of SGG and p-type BGG at temperatures of 100, 200, and 300 K, shown with squares, circles, and triangles, respectively, in Fig. 31. Note that with decreasing temperature the *width* of the peak around 4 meV increases. These behaviors coincide with the results of infrared absorption by Mori *et al.* (2009, 2011). The physical origin of this anomalous broadening is discussed in Sec. VII.

Here we mention interesting works on clathrate hydrates in terms of incoherent INS (Tse *et al.*, 2001; Gutt *et al.*, 2002; Baumert *et al.*, 2003) and nuclear resonant inelastic x-ray scattering experiments (Klug *et al.*, 2011) on the avoided crossing between low-lying optical modes and acoustic

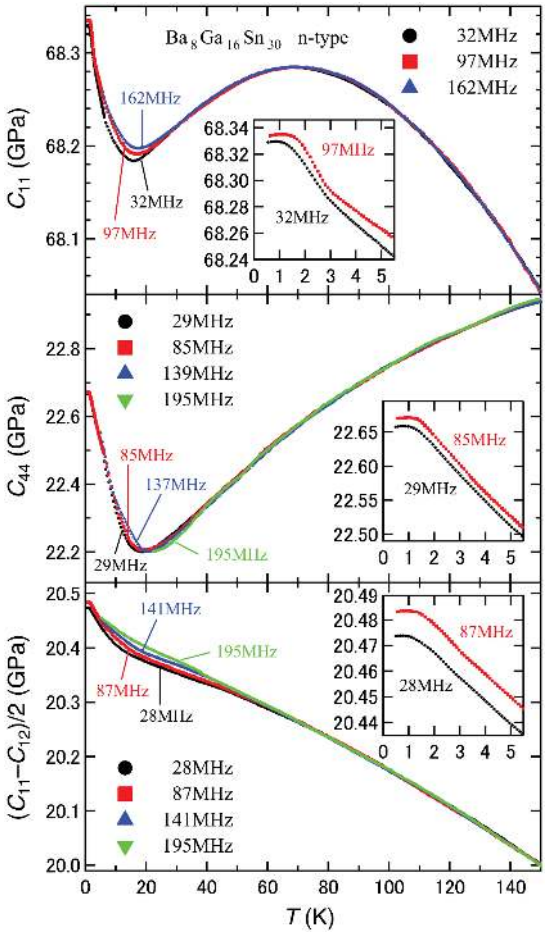

FIG. 32. (color online). Temperature dependences of elastic stiffness constants C_{11}, C_{44}, and $(C_{11} - C_{12})/2$ in n-type type-I $Ba_8Ga_{16}Sn_{30}$. The insets represent the data in an expanded scale below 5 K. From Ishii *et al.*, 2012.

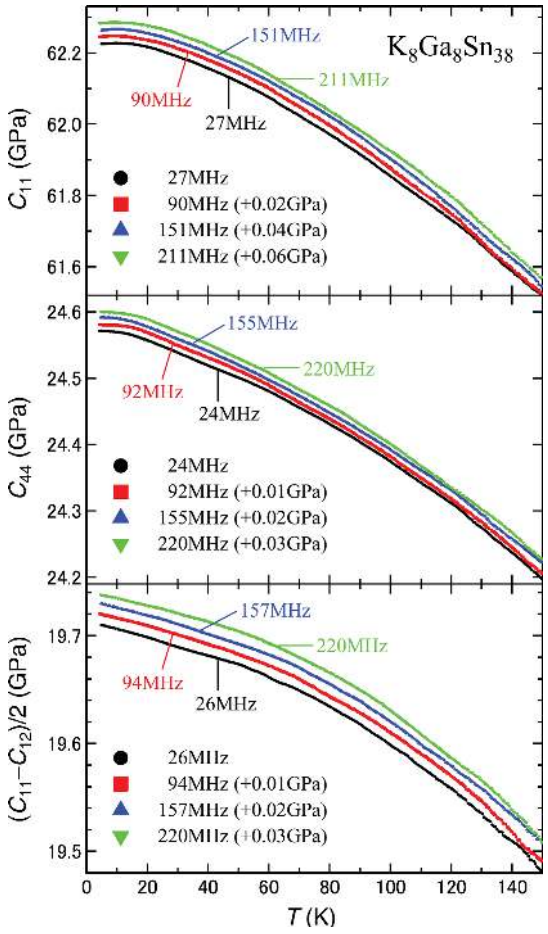

FIG. 33. (color online). Temperature dependences of elastic stiffness constants C_{11}, C_{44}, and $(C_{11}-C_{12})/2$ in type-I $K_8Ga_8Sn_{38}$. From Ishii *et al.*, 2012.

phonons. This was demonstrated as strong coupling between the local vibrations of guest molecules and water-framework vibrations.

Ishii *et al.* (2012) performed ultrasonic measurements on type-I $Ba_8Ga_{16}Sn_{30}$ (β-BGS) and $K_8Ga_8Sn_{38}$ (KGS) single crystals. They investigated the softening of the elastic stiffness constant C_{44} relevant to the strain component e_{xy}, which shows the softening of C_{44} up to 20 K for β-BGS. No charge-carrier dependence is observed between *n*-type and *p*-type β-BGS. For KGS, however, such tendencies have not been found, as shown in Figs. 32 and 33 (Ishii *et al.*, 2006, 2012). This is the evidence that local vibrations of the Ba(2) atom in β-BGS strongly couple with transverse ultrasonic waves. The significant softening on the bulk modulus in β-BGS contrasts with the continuous hardening in KGS.

VII. PHONON DISPERSION RELATIONS

A. Theoretical aspects of terahertz-frequency dynamics of type-I clathrate compounds

1. Molecular dynamics calculations

Molecular dynamics (MD) calculations have been done for clathrate hydrates with encaged guest atoms or molecules (Inoue, Tanaka, and Nakanishi, 1996; Tse *et al.*, 1997; Baumert *et al.*, 2003; English and Tse, 2009, 2011; English, Gorman, and MacElroy, 2012). It was pointed out (Tse *et al.*, 1997) that the avoided crossing arises from the coupling between local vibrations of guest atoms and acoustic phonons of network cages. Myles, Biswas, and Nenghabi (2007) performed MD calculations on the dispersion relations of acoustic and optical phonons of type-I $Ba_8Ga_{16}Ge_{30}$ and $Ba_8Ga_{16}Si_5Ge_{25}$. Their calculation is based on first-principles density functional theory (DFT) using a plane-wave basis and the pseudopotential method. Acoustic modes of both materials lie below 30–35 cm^{-1} (= 3.7–4.3 meV), and most of the optical modes show flat dispersion. However, the optical modes of type-I $Ba_8Ga_{16}Ge_{30}$ in the range 100–190 cm^{-1} (= 12.4–23.6 meV) and of type-I $Ba_8Ga_{16}Si_5Ge_{25}$ in the range 110–175 cm^{-1} (= 13.6–21.7 meV) display significant dispersion. The DFT calculations were made on the total energy and electric structures for type-I $Ba_8Ga_{16}Sn_{30}$ under hydrodynamic pressure (Li *et al.*, 2012).

Koza *et al.* (2010) carried out lattice-dynamical calculations in order to interpret the PDOSs obtained from INS measurements for $Ba_8Zn_6Ge_{40}$ and Ba_8Ge_{43} which are quasi-on-center systems. In both compounds, eigenmodes relevant to the Ba guest are primarily located in the energy regime below 14 meV. The low-energy modes at 3.10 meV are mainly due to Ba(2) cations, and Ba(1) cations contribute to the modes at 8.14 meV] The partial contributions of the host lattice constituents Ge and Zn indicate larger amplitudes in the energy range of Ba(1) than in that of Ba(2) eigenfrequencies. They pointed out that the suppression of the acoustic bandwidth is accomplished not only by the hybridization of Ba with Ge dynamics, but also by the lowest-energy eigenstates at the Brillouin-zone boundary.

Johnsen *et al.* (2010) carried out DFT calculations for $Ba_8\mathcal{T}_6Ge_{40}$ ($\mathcal{T}$ = Cu, Ag, and Au) to explain the atomic dynamics probed by their INS experiments. The DFT calculations were in good agreement with the PDOS data of INS concerning low-energy phonon modes of *n*-type Cu compounds, but showed discrepancies for *p*-type Ag and Au compounds with glasslike thermal conductivities.

Euchner *et al.* (2012) performed first-principles DFT calculations on the phonon dispersion relations of the following three cases: type-I $Ba_8Ge_{40}Ni_6$, a Ge_{46} framework without guest atoms, and a Ge diamond structure. They rescaled the energy axis to achieve an agreement with experimental data for $Ba_8Ge_{40}Ni_6$. The rescaling parameter of 1.4 is relatively large, indicating an underestimated Ba-Ge interaction within their DFT approach. They calculated the participation ratio (PR) characterizing the local or extended nature of the eigenmodes; a value of PR close to unity indicates extended modes with simultaneous displacements of relevant atoms. A PR close to zero indicates the local modes associated with local vibrations of the Ba(2) guest atom. The flat branches at 6–8 meV in $Ba_8Ge_{40}Ni_6$ were identified as the modes associated with the Ba(2) guest atom.

The constraints of the limited size in *ab initio* calculations make it difficult to treat the effect of disorder of the atomic configuration, whereas the quasi-on-center Ba-Ge-Ni makes it possible to create structures with different Ni content. These are $Ba_8Ge_{40}Ni_6$ and $Ba_8Ge_{42}Ni_4$, which have a different occupation of Ni at the 6*c* position. This is the only site that

exhibits disorder in the Ba-Ge-Ni clathrate structure. Since the 6*c* position is located in the large 24-atom trapezohedron, the Ni content yields distortions of the cages. Euchner *et al.* (2012) claimed that the disorder distribution of Ni and Ge yields a broadening of the guest modes.

Matsumoto *et al.* (2009) theoretically investigated the effect of a quadratic anharmonic potential to explain the temperature dependence of the optical conductivities (Mori *et al.*, 2009, 2011). They calculated the unequally spaced energy levels of a one-dimensional single-well and double-well potentials. The dipole interaction of the guest atoms with electric fields was assumed to induce transitions among vibrational states with unequally spaced energies. They calculated the natural line broadening and the shift of the peak frequency. In the case of a single-well potential, a softening of the peak frequency and an asymmetric narrowing of the linewidth with decreasing temperature were explained as a shift in the spectral weight to lower-level transitions. However, the calculated results for one-dimensional double wells showed that the spectral width of the lowest mode decreases with decreasing temperature. This is in conflict with the experimental results showing the reverse effect by Mori *et al.* (2011). This discrepancy indicates that this type of isolated potential for guest atoms is unsatisfactory for describing the experimental results.

Safarik, Llobet, and Lashley (2012) theoretically investigated the error arising from the use of the harmonic Debye-Waller factor to explain strong anharmonic vibrations of off-center Eu(2) guest atoms in type-I $Eu_8Ga_{16}Ge_{30}$ by assuming a one-dimensional anharmonic potential. They assessed the error in the values and temperature dependence of the thermal average mean-square displacement for Eu(2) guest atoms. The harmonic approximation led at most to a $\sim 25\%$ error. Yamakage and Kuramoto (2009) discussed the effect of the anharmonic potential on the temperature dependence of phonon spectra employing the self-consistent harmonic approximation for type-I SGG.

To summarize, MD calculations are powerful for gaining insight into the characteristics of vibrational properties of on-center systems with translational-invariance symmetry. It is obvious that MD calculations are not efficient for off-center systems without translational symmetry. However, the results of MD calculations definitely exclude an interpretation of the boson-peak-like hump of the PDOS at around 0.5 THz observed for off-center systems from adiabatic isolated-oscillator pictures such as the Einstein model or the soft potential model, since the hybridized modes between $\mathcal{R}(2)$ guest atoms and network cages are crucial.

2. Anharmonic potential expressed in terms of the relative coordinate

In this section, we describe the THz-frequency dynamics by constructing a model from simple and general points of view. This type of model enables us to grasp the essential points of physics involved. The atomic configuration of type-I clathrate compounds with off-center guest atoms has been given by means of diffraction measurements (Nolas, Weakley *et al.*, 2000; Bentien *et al.*, 2005; Christensen *et al.*, 2006, 2009) and EXAFS studies (Baumbach *et al.*, 2005; Jiang *et al.*, 2008).

As described in Sec. III, $\mathcal{R}(2)$ guest atoms in these compounds take on-center or off-center positions in 14-hedrons depending on the ratio of the cage size and the atomic radius of the guest atom. For example, the guest atoms in 14-hedrons in type-I $Ba_8Ga_{16}Sn_{30}$ (β-BGS) take the off-center position at $|\boldsymbol{U}_\ell| = 0.43$ Å from the center of the tetradecahedral cage (Suekuni, Avila *et al.*, 2008). Note that the amplitudes of $\mathcal{R}(2)$ guest atoms are of the order of 0.05 Å, which is sufficiently small compared with $|\boldsymbol{U}_\ell|$. The deviation $|\boldsymbol{U}_\ell| = 0.43$ Å is 7.4% of the nearest-neighbor distance $d = 5.84$ Å between Ba^{2+} atoms. Hence, the potential function for off-center guest atoms is shaped like the sheared bottom of a wine bottle. For example, four sites of 6*k* off-center positions are schematically illustrated in Fig. 34 (Avila *et al.*, 2008).

The THz-frequency dynamics is the most important part for elucidating peculiar thermal and dynamic properties of off-center systems. This frequency range is mainly concerned with the acoustic and the lowest optical bands. For this situation, we focus on the dynamics of cages and $\mathcal{R}(2)$ guest atoms. The cages are treated as possessing total mass M with effective charge $-e_C^*$, and guest atoms as having mass m with charge e_G^*. The position vector of the ℓth cage at time t was defined in Sec. VI.B.1 as $\boldsymbol{R}_\ell + \boldsymbol{r}_\ell(t)$, where $\boldsymbol{R}_\ell$ is the equilibrium position of the ℓth cage center. The vector $\boldsymbol{r}_\ell(t)$ represents a small deviation from $\boldsymbol{R}_\ell$. The position of an $\mathcal{R}(2)$ guest atom is defined by the vector $\boldsymbol{U}_\ell + \boldsymbol{u}_\ell(t)$, where $\boldsymbol{U}_\ell$ is the position of an $\mathcal{R}(2)$ guest atom measured from $\boldsymbol{R}_\ell$, and $\boldsymbol{u}_\ell(t)$ is a small deviation from $\boldsymbol{U}_\ell$ at time t. Note that $\boldsymbol{U}_\ell \neq \boldsymbol{0}$ corresponds to the case of an off-center guest

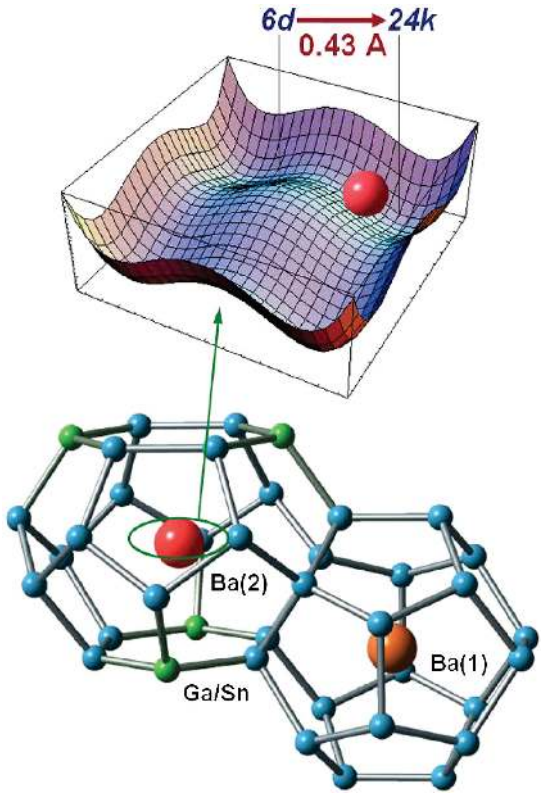

FIG. 34. (color online). Schematic illustration of the anharmonic potential for the $\mathcal{R}(2)$ guest atom in oversized cages in type-I clathrate compounds. From Avila *et al.*, 2008.

atom, whereas the on-center case has $\boldsymbol{U}_\ell = \mathbf{0}$. This clarifies the difference between on-center and off-center systems on the same theoretical basis. The definition of coordinates is given in Fig. 27.

Nakayama and Kaneshita (2011) employed the following form of the anharmonic potential, which is applicable to both the off-center and the on-center systems. This is expressed in terms of the "relative displacement" $\boldsymbol{w}_\ell(t) = \boldsymbol{u}_\ell(t) - \boldsymbol{r}_\ell(t)$ as

$$V_{\rm anh} = \sum_\ell \left[\frac{\xi}{2}|\boldsymbol{U}_\ell + \boldsymbol{w}_\ell(t)|^2 + \frac{\eta}{4}|\boldsymbol{U}_\ell + \boldsymbol{w}_\ell(t)|^4\right], \qquad (39)$$

where the parameter ξ takes a positive or negative value, and $\eta > 0$. This type of potential expressed by the relative coordinate $\boldsymbol{w}_\ell(t)$ allows us to legitimately treat the THz-frequency dynamics of hybridized modes consisting of guest atoms and network cages beyond the adiabatic approximation.

The potential $V_{\rm anh}$ of Eq. (39) involves two types of anharmonic potentials depending on positive or negative ξ, namely, a wine-glass or wine-bottle type of potential. Thus, Eq. (39) makes it possible to treat in a unified way both on-center and off-center systems.

3. Spontaneous symmetry breaking of off-center systems

For the case of off-center systems, the parameter set $\xi < 0$ and $\eta > 0$ in Eq. (39) yields a potential similar to the bottom of a wine bottle, in which the minimum becomes $V_{\rm anh,min} = -\xi^2/4\eta$ at $|\boldsymbol{U}_\ell|^2 = -\xi/\eta$. The nonzero $\boldsymbol{U}_\ell$ enables one to rewrite the potential of Eq. (39) as

$$V_{\rm anh} = \frac{\xi}{2}\sum_\ell |\boldsymbol{U}_\ell + \boldsymbol{w}_\ell(t)|^2\left[1 - \frac{|\boldsymbol{U}_\ell + \boldsymbol{w}_\ell(t)|^2}{2|\boldsymbol{U}_\ell|^2}\right]. \qquad (40)$$

We describe the vibrations around the equilibrium position of off-center guest atoms by the following complex number:

$$W_\ell = e^{i[\theta_\ell + \delta\theta_\ell(t)/\sqrt{2}]}\left[U_0 + \frac{h_\ell(t)}{\sqrt{2}}\right], \qquad (41)$$

where W_ℓ represents the vector $\boldsymbol{U}_\ell + \boldsymbol{w}_\ell$. The equilibrium position of the $\mathcal{R}(2)$ guest atom measured from the center of the cage is given by $U_0 e^{i\theta_\ell}$, which indicates that the potential of Eq. (40) preserves the *local* gauge symmetry. The phase factor can be considered as a dynamical variable representing the guest position trapped in one of our hindering potentials caused by local symmetry breaking. The variable $h_\ell(t)$ in Eq. (41) represents a small fluctuation along the radial direction from the randomly oriented angle θ_ℓ. Figure 35 depicts two parameters representing these two modes. It is straightforward to include another degree of freedom $\delta\varphi_\ell(t)$ perpendicular to the plane introduced in Eq. (41).

The reformed potential function with respect to small quantities $h_\ell(t)$ and $\delta\theta_\ell(t)$ is given from Eq. (40) for $|\boldsymbol{w}_\ell| < |\boldsymbol{U}_\ell|$ as

$$V_{\rm anh} = \frac{1}{2}\sum_\ell (\tilde{\xi}_s h_\ell^2 + \tilde{\xi}_\theta U_0^2 \delta\theta_\ell^2), \qquad (42)$$

where the effective force constants $\tilde{\xi}_s$ and $\tilde{\xi}_\theta$ in Eq. (42) are introduced to redefine ξ in Eq. (40) in order to express the differences between angular motion and stretching motion. In addition, these force constants involve the effect of the random orientation of $\{U_\ell\}$ and anharmonicity through the following definitions:

$$\tilde{\xi}_s = -\xi_s\left(\frac{1 + \langle h_\ell^2\rangle/U_0^2}{2}\right), \qquad \tilde{\xi}_\theta = -\xi_\theta\left(\frac{1 + \langle \delta\theta_\ell^2\rangle}{2}\right), \qquad (43)$$

where the angular brackets represent a thermal average over the anharmonic term in Eq. (40), which should be proportional to T at higher temperatures.

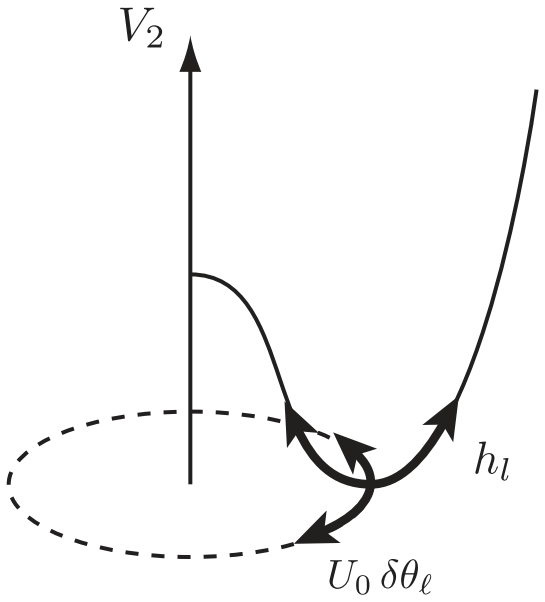

FIG. 35. The emergence of 2 degrees of freedom of motion: stretching $h_\ell(t)$ and libration $U_0\delta\theta_\ell(t)$.

B. Equations of motion

1. Effect of charge fluctuation

The relative displacements $\{\boldsymbol{w}_\ell\}$ from the center of the cage induce electric dipoles for both the on-center and off-center systems as in the case of ionic crystals (Fano, 1960). The total potential energy due to the intersite dipole-dipole interaction is expressed as

$$V_{\rm dip} = \sum_{\ell,m}\frac{e_G^{*2}}{2\boldsymbol{R}_{\ell m}^3}[\boldsymbol{w}_\ell\cdot\boldsymbol{w}_m - 3(\boldsymbol{w}_\ell\cdot\hat{\boldsymbol{R}}_{\ell m})(\boldsymbol{w}_m\cdot\hat{\boldsymbol{R}}_{\ell m})], \qquad (44)$$

where the dipole $\boldsymbol{p}_\ell$ is defined by $\boldsymbol{p}_\ell = e_G^*\boldsymbol{w}_\ell$, and $\hat{\boldsymbol{R}}_{\ell m}$ is a unit vector in the direction of the vector $\boldsymbol{r}_{\ell m} = \boldsymbol{r}_\ell - \boldsymbol{r}_m$. The Fourier-transformed expression of Eq. (44) under the random phase approximation is obtained as (Cohen and Keffer, 1955)

$$V_{\rm dip} = \frac{(e^*)^2}{4}\sum_{\ell,k,\mu}|\boldsymbol{q}_{k\mu}|^2 e^{-i\boldsymbol{k}\cdot\boldsymbol{r}_{0\ell}}\frac{1 - 3(\hat{\boldsymbol{q}}_{k\mu}\cdot\hat{\boldsymbol{R}}_{0\ell})^2}{R_{0\ell}^3} + \text{c.c.}, \qquad (45)$$

where $\boldsymbol{q}_{k\mu}$ means the normal coordinate for the Fourier transform of $\boldsymbol{w}_\ell$, and c.c. indicates the complex conjugate of the first term.

Equation (45) can be expressed, by using the Lorentz sums, as

$$V_{\rm dip} = \frac{m\omega_p^2}{2}\sum_{k\mu}|\boldsymbol{q}_{k\mu}|^2 L_\mu, \tag{46}$$

where $L_\mu = (\hat{\boldsymbol{q}}_{k\mu}\cdot\hat{\boldsymbol{k}})^2 - 1/3$ for small $\boldsymbol{k}$ for a cubic lattice, $\omega_p^2 = 4\pi n_C (e_G^*)^2/m$ is the squared plasma frequency of guest atoms with mass m, and charge e_G^* in cgs esu units, and $n_C = 1/a^3$ is the number density of charges. We note that $L_\parallel = 2/3$ for longitudinal modes and $L_\perp = -1/3$ for transverse modes (Cohen and Keffer, 1955).

2. Fourier-transformed representation of equations of motion

Each cage is elastically connected with nearest-neighbor cages. We denote the coupling strength by the harmonic force constants $f_\parallel$ and $f_\perp$, which represent longitudinal (dilation) and transverse (shear) modes. With these quantities, the potential energy is expressed by

$$V_{\rm lat} = \sum_{\ell,\mu}\frac{f_\mu}{2}|\boldsymbol{r}_{\ell,\mu} - \boldsymbol{r}_{\ell+1,\mu}|^2, \tag{47}$$

where μ denotes the species of the three modes $\parallel$, $\perp$, and $\perp'$.

Network cages compose a cubic lattice (Nolas, Weakley *et al.*, 2000; Baumbach *et al.*, 2005; Bentien *et al.*, 2005; Christensen *et al.*, 2006), which is invariant under translation by any lattice vector. This enables us to make the Fourier transformation of the potential function given by

$$V_{\rm lat} = 2\sum_{k,\mu} f_\mu |\boldsymbol{Q}_{k\mu}|^2 \sin^2\left(\frac{\boldsymbol{k}\cdot\boldsymbol{a}}{2}\right), \tag{48}$$

where $\boldsymbol{a}$ is a lattice vector. The Fourier transformation of the anharmonic potential expressed by the relative coordinate $\boldsymbol{w}_\ell$ is made as

$$\bar{V}_{\rm anh} = \frac{1}{2}\sum_{k,\mu}\bar{\xi}_\mu |\boldsymbol{q}_{k\mu}|^2, \tag{49}$$

where $\bar{\xi}$ represents the force constants of both the on-center and off-center systems.

The nature of the force constants $\bar{\xi}_\mu$ in Eq. (49) is quite different for on-center and off-center systems. The crucial difference is that $\tilde{\xi}_\mu$ for off-center systems involves both the librational ($\tilde{\xi}_\theta$) and radial ($\tilde{\xi}_s$) degrees of freedom, while $\hat{\xi}$ for on-center systems is *isotropic*, and independent of the mode μ, whether longitudinal or transverse. The equations of motion for two variables $\boldsymbol{q}_{k\mu}$ and $\boldsymbol{Q}_{k\mu}$ are obtained by replacing $\bar{\xi}_\mu \to \hat{\xi}$ in Eq. (50). On-center systems impose the condition $\xi > 0$, $\eta > 0$ in Eq. (39). This yields the equilibrium position of on-center guest atoms $\boldsymbol{U}_\ell(t) = \boldsymbol{0}$. In this case, the force constant $\bar{\xi}$ becomes $\hat{\xi} = \xi + \eta\langle|\boldsymbol{w}_\ell(t)|^2\rangle/2$ by taking into account the thermal average of the anharmonic terms.

The equations of motion for two variables $\boldsymbol{q}_{k\mu}$ and $\boldsymbol{Q}_{k\mu}$ with $\mu = \parallel, \perp$ are obtained from the Euler-Lagrange equation as

$$m\omega_{k\mu}^2(\boldsymbol{q}_{k\mu} + \boldsymbol{Q}_{k\mu}) = (\bar{\xi}_\mu + m\omega_p^2 L_\mu)\boldsymbol{q}_{k\mu}, \tag{50}$$

$$(m+M)\omega_{k\mu}^2\boldsymbol{Q}_{k\mu} = 4f_\mu\sin^2\left(\frac{\boldsymbol{k}\cdot\boldsymbol{a}}{2}\right)\boldsymbol{Q}_{k\mu} - m\omega_{k\mu}^2\boldsymbol{q}_{k\mu}. \tag{51}$$

Here the above equations of motion are applicable to both cases of on-center or off-center systems. It is straightforward to introduce the effect of random orientation of off-center guest atoms by taking $\bar{\xi}_\mu \to \bar{\xi}$ ($\tilde{\xi}_\theta \le \bar{\xi}_\mu \le \tilde{\xi}_s$).

C. Phonon dispersion relations for off-center and on-center systems in the terahertz-frequency region

1. On-center system

The force constants $f_\parallel$ and $f_\perp$ in Eq. (47) for $Ba_8Ga_{16}Ge_{30}$ for an on-center system are obtained using the sound velocities $v_\parallel = 4\,096$ m/s and $v_\perp = 2795$ m/s (Christensen *et al.*, 2008). These yield $f_\parallel = 26.4$ and $f_\perp = 12.3$ N/m using $M = 7.04m$ and $a = 10.78$ Å. The force constant $\hat{\xi}$ for n-type BGG on-center systems is obtained at 2 K in the same manner as for the data on Raman scattering $\omega_0/2\pi = 32$ cm^{-1} ($= 0.96$ THz) (Takasu *et al.*, 2006; Suekuni *et al.*, 2010) as $\hat{\xi} = 8.23$ N/m. Equation (50) involves the squared plasma frequency ω_p^2 arising from the fluctuation of charged guest atoms defined in Eq. (46). The magnitude of the plasma frequency should be $\omega_p/2\pi \cong 0.09$ THz using the mass ($m = 137$ u) and the charge of Ba^{2+} ($e_G^* = 2e$) by taking the number density $n_C = 0.628\times 10^{27}$ m^{-3} and the relative electric susceptibility $\epsilon_r/\epsilon_0 \cong 10$, the same as that of the Si crystal.

Nakayama and Kaneshita (2011) analytically calculated the dispersion relations for BGG on-center systems from Eqs. (50) and (51) using the force constants mentioned above, as shown in Fig. 36(a). The acoustic phonon dispersions in Fig. 36(a) for BGG are flattened below $\omega_{0\mu}$ for both transverse and longitudinal modes. The eigenfrequencies of optical

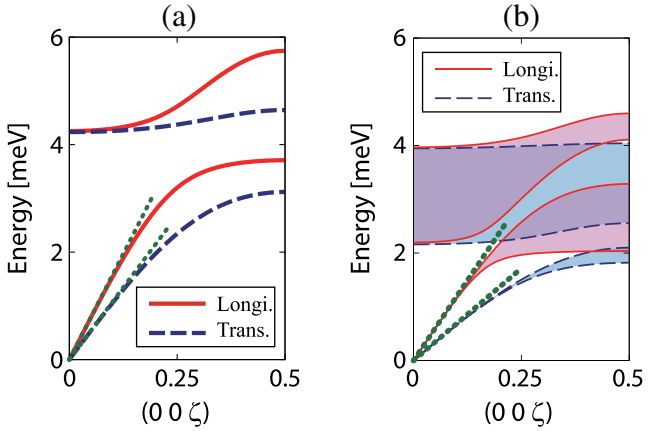

FIG. 36. (color online). (a) Phonon dispersion curves along the [001] direction for BGG on-center systems. Dispersion relations for longitudinal modes are plotted with solid lines and for transverse modes with dashed lines. Dotted linear lines from the origin represent the long-wave limit of the acoustic dispersion relations. The degeneracy of optical modes at the Γ point is observed at 4.2 meV arising from the on-centered symmetric potential. (b) Phonon dispersion curves along the [001] direction for β-BGS off-center systems. Dispersion relations for longitudinal (transverse) modes are illustrated by the region bounded by solid (dashed) lines. Dotted linear lines from the origin again represent the long-wave limit of acoustic dispersion relations. Note that optic modes observed at the Γ point are not separated at 2.2 and 4.1 meV. Adapted from Nakayama and Kaneshita, 2011.

modes at the Γ point are degenerate, reflecting the fact that the isotropic force constant $\tilde{\xi}$ is independent of the mode μ.

Experimental data on the dispersion relations in terms of coherent inelastic neutron scattering are available for *n*-type BGG on-center systems (Lee *et al.*, 2007; Christensen *et al.*, 2008). The calculated results shown in Fig. 36(a) using the smallest number of parameters of f_μ and $\tilde{\xi}$ recover well the inelastic neutron scattering data for BGG (Lee *et al.*, 2007; Christensen *et al.*, 2008).

2. Off-center system

Equations (50) and (51) describe the hybridization between the vibrations of cages and the off-center $\mathcal{R}(2)$ guest atoms in addition to the effect of the random orientation of off-center guest atoms on the spectral width of the phonon dispersion relations. The hybridization occurs as a result of the coupling between *parallel* components of displacements regardless of the transverse (⊥) or longitudinal (∥) modes. Figures 37(a) and 37(b) illustrate the physical meaning of this "vector" coupling. For example, consider the case in which longitudinal acoustic phonons with polarization vector parallel to the y axis are incident along the y axis when the $\mathcal{R}(2)$ guest atom takes the far-side position as depicted in Fig. 37(a). These longitudinal acoustic phonons predominantly couple with the stretching component $h_\ell(t)$ parallel to the polarization vector. Provided that the $\mathcal{R}(2)$ guest atom is on the right side along the x axis as shown in Fig. 37(b), the longitudinal acoustic phonons incident along the y axis couple with the libration component $U_0\delta\theta_\ell$, which is parallel to the polarization vector of the acoustic phonons. Thus, the coupling constant continuously spans from the librational one $\tilde{\xi}_\theta$ to the stretching one $\tilde{\xi}_s$. The same arguments hold for the coupling of transverse acoustic phonons. These cause the broadening of the spectral width through the distribution of force constants $\tilde{\xi}_\theta \le \tilde{\xi}_\mu \le \tilde{\xi}_s$ with the definition $\mu = \perp$ or ∥ (Nakayama and Kaneshita, 2011). It should be noted that the first demonstration, to our knowledge, on the relevance of this type of hybridization to the boson peak in glasses was made using a simple model full of implications by Nakayama (1998) and Nakayama and Sato (1998).

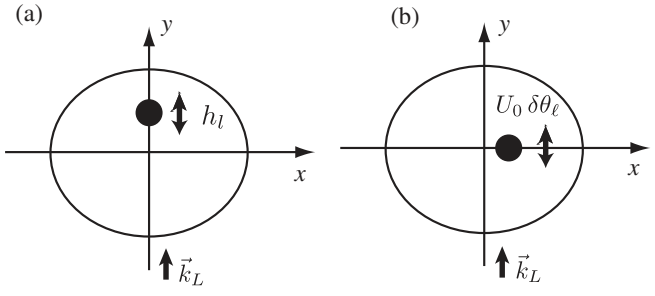

FIG. 37. Illustration showing the coupling mechanism between acoustic phonons and $\mathcal{R}(2)$ guest atoms. (a) The case in which the off-center guest atom takes the far-side position for incident longitudinal (∥) acoustic phonons with the wave vector $\boldsymbol{k}_{\rm ph}$; (b) the $\mathcal{R}(2)$ guest atom is perpendicular to the same longitudinal acoustic phonons. The coupling to parallel components of relevant displacements becomes effective regardless of whether the mode is transverse or longitudinal.

The force constants $f_\parallel$ and $f_\perp$ in Eq. (51) can be obtained from the sound velocities $v_\parallel = 3\,369$ m/s and $v_\perp = 1936$ m/s for type-I $Ba_8Ga_{16}Sn_{30}$ (β-BGS), an off-center system, measured by Suekuni, Avila *et al.* (2008) using $v_\mu = a\sqrt{f_\mu/(m+M)}$, which provides $f_\parallel = 18.1$ N/m and $f_\perp = 5.77$ N/m by employing masses $m = 136$ u for the Ba^{2+} atom and $M = 8.55m$ for the cage, and the lattice spacing between unit cells $a = 11.68$ Å.

The force constants $\tilde{\xi}_\mu$ in Eq. (42) can be determined from optical spectroscopy data since the spectra for optical modes provide the information at $\boldsymbol{k} = \boldsymbol{0}$, namely, at the Γ point. Taking $\boldsymbol{k} \to \boldsymbol{0}$ in Eq. (51) and combining it with Eq. (50), the squared eigenfrequency for optical modes is given by

$$\omega_{0\mu}^2 = \frac{\tilde{\xi}_\mu + m\omega_p^2 L_\mu}{m}\left(1 + \frac{m}{M}\right), \tag{52}$$

where μ denotes the longitudinal or transverse polarization of the optical modes. The electrostatic interaction $V_{\rm dip}$ for off-center systems becomes the same as in the case of on-center BGG.

The force constant $\tilde{\xi}_\mu$ in Eq. (52) for β-BGS off-center systems is obtained from the Raman scattering (Takasu *et al.*, 2006, 2010) and far-infrared spectroscopy (Mori *et al.*, 2009 data, 2011). Mori *et al.* (2009, 2011) observed infrared-active spectra at 7 K, with the lowest-lying peak at 0.71 THz, and with a linewidth broadening of 0.57 THz for β-BGS off-center systems by means of THz time-domain spectroscopy. This spectrum should be assigned to the librational mode of off-center rattling guest ions, which couples with the transverse acoustic mode.

The spectrum of the A_{1g} stretching mode coupled with the longitudinal mode is not observed for β-BGS off-center systems for technical reasons (Takasu *et al.*, 2006; Suekuni *et al.*, 2010). For another type of off-center system, SGG, spectra at 2 K were obtained at 48 cm^{-1}, and for β-EGG off-center systems the spectrum at 36 cm^{-1} for the A_{1g} mode (Takasu *et al.*, 2006; Suekuni *et al.*, 2010). By extrapolating these data, the eigenfrequency of the A_{1g} mode of β-BGS is estimated as $\omega_0/2\pi = 30$ cm^{-1} (= 0.9 THz), from which the force constant $\tilde{\xi}_\parallel$ associated with the longitudinal optical mode can be evaluated. These assignments lead to $\tilde{\xi}_\parallel = 7.32(1 \pm 0.25)$ N/m and $\tilde{\xi}_\perp = 2.21(1 \pm 0.25)$ N/m, taking the plasma frequency $\omega_p/2\pi = 0.09$ THz from Eq. (52). The contribution from this plasma frequency is only 10% at the Γ point.

The calculated dispersion relations for β-BGS off-center systems are given in Fig. 36(b). It is remarkable [see Fig. 36(b)] that the spectral width becomes broader and gapless in the region of avoided crossing. This is attributable to the random orientation of guest atoms.

Experimental far-infrared spectroscopy data at low temperatures (Mori *et al.*, 2009, 2011) for off-center systems provide interesting linewidth broadening features. The spectral width of about 0.57 THz of the lowest-lying infrared-active optical modes 0.71 THz at 7 K decreases with increasing temperature. This feature contradicts the assumption that the anharmonicity of the potential Eq. (39) is a key element for interpreting the origin of the linewidth broadening (Matsumoto *et al.*, 2009).

These experimental results (Mori *et al.*, 2009, 2011) suggest that the random configuration of $\boldsymbol{U}_\ell$ yields the broadening of optical spectra at low temperatures.

The thermal-averaged squared displacements $\langle h_\ell^2 \rangle$ and $\langle \delta\theta_\ell^2 \rangle$ are proportional to temperature T. Raman scattering (Takasu *et al.*, 2006, 2010; Suekuni *et al.*, 2010) and far-infrared spectroscopy (Mori *et al.*, 2009, 2011) experiments have shown that the spectral energies belonging to the lowest band monotonically decrease with decreasing temperature T. These observations can be interpreted by means of thermal-averaged anharmonic terms given by $\langle h_\ell^2 \rangle$ and $\langle \delta\theta_\ell^2 \rangle$ from Eqs. (42) and (43), which are proportional to T at high temperatures under the self-consistent phonon approximation.

Equations (50) and (51) yield the frequency range of the avoided crossing given by

$$\delta\omega_{c\mu} \cong \left[\frac{m}{M}\left(\frac{\bar{\xi}_\mu}{m} + \omega_p^2 L_\mu\right)\right]^{1/2} \cong \omega_{0\mu}\sqrt{\frac{m}{M}}, \tag{53}$$

where the last relation gives a small contribution arising from the plasma frequency compared with the first term in parentheses. This relation is valid since the contribution from the plasma frequency is only 10% of $\omega_{0\perp}$ for β-BGS. Equation (53) indicates that the frequency $\delta\omega_{c\mu}$ at the avoided crossing is governed by the quantities $\omega_{0\mu}$ and the square root of the mass ratio $\sqrt{m/M}$. The frequency $\delta\omega_{c\mu}$ for off-center systems is much smaller than for on-center systems due to the inequality $\bar{\xi}_\mu < \hat{\xi}$.

3. Comparison of calculated dispersion relations to INS experiments

Coherent INS measurements for both BGG and β-BGS were performed in the temperature range from 5 to 290 K using the cold neutron disk-chopper spectrometer AMATERAS installed in the Materials and Life Science Experimental Facility (MLF), Japan Proton Accelerator Research Complex (J-PARC) (Nakamura and Arai, 2010). The results integrated in the range from 0.4 to 0.7 Å^{-1} are given in Fig. 38(a) for BGG and in Fig. 38(b) for β-BGS. These data provide important information on the THz-frequency dynamics of clathrate compounds.

First, for the data on quasi-on-center BGG, Fig. 38(a) shows three sharp peaks at 4.0, 7.5, and 11 meV. The assignments of these spectra can be made in comparison with the results of optical spectroscopies described in Sec. VI.A. The lower peaks at 4.0 and 7.5 meV have been observed in both Raman scattering (Takasu *et al.*, 2006) and infrared spectroscopies (Mori *et al.*, 2009; Iwamoto *et al.*, 2013). These have been assigned as T_{2g} and E_g modes attributable to Ba(2) guest atoms encapsulated in 14-hedrons. The higher spectrum at 11 meV corresponds to Ba(1) guest atoms in 12-hedrons. The lower peak at around 4.0 meV varies considerably with T from 5 to 290 K, while the two higher peaks do not show such a strong temperature dependence. The strong dependence on temperature manifests the relevance of the "wine-glass-type" anharmonic potential employed in Eq. (39) for Ba(2) guest atoms in BGG. Calculated results for dispersion relations for BGG are given in Fig. 36(a).

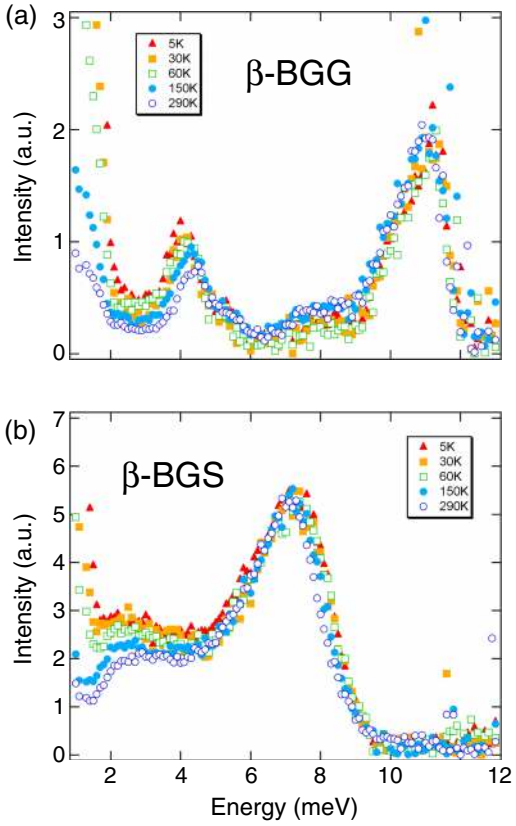

FIG. 38. (color online). Phonon densities of states for both type-I (a) $Ba_8Ga_{16}Ge_{30}$ (BGG) and (b) $Ba_8Ga_{16}Sn_{30}$ (β-BGS) obtained by means of coherent INS experiments in the temperature range from 5 to 290 K. The data provide integrated densities of states from 0.4 to 0.7 Å^{-1} in $\boldsymbol{k}$ space. See text for the assignments of the spectra. From Nakamura and Arai, 2010.

Figure 38(b) for off-center β-BGS shows two peaks at 2–4 and 7 meV. The lower hump arises from the vibrations of Ba (2) guest atoms in the 14-hedrons, and the peak at 7 meV is attributable to Ba(1) guest atoms in the 12-hedrons. There is no clear gap between 2 and 4 meV, which is distinctly different from the result for BGG given in Fig. 38(a). The data in Fig. 38(b) indicate that the lower-energy side of the hump at around 2 meV is more strongly affected by temperature than the higher-energy side at around 4 meV.

The calculations given in Fig. 36(b) clarified the fact that the lower side is concerned with the hybridization between libration vibrations of guest atoms and the transverse acoustic modes from networked cages. At the same time, the higher-energy side of the hump results from the hybridization between the stretching vibrations of guest atoms and the longitudinal acoustic phonons. Thus, the INS data indicate that the libration motion of Ba(2) guest atoms in β-BGS experiences much stronger anharmonicity compared with that of the stretching motion. This is consistent with the view that the thermal-averaged anharmonic term $\langle \delta\theta_\ell^2 \rangle$ in Eq. (43) is large compared with the stretching term $\langle h_\ell^2 \rangle$. This is a reasonable interpretation for the observations in INS experiments by Nakamura and Arai (2010) for BGG and β-BGS.

To conclude this section, we emphasize that the observed densities of states given in Fig. 38 recover the calculations on BGG and β-BGS shown in Fig. 36 very well. In particular, the gapless density of states given in Fig. 38(b) for β-BGS is well reproduced in Fig. 36(b).

4. The origin of boson-peak-like excess density of states

Since the specific heats of type-I clathrate compounds containing off-center guest atoms, for example, β-BGS or SGG, exhibit a hump at around $T \simeq 4$ K, the corresponding modes have been observed by Raman scattering (Takasu *et al.*, 2006, 2010; Kume *et al.*, 2010; Suekuni *et al.*, 2010) and infrared measurements (Mori *et al.*, 2009, 2011).

The relation between the phonon specific heat $C_{\rm ph}(T)$ and the phonon density of states $D(\omega)$ is expressed by

$$C_{\rm ph}(T) = \frac{-1}{k_{\rm B}T^2}\sum_{\mu}\left[\int_0^{\infty}\frac{\partial n_{\rm B}(\beta\hbar\omega)}{\partial\beta}\hbar\omega_{\mu}D(\omega_{\mu})d\omega_{\mu}\right], \quad (54)$$

where $n_{\rm B}$ is the Bose-Einstein distribution function and the inverse temperature is defined by $\beta = 1/k_{\rm B}T$. The density of states $D(\omega)$ can be obtained in principle by inverting Eq. (54) using the observed data for $C_{\rm ph}(T)$, although this procedure involves an uncertainty. However, specific-heat measurements are not affected by the mode-selection rule on excited modes as in the case of optical spectroscopies, in which active modes are distinguished by infrared absorption, Raman scattering, and hyper-Raman scattering experiments. Optical spectroscopies provide information close to the Γ point. These are different from humps observed in specific heats that represent averaging over a wide sector of $\boldsymbol{k}$ space.

The characteristic frequency of guest atoms in cages is much smaller than the Debye frequency $\omega_{\rm D}$ expressing the upper limit of propagating acoustic phonons of the network cages without guest atoms. The coupling of guest atoms and cages yields the hybridization of dispersion curves and creates the flat and broad band. This is the origin of the boson-peak-like mode observed in type-I clathrate compounds containing off-center guest atoms. Thus, the flat band with broad spectra at around 0.5 THz shown in Fig. 36(b) is the origin of the boson-peak-like excess density of states.

VIII. GLASSLIKE SPECIFIC HEATS BELOW 1 K

A. Low-temperature specific heats and two-level tunneling states

1. Two-level tunneling model

In off-center type-I clathrate compounds, the disorder is introduced by randomly oriented guest atoms. This is the origin of glasslike specific heats observed for off-center systems at low temperatures. At $T \lesssim 1$ K, a quantum-mechanical description is needed to describe the states contributing to T-linear specific heats. For structural glasses, it was postulated that an atom or a group of atoms can occupy one of two potential minima (Anderson, Halperin, and Varma, 1972; Phillips, 1972); see the reviews by Hunklinger and Raychaudhuri (1986) and Phillips (1987). Each tunneling state can be simply represented by assuming a double-well potential shown in Fig. 39, where the abscissa gives the position of the tunneling element in multidimensional configuration space. This tunneling model provides a good phenomenological basis on which various observations can be consistently explained. It should be emphasized that the idea of a double-well potential is based on the adiabatic approximation. This is acceptable since the wavelengths of excited acoustic phonons below 1 K are sufficiently larger than the scale of tunneling elements. The THz-frequency dynamics attributable to the hybridization between local vibrations of guest atoms and acoustic phonons due to network cages should take into account the nonadiabatic aspect as described in Sec. VII.

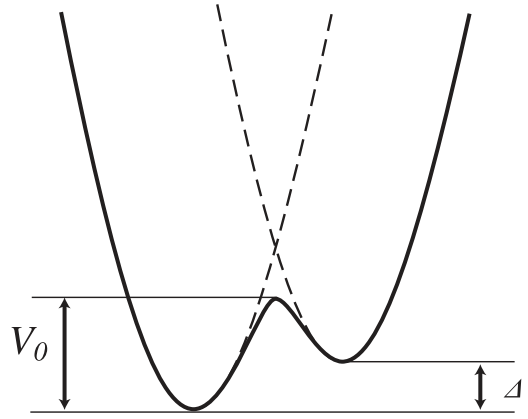

FIG. 39. Schematic illustration of a double-well potential representing the two-level tunneling state.

We choose a basis set of (φ_1, φ_2) of the appropriate potentials V_1 and V_2 belonging to ground energies (E_1, E_2). By taking the zero of energy as the mean of E_1 and E_2, the Hamiltonian matrix becomes

$$\mathcal{H} = \frac{1}{2}\begin{pmatrix} -\epsilon & \Delta \\ \Delta & \epsilon \end{pmatrix}, \quad (55)$$

where the tunnel splitting Δ due to the overlap of the wave functions is given by

$$\Delta = 2\langle\varphi_1|H|\varphi_2\rangle. \quad (56)$$

The overlap integral Δ generally involves an exponential decay given by

$$\Delta = \hbar\Omega e^{-\lambda} = \hbar\Omega e^{-\ell\sqrt{2mV_0}/\hbar}, \quad (57)$$

where $\hbar\Omega$ is approximately equal to $(E_1 + E_2)/2$, while ℓ and V_0 are the separation and the barrier height between the two wells, and m is the mass of the tunneling element. Typical values of the tunneling parameter λ can be estimated from the requirement that Δ must be approximately equal to $k_{\rm B}T$ if the tunneling states predominantly contribute to thermal properties at temperature T. This requires, for example, $\Delta \cong 1$ K at 1 K, which gives approximately 5 for λ with $\hbar\Omega$ equal to 100 K.

For off-center guest atoms, the overlapping integral Δ is due to the angular rotation of off-center guest atoms given by

$$\Delta = \hbar\Omega e^{-\sqrt{2IV_0}\delta\theta/\hbar}, \quad (58)$$

where the moment of inertia $I = 25.4$ u Å^2 for β-BGS. The zero-point energy scale $\hbar\Omega$ of the guest atom trapped in one of four local-potential minima is estimated, from the uncertainty principle, to be $\hbar\Omega \approx 4.6$ K for an actual spatial size $\approx (0.3$ Å$)^3$ for β-BGS. This energy scale $\hbar\Omega \approx 4.6$ K $(= 4$ meV$)$ is comparable with that of the boson-peak-like hump in β-BGS observed from specific heats and spectroscopic measurements.

The Hamiltonian matrix of Eq. (55) provides eigenvalues

$$E = \pm\tfrac{1}{2}(\epsilon^2 + \Delta^2)^{1/2}. \quad (59)$$

The distribution function of ϵ must be an even function because both the positive and negative values of ϵ are equally likely. The range of energy variation of ϵ is determined by the thermal energy at which atoms or molecules become free from the constraint of neighboring atoms. In structural glasses, this corresponds to the glass-transition temperature T_g. The glass-transition temperature obeys Tammann's rule of the form $T_g \cong 2T_{\rm melt}/3$ K. Thus, the distribution function $f(\epsilon, \Delta)$ is a reasonably slowly varying function of ϵ in the range of interest 10 mK $< \epsilon/k_{\rm B} <$ 1 K, so that $f(\epsilon, \Delta)$ can be taken as independent of ϵ. Because of the exponential dependence of Δ on λ, only a relatively small range of λ is sampled for a large range of Δ.

Note that ϵ expresses the asymmetry energy of *two-level* systems, i.e., the thermal activation energy needed for the rearrangement of local microscopic structures in the regime $\epsilon/k_{\rm B} \gg 1$ K. Thus, ϵ does not manifest the energies of the excess density of states related to the boson peak observed at 3–10 K for structural glasses.

2. Specific heats below 1 K

By introducing the density of states $n(E)$ per volume per unit of energy, the specific heat at low temperatures is given by

$$C_{\rm tun}(T) = \frac{1}{4k_{\rm B}T^2}\int_0^{\Delta_0/2} n(E)E^2 {\rm sech}^2\left(\frac{\beta E}{2}\right)dE, \quad (60)$$

where $\beta = (k_{\rm B}T)^{-1}$. The form of the distribution function $n(E)$ is not known *a priori*, but $n(E)$ should be a continuous function in the temperature regime $T \ll \Delta_0/k_{\rm B}$, where Δ_0 is the upper bound of E.

If we employ a simpler view in which the states are distributed uniformly from $-\Delta_0/2$ to $\Delta_0/2$ such as $n(E) = \bar{N}/\Delta_0$, where $\bar{N}$ is the number density of tunneling states per volume, Eq. (60) yields at $T \ll \Delta_0/k_{\rm B}$,

$$C_{\rm tun} \cong \frac{\pi^2\bar{N}}{3\Delta_0}k_{\rm B}^2 T. \quad (61)$$

Above 1 K, the part of the asymmetry energy ϵ in Eq. (59) is a dominant term in Eq. (61). In this case, using observed values of specific heats of silica glass of $C_{\rm tun} \cong 2.5 \times 10^{-4}$ mJ cm^{-3} K^{-1} at $T = 0.1$ K and the upper bound of $\Delta/k_{\rm B} \cong 1$ K in Eq. (61), the number density of tunneling states is estimated as $\bar{N} \cong 10^{17}$ cm^{-3}. Therefore, in silica glass only 10^{-5} states per SiO_2 element contribute to tunneling (Kittel, 2005).

The structural glasses are in nonequilibrium states, so that observed specific heats should vary logarithmically with the measuring time, implying the relaxation in a multivalley potential in configuration space (Anderson, Halperin, and Varma, 1972; Phillips, 1972). Here we do not enter into the details of this interesting phenomenon. One can find the expressions for specific heats involving relaxation time τ in Hunklinger and Raychaudhuri (1986) and Phillips (1987).

The two-level tunneling model provides a good phenomenological picture of observed universal phenomena. However, it is difficult to identify the tunneling entity in glasses due to its structural complexity. Compared with structural glasses, type-I clathrate compounds containing off-center guest atoms are microscopically well defined, and it is possible to identify the tunneling entity on an atomic scale. This is the major goal of Sec. VIII.

3. Failure of the noninteracting picture for tunneling elements

One of the important features of type-I clathrate compounds found in experiments (Nolas *et al.*, 1995, 1996; Sales, Mandrus, and Williams, 1996; Nolas, Slack *et al.*, 1998; Nolas, Cohn *et al.*, 1998; Nolas, Cohn, and Slack, 1998; Sales, 1998; Cohn *et al.*, 1999; Nolas, Weakley *et al.*, 2000; Nolas, Sharp, and Goldsmid, 2001; Sales *et al.*, 2001; Bentien *et al.*, 2004, 2005; Avila, Suekuni, Umeo, and Takabatake, 2006; Avila, Suekuni, Umeo, Fukuoka *et al.*, 2006; Suekuni *et al.*, 2007, 2010; Suekuni, Avila *et al.*, 2008; Suekuni, Yamamoto *et al.*, 2008; Xu *et al.*, 2010) is that guest atoms take either the on-center or off-center position depending on the size of cages or, equivalently, the ionic radii of guest atoms.

A typical deviation $r_0 = 0.43$ Å in β-BGS has been obtained from diffraction experiments (Avila, Suekuni, Umeo, Fukuoka *et al.*, 2006; Avila *et al.*, 2008). p-type BGG is slightly off center by 0.15 Å (Christensen *et al.*, 2006; Jiang *et al.*, 2008). In this connection, it should be noted that n-type BGG shows crystal-like thermal conductivity, while p-type BGG behaves with glasslike thermal properties (Avila, Suekuni, Umeo, and Takabatake, 2006; Avila *et al.*, 2008). This is one piece of evidence showing that the long-range dipole interaction plays a crucial role in type-I clathrates, since the Coulomb interaction between the cages and the guest cation Ba^{2+} in BGG is shielded in n-type electron-rich BGG, while the dipole interaction in p-type BGG becomes relevant even for small dipole moments. The network configuration consisting of off-center guest atoms is schematically illustrated in Fig. 40.

At first glance, individual off-center guest atoms seem to independently contribute to glasslike thermal properties at low temperatures. This naive view misleads in that it suggests that an isolated noninteracting picture could explain the observed glasslike behaviors. Such a noninteracting picture does not reproduce the observed temperature dependence or the magnitudes of the specific heats for type-I clathrate compounds with off-center guest atoms at 1 K and below (Nakayama and Kaneshita, 2008). In fact, as discussed in Sec. VIII.B, the tunneling between the nearby potential minima in

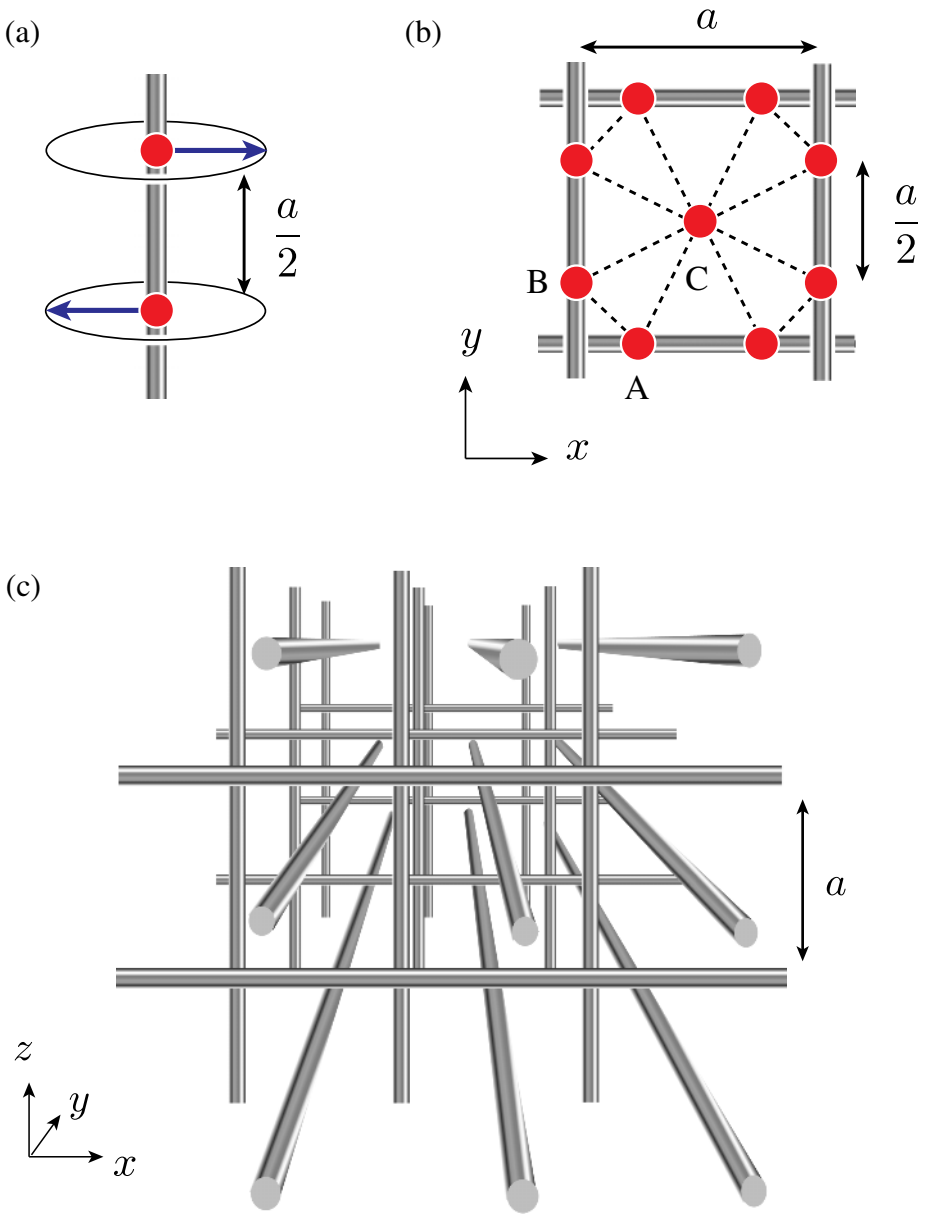

FIG. 40 (color online). Schematic illustration of the configuration of the guest atoms in the oversized cages in β-BGS. The fourfold inversion axes are directed along x, y, and z. (a) The deviation from the on-center position (filled circles) induces the electric dipoles (arrows). Here two nearest dipoles are depicted. The electric dipoles rotate in the plane perpendicular to the axis linking the nearest dipoles. (b) The configuration of the on-center positions of the guest atoms. The filled circles represent the positions of off-center guest atoms, around which the electric dipoles are induced. The sites A, B, and C in (a) are seated on the chains parallel to x, y, and z, respectively: $A = (a/4, 0, a/4)$, $B = (0, a/4, 3a/4)$, and $C = (a/2, a/2, a/2)$. The distance between the next-nearest neighbors (dashed lines) is $\sqrt{3/8}a$. Note that these three dipoles constitute an *equilateral triangle* and easily generate a frustrated situation. (c) The 3D configuration of the dipole chains is illustrated.

configuration space generated by a combination of interacting dipoles is crucial for interpreting glasslike thermal properties at low temperatures.

In an isolated noninteracting picture, the problem is reduced to the state of a single cage where $\mathcal{R}(2)$ guest atoms experience a *hindering* potential $V_h(\theta)$ along the azimuthal direction (Nolas, Sharp, and Goldsmid, 2001; Sales *et al.*, 2001). The barrier height of the hindering potential V_h between nearby potential wells is estimated to be of the order of 10 K. Actually, first-principles calculations have shown V_h to be $\cong 20$ K for $Sr^{2+}(2)$ guest atoms in SGG (Madsen and Santi, 2005).

The separation of neighboring wells is small, for example, $\pi U_0/2 = 0.67$ Å in β-BGS. This allows the $\mathcal{R}(2)$ guest atom to tunnel to a nearby potential minimum at lower temperatures than the barrier height $T \ll V_h/k_B$, where the off-center guest atom executes zero-point motion at one of the wells with an energy $\hbar\Omega$.

The tunneling splitting Δ due to the angular rotation of off-center guest atoms is given by

$$\Delta = \hbar\Omega e^{-\sqrt{2IV_h}\delta\theta/\hbar}, \tag{62}$$

where $\delta\theta \le \pi/2$ is the angle between two nearby minima. Since the zero-point energy $\hbar\Omega$ of the guest atom is estimated to be $\hbar\Omega \approx 4.6$ K for β-BGS, we can estimate the most probable lower bound as $\Delta_{\min} = 0.03$ K by using the hindering potential height $V_h(\theta) \approx 10$ K and the moment of the inertia of dipoles $I = 25.4$ u Å^2 for β-BGS in Eq. (62).

The lower bound of the integral in Eq. (60) should be $\Delta_{\min}/2$. Introducing the dimensionless variable x defined by $x = E/(2k_BT)$, the function $x^2\mathrm{sech}^2(x)$ in the integrand of Eq. (60) has a maximum at around $x = 1$. The contribution to the integral of the product of $x^2\mathrm{sech}^2(x)$ and $n(2xk_BT)$ should become sharply smaller at temperatures below $T \lesssim \Delta_{\min}/k_B \approx 0.03$ K, but the experimental data on specific heats for type-I clathrate compounds do not show this tendency.

Furthermore, the isolated noninteracting picture is based on the idea that every off-center guest atom contributes to the specific heat. Taking the distribution function $n(E) = \bar{N}/\Delta_0$ with $\Delta_0/k_B \approx V_h/k_B \approx 20$ K and $\bar{N} = 6$, where six is the number of guest atoms in a unit cell of β-BGS, Eq. (60) becomes

$$C_{\mathrm{tun}} \cong 1.0 \times 10^4 T \ [\mathrm{mJ\,mol^{-1}\,K^{-1}}], \tag{63}$$

which is 2 orders of magnitude larger than the observed value for β-BGS $C_{\mathrm{tun}} \cong 30T$ mJ mol^{-1} K^{-1} (Suekuni, Avila *et al.*, 2008; Suekuni, Yamamoto *et al.*, 2008). Thus, the noninteracting picture based on the assumption that every off-center guest ion independently contributes to the tunneling states yields a specific heat $C_{\mathrm{tun}}(T)$ of 2 orders of magnitude larger than the observed values at 1 K, in conflict with observations. It is therefore not reasonable to employ the noninteracting picture to explain glasslike properties of type-I clathrate compounds observed at $T \lesssim 1$ K (Nakayama and Kaneshita, 2008).

B. Interacting dipoles in type-I clathrate compounds

1. Multivalley potentials in configuration space

In type-I clathrate compounds with divalent guest ions, the deviation of the guest ion from the center of the cage induces an *electric dipole moment* due to the difference of the charges between the guest atom with charge $+2e$ and the ion with charge $-e$ constituting cages. The strength of the electric dipole moment can be estimated to be $p = 4.1$ D in the case of β-BGS with the deviation $U_0 = 0.43$ Å from the center. The deviation is about 7.2% of the distance between the neighboring 14-hedrons ($a/2 = 5.84$ Å, where a is the lattice constant). Thus, the cages with off-center guest atoms intrinsically possess electric dipoles, and it is crucial to take these characteristics into account; see Fig. 41.

Bentien *et al.* (2005) pointed out, from crystallographic studies (Bentien *et al.*, 2000, 2002) and thermal conductivity measurements (Bentien *et al.*, 2004), that the Ba(2) guest can be off center in p-type $Ba_8Ga_{16}Ge_{30}$. Avila, Suekuni, Umeo, Fukuoka *et al.* (2006) found that p-type BGG shows crystallike thermal conductivity, while n-type BGG behaves as glasslike. This indicates that the long-range interaction between divalent guest atoms becomes relevant owing to antishielding by doped holes in p-type BGG, while n-type BGG has the opposite tendency. p-type BGG is slightly off center by 0.15 Å (Christensen *et al.*, 2006; Jiang *et al.*, 2008) with much smaller dipole moments compared with the case of β-BGS. This is one piece of evidence showing that the long-range dipole interaction is crucial for interpreting the thermal properties of type-I clathrates since the Coulomb interaction between the cation guest ion Ba^{2+} in BGG is shielded in n-type electron-rich BGG, while the dipole-dipole interaction in p-type BGG becomes relevant even for small dipole moments.

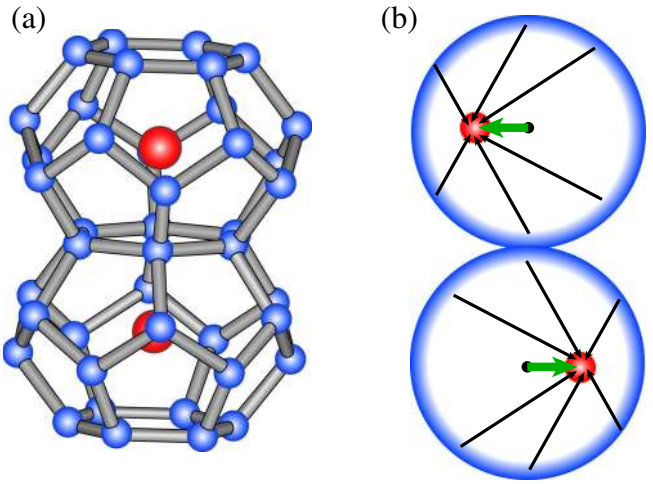

FIG. 41 (color online). (a) Illustration of two 14-hedron cages along the z direction consisting of anions and guest cations. (b) The cage (outer circle) and the symmetry-broken off-center guest atom compose an effective electric dipole moment (thick arrow), which is the vector sum of each dipole (thin arrow).

In type-I clathrate compounds, off-center guest atoms are in 14-hedron cages, and the nearest-neighbor off-center guest atoms are located in the next two 14-hedron cages, which share the same fourfold inversion axis. The fourfold inversion axes are directed along the x, y, and z axes due to the cubic symmetry of β-BGS, as illustrated in Fig. 40(a). The key for yielding glasslike behavior is that these dipoles constitute an equilateral-triangle structure among next-nearest-neighbor dipoles, as depicted in Fig. 40(b). This configuration generates a frustrated situation necessary for the emergence of glasslike behavior below 1 K.

To make our argument clear, we consider two electric dipoles $\boldsymbol{p}_\ell$ and $\boldsymbol{p}_m$ separated by a distance $|\boldsymbol{R}_{\ell m}|$. The dipolar interaction is given by the following form:

$$V_{\ell m} = \frac{1}{4\pi\varepsilon_r|\boldsymbol{R}_{\ell m}|^3}[\boldsymbol{p}_\ell\cdot\boldsymbol{p}_m - 3(\boldsymbol{p}_\ell\cdot\hat{\boldsymbol{R}}_{\ell m})(\boldsymbol{p}_m\cdot\hat{\boldsymbol{R}}_{\ell m})], \tag{64}$$

where ε_r is the dielectric constant of the clathrate, and $\hat{\boldsymbol{R}}_{\ell m} = \boldsymbol{R}_{\ell m}/|\boldsymbol{R}_{\ell m}|$ is a unit vector. The potential function for two coupled dipoles $\boldsymbol{p}_1$ and $\boldsymbol{p}_2$ along an axis becomes $V_{12} = V_h(\theta_1) + V_h(\theta_2) + W_{12}(\theta_1,\theta_2)$ with $W_{12} = p^2\cos(\theta_1-\theta_2)/4\pi\varepsilon_r R_{12}^3$, where two global minima (maxima) in (θ_1,θ_2) configuration space appear at $|\theta_1-\theta_2| = \pi(2\pi)$ since the

dominant term for a nearest-neighbor pair is the first term in Eq. (64). This configuration acts as a new hindering potential in addition to the fourfold inversion-symmetric potential V_h. This argument can be straightforwardly extended to the case of multiple pairs, providing many potential minima in configuration space $\mathcal{P} = (\theta_1, \theta_2, \theta_3, \ldots)$, where the potential function is $V_{123\ldots} = \sum V_h(\theta_\ell) + \sum V_{\ell m}$.

The energy scale of the dipole-dipole interactions between nearest neighbors is given by its maximum value,

$$J_1 = \frac{p^2}{4\pi\varepsilon_r R_1^3}, \tag{65}$$

where R_1 is the distance between the nearest neighbors. The actual distance between nearest-neighbor guest atoms in β-BGS is $R_1 = a/2 = 5.84$ Å. The characteristic energy scale for nearest-neighbor coupling is then estimated as $J_1 \cong 6\varepsilon_r/\varepsilon_0$ [K]. Taking into account the dielectric constant for semiconductors in the range $5 \lesssim \varepsilon_r/\varepsilon_0 \lesssim 20$, it turns out that $\mathcal{R}(2)$ guest atoms experience strong electric fields. The energy scale of the dipole-dipole interaction is estimated to be of the order of a few tens of kelvin. They are no longer regarded as isolated dipoles. Combining the fourfold inversion symmetry of dipoles with the frustrated situation due to the equilateral triangle [see Fig. 40(b)], many local minima are created in a hierarchical potential map in configuration space $\mathcal{P}$, where tunneling should occur in a multivalley potential in configuration space with simultaneous local structural rearrangements of an appropriate number of guest atoms. See the illustration of the multivalley potential depicted in Fig. 42.

2. Explicit form of specific heats below 1 K

The range of the energy distribution $n(E)$ can be determined from the energy at which the dipoles become free from the constraint of neighboring dipoles. The maximum coupling strength with neighbor dipoles is $\Delta_0 \cong z_1 J_1 + z_2 J_2 \cong 6J_1$ with configuration numbers $z_1 = 2$ and $z_2 = 8$ ($J_3 \ll J_1, J_2$). We introduce the ratio between the number of tunneling states $\bar{N}$ and the total number of off-center guest atoms N given by

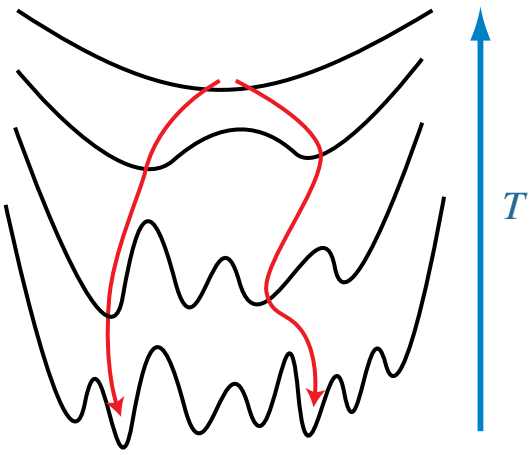

FIG. 42 (Color online) (color online). Schematic illustration of free-energy landscape representing nonequilibrium states.

$\eta = \bar{N}/N < 1$. Since $\bar{N}/J_1 = 3\pi\varepsilon_r\eta/p^2$ using $R_1 = a/2$ in Eq. (65), Eq. (61) assumes the simple form

$$C_{\rm tun} \cong \frac{6\pi^3\varepsilon_r\eta}{p^2} k_{\rm B}^2 T. \tag{66}$$

Equation (66) predicts larger specific heats for smaller dipole moments p, but η vanishes as $p \to 0$ (Nakayama and Kaneshita, 2008).

A carrier-type dependence on $C_{\rm tun}(T)$ was observed by Suekuni, Avila *et al.* (2008) for n-type and p-type β-BGS with deviations $U_0 = 0.434$ and 0.439 Å, respectively. The observed $C_{\rm tun}(T)$ below 1 K for n-type β-BGS is a few percent larger than that of the p type, as shown in Fig. 18. This is in accordance with the prediction of Eq. (66).

A comparison of Eq. (66) with the observed magnitude of the specific heat $C_{\rm tun}(T) \cong 30T$ mJ mol^{-1} K^{-1} below 1 K for β-BGS (Suekuni, Avila *et al.*, 2008; Suekuni, Yamamoto *et al.*, 2008) provides important information on the tunneling states. Taking $\varepsilon_r \cong 10\varepsilon_0$, η becomes $\cong 0.06$ from $C_{\rm tun}(T) \cong 50(\varepsilon_r/\varepsilon_0)\eta T$ mJ mol^{-1} K^{-1}. This indicates that only 6% of the off-center guest ions contributes to the specific heats on average. This implies that the averaged number of dipoles simultaneously rearranged by tunneling is $1/\eta \cong 20$.

The formulation of the specific heat from Eq. (66) is based on the tunneling states caused by the dipole-dipole interaction; thus $C_{\rm tun}(T)$ vanishes when the dipole-dipole interaction becomes irrelevant. This explains why the specific heats of on-center clathrate compounds show the Debye specific heat at low temperatures.

3. Tunneling states in alkali-halide crystals containing CN^- ions

Section VIII.B.2 highlighted the role of off-center dipoles in type-I clathrate compounds. In this connection, we mention the low-temperature thermal properties of alkali-halide crystals containing CN^- ions which provide good examples showing the relevance of long-range dipole-dipole interactions. The alkali-halide mixed crystals have served as a model for the exploration of the low-energy excitations characteristic of structural glasses (Narayanamurti and Pohl, 1970; De Yoreo *et al.*, 1986; Loidl *et al.*, 1988; Winterlich, Böhmer, and Loidl, 1995; Topp and Pohl, 2002). The low-temperature thermal properties of $(KBr)_{1-x}(KCN)_x$ single crystals in the range of $0.25 \le x \le 0.70$ were investigated by De Yoreo *et al.* (1986) and Topp and Pohl (2002).

Although $(KBr)_{1-x}(KCN)_x$ is crystalline, it is disordered in two ways. The CN^- ions and the Br^- ions are randomly distributed over the anion sublattice. This disorder by itself is unlikely to produce emergence of a glasslike behavior since mixed crystals such as KBr : KI involve the same disorder, but do not show glasslike behavior (Nathan, Lou, and Tait, 1976). In the case of KBr:KCN, the CN^- molecules are disordered with respect to their orientations in the cubic lattice.

The observed specific heats are well described by the relation given in Eq. (28). For $x = 0.25$, 0.50, and 0.70, the values of the small factor δ giving the best fit for the long-time data are $\delta = 0.03$, 0.00, and 0.08, respectively. The observed values of specific heats below 1 K for the case of $x = 0.25$ yield the number density of $\bar{N} \cong 10^{17}$ cm^{-3}. This is

evidence that all CN^- elements do not contribute to tunneling states, as in the case of off-center clathrate compounds described in Sec. VIII.B.2. The role of long-range interactions between elastic dipoles randomly distributed in crystals has been theoretically investigated (Randeria and Sethna, 1988; Grannan, Randeria, and Sethna, 1990a, 1990b).

We mention the INS experiments performed for the KCN:CN system by Walton, Mook, and Nicklow (1974). They observed at 5 K a clear anticrossing of the acoustic phonon dispersion relation between 0.4 and 0.5 THz corresponding to T_{1u} and T_{2u} modes of a CN^- molecule in a KCl crystal doped with $6\times10^{19}CN^-$ [cm^{-3}]. However, the anticrossing was not observed at room temperature. The strong dependence of INS intensities on temperature indicates that the coupling between acoustic phonons and libration modes of CN^- depends on the state of the CN^- molecule, namely, the libration modes are well characterized at low temperatures compared with those at room temperature.

IX. UNDERLYING MECHANISMS OF GLASSLIKE THERMAL CONDUCTIVITIES

The reduction of phonon thermal conductivities $\kappa_{\rm ph}(T)$ is the key element in increasing the dimensionless figure of merit ZT according to the phonon-glass electron-crystal concept (Slack, 1995). Berman (1949) discovered in structural glasses an unexpected anomaly of $\kappa_{\rm ph}(T)$. He measured $\kappa_{\rm ph}(T)$ of several samples of silica glass in the temperature range 2.2–90 K and found plateau behavior in the temperature range 5–10 K with a magnitude several orders of magnitude smaller than that of crystal silica. However, these properties attracted little attention until the work of Zeller and Pohl (1971), who discovered three characteristic temperature regions: (i) $\kappa_{\rm ph}(T)\propto T^{2-\delta}$ below 1 K, (ii) a plateau region of $\kappa_{\rm ph}(T)$ at around 5–10 K, and (iii) $\kappa_{\rm ph}(T)$ shows a T-linear rise subsequent to the plateau region above 10 K. The same features of $\kappa_{\rm ph}(T)$ have been found for a variety of glasses and amorphous materials (Zeller and Pohl, 1971; Freeman and Anderson, 1986; Graebner, Golding, and Allen, 1986).

Nolas, Cohn *et al.* (1998) pointed out that the $\kappa_{\rm ph}(T)$ of off-center SGG polycrystalline samples behaves like those of structural glasses. The same characteristics have been observed for other type-I clathrate compounds containing off-center guest atoms (Nolas *et al.*, 1995, 1996; Sales, Mandrus, and Williams, 1996; Nolas, Slack *et al.*, 1998; Nolas, Cohn *et al.*, 1998; Nolas, Cohn, and Slack, 1998; Sales, 1998; Cohn *et al.*, 1999; Nolas, Weakley *et al.*, 2000; Nolas, Sharp, and Goldsmid, 2001; Sales *et al.*, 2001; Bentien *et al.*, 2004, 2005; Avila, Suekuni, Umeo, and Takabatake, 2006; Avila, Suekuni, Umeo, Fukuoka *et al.*, 2006; Suekuni *et al.*, 2007, 2010; Suekuni, Avila *et al.*, 2008; Suekuni, Yamamoto *et al.*, 2008; Xu *et al.*, 2010), where the temperature dependence and the magnitude of $\kappa_{\rm ph}(T)$ are almost identical to those of structural glasses; these are the power law of $\kappa_{\rm ph}(T)\propto T^{2-\delta}$ in the temperature below $T\simeq1$ K, the plateau-temperature region at $T=$ 1–10 K, and the subsequent rise of $\kappa_{\rm ph}(T)$ proportionally to T at the high-temperature end of the plateau.

This section describes theoretical interpretations taking into account the quantum-mechanical aspects of these unique behaviors observed in type-I clathrate compounds that are off-center systems.

A. Thermal conductivities below 1 K

$\kappa_{\rm ph}(T)$ can be evaluated on the assumption that heat is carried by acoustic phonons obeying linear dispersion relations. This is expressed by

$$\kappa_{\rm ph}(T)=\frac{1}{3}\sum_{\mu}\int_0^{\omega_{c\mu}}\hbar\omega_\mu\frac{\partial n_{\rm B}}{\partial T}v_\mu^2\tau_\mu(T,\omega)D(\omega_\mu)d\omega_\mu, \quad (67)$$

where $n_{\rm B}$ is the Bose-Einstein distribution function, and $D(\omega_\mu)$, $v_\mu=\partial\omega_\mu(k)/\partial k$, and τ_μ are the Debye density of states, the group velocity, and the lifetime of acoustic phonons of the mode μ, respectively. Note that Matthiessen's rule for the lifetime $1/\tau_\mu=\sum_i 1/\tau_i$ should hold for the independent scattering process i.

The cutoff frequency $\omega_{c\mu}$ is the crossover frequency from linear dispersion to flat dispersion of acoustic phonons of the mode μ, at which the group velocity v_μ of acoustic phonons of the mode μ almost vanishes. At temperatures below 1 K, this cutoff frequency becomes irrelevant, whereas it becomes crucial above 1 K.

For type-I clathrates with off-center guest atoms at $T\lesssim1$ K, the predominant scattering arises from the interaction between tunneling states and thermally excited acoustic phonons. The scattering rate of a phonon of the mode μ due to the interaction with a tunneling state is given by (Phillips, 1987)

$$\frac{1}{\tau_\mu(\omega)}=\sum_E\frac{\pi g_\mu^2\omega_\mu}{\rho v_\mu^2}\left(\frac{\Delta}{E}\right)^2\tanh\left(\frac{\beta\hbar\omega}{2}\right)\delta(\hbar\omega-E), \quad (68)$$

where g_μ is the deformation coupling constant and ρ is the mass density ($\rho=6.01\times10^3$ kg m^{-3} for β-BGS). The averaging procedure by the distribution function $f(\varepsilon,\lambda)$ defined in Sec. VIII.A.1 can be simplified by replacing $\sum_E\delta(\hbar\omega-E)\to\int n(E)dE$ as in the case of Eq. (60). The dominant tunneling process occurs at $\Delta\cong E$; then Eq. (68) provides

$$\frac{1}{\tau_\mu(T,\omega)}=\frac{\pi^2g_\mu^2\omega_\mu}{2\rho v_\mu^2}\left(\frac{\varepsilon_r\eta}{p^2}\right)\tanh\left(\frac{\beta\hbar\omega}{2}\right), \quad (69)$$

where the density of states is taken as $\bar{N}/\Delta_0\cong\pi\varepsilon_r\eta/2p^2$ due to the interacting-dipole picture given in Sec. VIII.B.2. By combining the above scattering rate with Eq. (67), $\kappa_{\rm tun}(T)$ becomes

$$\kappa_{\rm tun}(T)\cong\frac{\rho k_{\rm B}^3v_s}{2\pi^2\hbar^2g^2(\varepsilon_r\eta/p^2)}T^2, \quad (70)$$

where the velocity v_s and the deformation coupling constant g refer to the average values for the three modes of acoustic phonons. A more convenient form involving the specific heat $C_{\rm tun}$ is obtained as

$$\kappa_{\rm tun}(T)\cong\left(\frac{3\pi\rho v_s\eta k_{\rm B}^3}{\hbar^2C_{\rm tun}/T}\right)\left(\frac{T}{g/k_{\rm B}}\right)^2. \quad (71)$$

This relation suggests that the thermal conductivities $\kappa_{\rm tun}(T) \propto T^{2-\delta}$ with the small factor δ reflecting $C_{\rm tun}(T) \propto T^{1+\delta}$ (Kaneshita and Nakayama, 2009). The small factor δ originates from the distribution function $f(\epsilon,\lambda)$ as discussed in Sec. VIII.B.2. Equation (71) predicts that the magnitude of $\kappa_{\rm tun}(T)$ should be proportional to the inverse of $C_{\rm tun}(T)$, namely, $\kappa_{\rm tun}(T) \to$ small when $C_{\rm tun}(T) \to$ large. This relation holds for $\kappa_{\rm tun}(T)$ of n-type and p-type β-BGS as observed in Figs. 7 and 18.

We employ the following physical parameters of β-BGS. The average value of v_μ is $v_s = 2.3 \times 10^3$ m s^{-1} from the actual values of velocities, $v_{C_{11}} = 3369$ m s^{-1}, $v_{C_{11}-C_{12}} = 1969$ m s^{-1}, and $v_{C_{44}} = 1844$ m s^{-1}. These yield

$$\kappa_{\rm tun}(T) = 2.0 \times 10^5 \left(\frac{T}{g/k_{\rm B}}\right)^2 [\mathrm{W\,K^{-1}\,m^{-1}}]. \qquad (72)$$

Using the experimental data of $\kappa_{\rm tun}(T) \cong 0.02T^2$ W K^{-1} m^{-1} for β-BGS (Suekuni, Avila *et al.*, 2008), the deformation coupling g is estimated as $g \simeq 0.3$ eV. This is a reasonable value because the deformation coupling constants g in glasses are in the range of 0.1–1 eV (Anderson, Halperin, and Varma, 1972; Phillips, 1972).

B. Plateau region of thermal conductivities at around 5 K

For off-center type-I clathrate compounds, some mechanisms have been proposed to explain $\kappa_{\rm ph}(T)$ in the plateau-temperature region (Dong, Sankey, and Myles, 2001; Bridges and Downward, 2004; Hermann, Grandjean, and Long, 2005; English and Tse, 2009; English, Gorman, and MacElroy, 2012). Bridges and Downward (2004) argued for a mechanism for plateau thermal conductivities of off-center clathrate compounds. Hermann, Grandjean, and Long (2005) considered the role of Einstein oscillators in filled skutterudites with the aim of explaining their lattice dynamics. Dong, Sankey, and Myles (2001) performed MD calculations for $\kappa_{\rm ph}(T)$ on clathrate compounds with and without guest atoms in cages. The addition of guest atoms in cages produced a reduction of phonon thermal conductivity. English and Tse (2009) investigated the mechanism for $\kappa_{\rm ph}(T)$ in methane hydrate, which shows the same plateau-temperature region do off-center clathrate compounds. These works employed MD calculations combined with the linear response formula for $\kappa_{\rm ph}(T)$, not taking into account quantum aspects such as the annihilation or creation of acoustic phonons via anharmonic interactions. The importance of the three-phonon process, the umklapp process, was first indicated by Peierls (1929) to explain the peak of $\kappa_{\rm ph}$ observed at about 10 K for crystals. MD calculations at the present stage cannot reproduce these quantum processes. This is the most difficult task in MD calculations on heat-transport simulations.

1. Umklapp process for on-center systems

Type-I clathrate compounds belonging to on-center systems possess the symmetry of translational invariance. This implies that the wave vector $\boldsymbol{k}$ of acoustic phonons carrying heat is well defined in the whole Brillouin zone. Acoustic phonons are scattered mainly by two mechanisms: Rayleigh elastic scattering due to imperfections and the anharmonic phonon-phonon inelastic scattering. The Rayleigh scattering due to the static imperfections proportional to $1/\tau_{\rm R}(\omega) \propto \omega^4$ does not become the dominant scattering mechanism in type-I clathrate compounds. This is because the wavelength of excited phonons is much larger than the scale of imperfections. So we have the situation $v_\mu \tau_\mu(T,\omega) > L$ at low temperatures, where L is the size of the crystalline part. This leads to $\kappa_{\rm ph}(T) \propto C_{\rm ph} \propto T^3$ for on-center type-I clathrate compounds.

With increasing temperature above 1 K, the wave vectors of thermally excited phonons approach the middle of the Brillouin zone, and the umklapp process starts to contribute to the decrease of $\kappa_{\rm ph}(T)$ at around $T \sim 10$ K; see Figs. 14 and 16.

Coherent INS data for on-center BGG given in Fig. 29 show that the avoided crossings for transverse acoustic phonons occur at $|\boldsymbol{k}| \gtrsim |\boldsymbol{G}|/4$ with the reciprocal lattice vector $\boldsymbol{G}$. This allows the umklapp process $\boldsymbol{k}_1 + \boldsymbol{k}_2 = \boldsymbol{k}_3 + \boldsymbol{G}$ for acoustic phonons which simultaneously satisfy the energy conservation law for anharmonic three-phonon processes. These crystalline features of $\kappa_{\rm ph}(T)$ are clearly manifested in experimental data of on-center clathrate compounds shown in Figs. 14 and 16.

At high temperatures $T \geq \hbar\omega_{c\mu}/k_{\rm B}$, the number of excited phonons are proportional to T. The scattering probability $1/\tau_\mu$ due to anharmonic interactions of acoustic phonons of the mode μ is proportional to the number of excited phonons, which is proportional to T, resulting in the mean free path $\ell_\mu = v_\mu \tau_\mu \propto 1/T$. Since the average velocity v_μ^2 in Eq. (67) should be independent of T, $\kappa_{\rm ph}(T) \propto T^{-1}$ as observed in Figs. 14 and 16.

2. Plateau-temperature region of off-center systems

$\kappa_{\rm ph}(T)$ of type-I clathrate compounds containing off-center guest atoms take the universal form described in Sec. V.B. The energy range of the plateau region in $\kappa_{\rm ph}(T)$ overlaps with that of the boson-peak-like excess density of states in off-center type-I clathrate compounds in the THz-frequency region. The physical origin of the plateau-temperature region should be interpreted with reference to this excess density of states.

The upper cutoff frequency $\omega_{c\mu}$ of the integral in the general formula for $\kappa_{\rm ph}(T)$ in Eq. (67) represents the crossover frequency from the linear-dispersion relation to the flat dispersion relation of acoustic phonons, where the group velocity of acoustic phonons of the mode μ vanishes. The frequency $\omega_{c\mu}$ behaves as a mobility edge for acoustic phonons. Thus, the crossover frequency $\omega_{c\mu}$ is crucial in revealing the plateau behavior of $\kappa_{\rm ph}(T)$.

Transverse acoustic phonons with 2 degrees of freedom of the modes mainly contribute to phonon thermal transport. The dispersion relations of β-BGS theoretically calculated in Fig. 36(b) show a wide flat region for the acoustic branch of transverse phonons arising from the coupling with the low-lying librational modes (Nakayama and Kaneshita, 2011). The calculated results given in Fig. 36(b) definitely show that the avoided crossing starts in the region below $|\boldsymbol{k}| \cong |\boldsymbol{G}|/4$. This result indicates that acoustic phonons carrying heat are limited to those with the wave number $|\boldsymbol{k}| \lesssim |\boldsymbol{G}|/4$. This leads to the plateau-temperature region of $\kappa_{\rm ph}(T)$ similarly to the case of

the Dulong-Petit limit of the Debye specific heats, i.e., $\kappa_{\rm ph}(T) = \text{const}$. Namely, conventional heat transport occurs via already excited phonons, yielding a saturation in $\kappa_{\rm ph}(T)$, which is referred to as the plateau.

The crossover frequency $\omega_{c\mu}$ is obtained by subtracting the frequency $\delta\omega_{c\mu}$ given by Eq. (53) as $\omega_{c\mu} = \omega_{0\mu} - \delta\omega_{c\mu}$. The use of Eq. (51) leads to

$$\omega_{c\mu} \cong \omega_{0\mu}\left(1 - \sqrt{\frac{m}{M}}\right). \tag{73}$$

The peak frequency of the thermal distribution at the temperature T becomes $\hbar\omega_{c\mu} \cong 3.83 k_{\rm B} T$, taking into account the Stefan shift. Then the relation between the lowest optical eigenfrequency $\omega_{0\perp}$ and the onset temperature T_p of the plateau becomes, from Eq. (73),

$$T_p \cong \hbar\omega_{0\perp} \frac{(1 - \sqrt{m/M})}{3.83 k_{\rm B}}. \tag{74}$$

The above relation between T_p of $\kappa_{\rm ph}(T)$ and $\hbar\omega_{c\mu}$ of the phonon dispersion relation holds for type-I clathrates with off-center rattling guest atoms.

C. *T*-linear rise above the plateau-temperature region

1. Thermal transport due to the hopping of local modes associated with guest atoms

At the temperature regime $T \gtrsim 10$ K above the plateau, the $\kappa_{\rm ph}(T)$ values of off-center type-I clathrate compounds exhibit the empirical law $\kappa_{\rm ph}(T) = \kappa_{\rm plateau} + \kappa_{\rm add}$, where $\kappa_{\rm add} = \alpha T$ (Cohn *et al.*, 1999; Nolas, Weakley *et al.*, 2000; Nolas, Sharp, and Goldsmid, 2001; Sales *et al.*, 2001; Bentien *et al.*, 2005; Avila, Suekuni, Umeo, and Takabatake, 2006; Suekuni *et al.*, 2007; Avila *et al.*, 2008; Suekuni, Avila *et al.*, 2008). The prefactors α become $\alpha = 0.009\ \mathrm{W\,K^{-2}\,m^{-1}}$ for n-type and $\alpha = 0.007\ \mathrm{W\,K^{-2}\,m^{-1}}$ for p-type β-BGS (Avila, Suekuni, Umeo, and Takabatake, 2006; Suekuni *et al.*, 2007; Avila *et al.*, 2008; Suekuni, Avila *et al.*, 2008). It is of importance that $\kappa_{\rm ph}(T)$ vanishes when extrapolating the temperature $T \to 0$, as seen from Fig. 14. It implies that a new additional heat-transport channel opens up above the plateau-temperature region. This feature, termed $\kappa_{\rm add}(T)$, at high temperatures is the same as those occurring in structural glasses or amorphous materials (Zeller and Pohl, 1971; Stephens, 1973; Freeman and Anderson, 1986; Cahill and Pohl, 1987). This is very different from the cases of on-center type-I clathrate compounds that behave as $\kappa_{\rm ph}(T) \propto 1/T$ above $T \gtrsim 10$ K.

Plateau-temperature regions of $\kappa_{\rm ph}(T)$ are also observed for silica aerogels (Bernasconi *et al.*, 1992). In silica aerogels, there are two types of phonon, low-energy extended acoustic phonons and high-energy localized phonons separated at the crossover frequency ω_c. Alexander, Entin-Wohlman, and Orbach (1986) proposed a hopping mechanism of localized modes to explain the T-linear dependence of $\kappa_{\rm add}(T)$ of silica aerogels. Jagannathan, Orbach, and Entin-Wohlman (1989) and Nakayama and Orbach (1999a, 1999b) introduced this mechanism to explain the T-linear rise of $\kappa_{\rm add}(T)$ above the plateau in structural glasses. Hashimoto and Shimizu (2011) demonstrated for silica glass the hopping of local modes associated with the boson peak. They employed transient saturation spectroscopy for $^{167}Er^{3+}$ ions doped in a silica glass fiber in the range 2.5–30 K, a temperature range above the plateau region. The result is consistent with the idea that local modes carry heat by their hopping assisted by acoustic phonons.

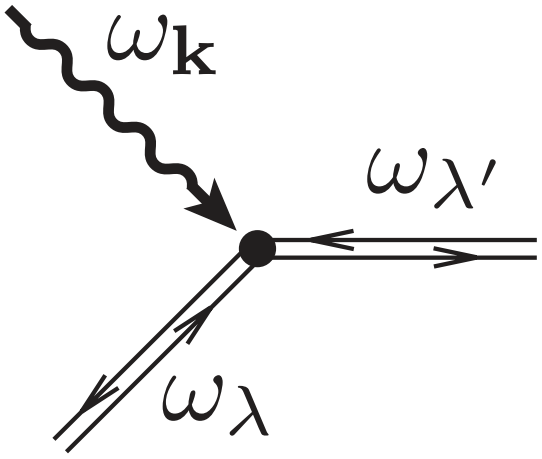

FIG. 43. A first-order process of local-mode hopping. The local mode (double lines) interacts with the acoustic phonon (wavy line) with the eigenfrequency $\omega_{\boldsymbol{k}}$, hopping from the initial state with ω_λ to the final state with $\omega_{\lambda'}$, where $\omega_{\lambda'} > \omega_\lambda > \omega_{\boldsymbol{k}}$. The set of arrowheads in the opposite directions on the double lines indicate that the local modes consist of the superposition of plane waves with opposite directions.

Here we present a simple explanation for the hopping mechanism contributing to $\kappa_{\rm ph}(T)$ in the temperature regime above the plateau. The formula of Eq. (67) for the thermal conductivity based on the propagation of extended acoustic phonons is not applicable to the hopping mechanism. At such high temperatures, the additional channel of heat transfer is opened up via the diffusion of local modes associated with guest atoms, where the hopping of local modes occurs via the anharmonic interaction with extended acoustic phonons as shown in Fig. 43.

The thermal conductivity due to phonon-assisted hopping is given by (Alexander, Entin-Wohlman, and Orbach, 1986; Nakayama, Yakubo, and Orbach, 1994)

$$\kappa_{\rm hop}(T) = \sum_\lambda C_\lambda(T) \frac{R_\lambda^2}{3\tau_\lambda(T)}, \tag{75}$$

where R_λ is the hopping distance of the local mode λ and R_λ^2/τ_λ is the thermal diffusivity due to the local-mode hopping. The decay rate $1/\tau_\lambda(T)$ is caused by the interaction with acoustic phonons, and C_λ is the specific heat associated with the local mode λ. In the higher-temperature regime above the plateau region $T \geq \hbar\omega_{c\mu}/3.83 k_{\rm B}$, the specific heat C_λ follows the Dulong-Petit relation in the form $C_\lambda = k_{\rm B}/V$, where V is the volume of the system. Substituting this relation into Eq. (75), we have the thermal conductivity formula given by

$$\kappa_{\rm hop} \cong \frac{k_{\rm B}}{3V}\sum_{\lambda}\frac{R_\lambda^2}{\tau_\lambda(T)}, \tag{76}$$

where the sum over λ means that the integral on ω_λ is defined by

$$\sum_{\lambda} \to \sum_{\mu}\int_{\omega_{c\mu}}^{\omega_{c\mu}+\Delta\omega_\lambda} d\omega_\lambda N_{\rm ex}(\omega_\lambda). \tag{77}$$

Here $N_{\rm ex}$ is the excess density of states and $\Delta\omega_\lambda$ is its bandwidth. The decay rate $1/\tau_\lambda(T)$ is proportional to the Bose-Einstein distribution function $n_{\rm B}(T)$ of acoustic phonons of the form $n_{\rm B} \cong k_{\rm B}T/\hbar\omega_{c\mu}$ in the high-temperature regime $T \gtrsim \hbar\omega_{c\mu}/3.83k_{\rm B}$. These procedures give rise to the following simple relation for $\kappa_{\rm hop}(T)$:

$$\kappa_{\rm hop}(T) \simeq \frac{Nk_{\rm B}^2}{V}\frac{R(\omega_{c\mu})^2 T}{\hbar\omega_{c\mu}\tau(\omega_{c\mu})}, \tag{78}$$

where the factor of 3 is canceled out by taking into account the contribution from the three acoustic phonon modes. We can estimate from Eq. (78) the actual value of the hopping contribution to $\kappa_{\rm hop}(T)$ above the plateau region by the following arguments.

With increasing temperature above $T \gtrsim \hbar\omega_{c\mu}/3.83k_{\rm B}$, acoustic phonons are hybridized with vibrations of guest atoms manifesting the Ioffe-Regel limit $kR(\omega_{c\mu}) \cong 1$, or equivalently $\omega_{c\mu}\tau(\omega_{c\mu}) \cong 1$ (Ioffe and Regel, 1960). This is the limit in which a quantum-mechanical treatment is applicable. The average hopping distance $R(\omega_{c\mu})$ is surely the distance between the nearest-neighbor off-center guest atoms of the order of 1 nm. Substituting these relations into Eq. (78) together with the number density of the local mode λ of $N/V = 1/R(\omega_{c\mu})^3$, we have

$$\kappa_{\rm hop} \simeq 0.002\ {\rm W\,K^{-1}\,m^{-1}}. \tag{79}$$

The estimated value agrees well with the observed prefactor α for off-center type-I clathrate compounds, showing that the T-linear rise above the plateau region is a universal phenomena.

Quantitative microscopic calculations for $\kappa_{\rm hop}$ should be made by taking into account the anharmonic interaction Hamiltonian between the acoustic phonon with the wave vector $\boldsymbol{k}$ and the local modes $|\lambda\rangle$, $|\lambda'\rangle$, which is expressed as follows:

$$H_{\rm hop} = C_{\rm eff}\sum_{\boldsymbol{k},\lambda,\lambda'}(A_{\boldsymbol{k},\lambda,\lambda'}c_\lambda^\dagger c_{\lambda'}b_{\boldsymbol{k}} + {\rm H.c.}), \tag{80}$$

where the operators $b_{\boldsymbol{k}}^\dagger$ and $c_\lambda^\dagger$ ($b_{\boldsymbol{k}}$ and c_λ) are the creation (annihilation) operators for an acoustic phonon and a local mode, respectively. $H_{\rm hop}$ is proportional to the dilatation of cages due to incoming acoustic phonons. The explicit form of the coupling constant $A_{\boldsymbol{k},\lambda,\lambda'}$ in Eq. (80) is given by (Nakayama and Orbach, 1999a, 1999b; Kaneshita and Nakayama, 2009)

$$A_{\boldsymbol{k},\lambda,\lambda'} = \sqrt{\frac{1}{V}}\left(\frac{\hbar}{2\rho}\right)^{3/2}\sqrt{\frac{\omega_{\boldsymbol{k}}}{\omega_\lambda\omega_{\lambda'}}}\left(\frac{I}{v_\mu\ell_\lambda\ell_{\lambda'}}\right), \tag{81}$$

where ρ is the mass density. The localization length ℓ_λ is the size of cages containing guest atoms, which is comparable with the hopping distance of the local mode λ. The factor I in Eq. (81) is the overlap integral between local modes represented by

$$I \cong \left(\frac{16}{\pi}\right)e^{-R_\lambda/\ell_\lambda + i\boldsymbol{k}\cdot\boldsymbol{R}_\lambda}, \tag{82}$$

where the local mode decays exponentially. As seen above, the explicit form of the local mode is not necessary, but only the order of R_λ and ℓ_λ.

For the process $|\boldsymbol{k};\lambda\rangle \to |\lambda'\rangle$ illustrated in Fig. 43, first-order perturbation theory provides the hopping lifetime of the local mode λ at temperatures $k_{\rm B}T \gg \hbar\omega_{c\mu}$ of the form

$$\frac{1}{\tau_\lambda(T)} = \frac{2\pi}{\hbar^2}\sum_{\lambda,\lambda'}|A_{\boldsymbol{k},\lambda,\lambda'}|^2 \times [1 + n(\omega_{\boldsymbol{k}}) + n(\omega_{\lambda'})]\delta(\omega_{\boldsymbol{k}} - \omega_{\lambda'} + \omega_\lambda). \tag{83}$$

The substitution of Eq. (83) into Eq. (76) yields the hopping contribution to the thermal conductivity given by

$$\kappa_{\rm hop}(T) = \frac{12^2 C_{\rm eff}^2 k_{\rm B}^2 T}{\pi^4\rho^3 v_s^5 \ell_\lambda^5}, \tag{84}$$

where the mass density $\rho = 6.01\times10^3$ kg m^{-3} is for β-BGS, $\ell_\lambda \simeq 1$ nm, and $1/v_s^5$ is the average of $1/v_\mu^5$ taking $\cong 3.6\times10^{-17}$ m^{-5} s^5 for β-BGS. Since the magnitude and temperature dependence of the thermal conductivities above the plateau-temperature region of off-center type-I clathrate compounds are almost identical to those of structural glasses, it is appropriate to take the coupling constant $C_{\rm eff}$ of structural glasses, which provides $C_{\rm eff} = -2.0\times10^{12}$ N m^{-2} (Nakayama and Orbach, 1999a, 1999b; Kaneshita and Nakayama, 2009). As a result, the thermal conductivity for β-BGS becomes $\kappa_{\rm ph}(T) \cong 0.003T$ W K^{-1} m^{-1} above the plateau $T \geq 10$ K. This coincides well with the experimental values of β-BGS (Avila, Suekuni, Umeo, and Takabatake, 2006; Suekuni *et al.*, 2007; Avila *et al.*, 2008; Suekuni, Avila *et al.*, 2008).

2. Overall interpretation of glasslike thermal conductivities

The analyses described in Secs. VII and VIII lead to the following interpretation of $\kappa_{\rm ph}(T)$ of off-center type-I clathrate compounds. These are summarized as follows: (i) two-level tunneling states generated by *interacting* electric dipoles explain the observed $\kappa_{\rm ph}(T) \propto T^{2-\delta}$ with a small value of δ below 1 K, (ii) the plateau region $\kappa_{\rm ph}(T) = $ const is a direct consequence of the *flattening* of acoustic modes due to the hybridization with local vibrations of off-center guest atoms, and (iii) the subsequent T-linear rise above the plateau originates from the hopping of local modes assisted by acoustic modes of networked cages.

There is an additional complication at much higher temperatures, as shown in Figs. 14 and 18, where the T-linear rise in $\kappa_{\rm ph}(T)$ does not continue, but $\kappa_{\rm ph}(T)$ shows a curling over above $T \simeq 100$ K. This temperature regime is important for practical application of type-I clathrates to efficient thermoelectric materials. In this regime, quenching

of phonon-assisted hopping occurs via the breakdown of three-phonon anharmonic scattering (Simons, 1964). The hysteresis becomes larger in adjusting to an instantaneous thermal equilibrium distribution, which leads to a curling over of $\kappa_{\rm ph}(T)$ attributable to the hydrodynamic or Akhieser limit (Akhieser, 1939). Thus, the key aspects of thermal conductivities of type-I clathrate compounds containing off-center guest atoms can be completely understood over the entire temperature range in a consistent way.

X. SUMMARY AND CONCLUSIONS

This article reviewed the development of research on phonon-glass electron-crystal thermoelectric materials, in particular, focusing on experimental and theoretical aspects of type-I clathrate compounds. After the PGEC concept was described by Slack (1995), much effort was spent in exploring efficient thermoelectric materials. As candidates for PGEC materials, Slack (1995) promoted clathrate compounds encapsulating guest atoms in cages. Type-I clathrate compounds manifest the PGEC concept when the size mismatch is large enough between the guest ion and the tetrakaidecahedoral cage. Thereby, the guest atoms take off-center positions in the tetrakaidecahedron.

The microscopic structure of type-I clathrate compounds has been clarified by means of the following experimental techniques: x-ray diffraction, neutron diffraction, resonant x-ray diffraction, and extended x-ray absorption fine-structure spectroscopy. These have been described in detail in Sec. III. Specific-heat measurements on type-I clathrate compounds with off-center guest atoms revealed the existence of the boson-peak-like excess density of states over the Debye phonons at around several kelvin. The characteristic temperatures θ of guest atom $\mathcal{R}(2)$ were estimated from the peaks in the plot of $C_V(T)/T^3$ vs T. These results are summarized in Table I. In addition, T-linear specific heats identical to those of glasses have been experimentally verified below about 1 K, as described in Sec. IV.

Excess densities of states over those of the Debye phonons have also been found by means of spectroscopic measurements: infrared absorption, Raman scattering, Mössbauer spectroscopy, and inelastic neutron scattering. Optical spectroscopies have made possible the identification of the relevant modes contributing to the excess densities of states. Raman scattering and infrared absorption experiments for type-I clathrate compounds containing off-center guest atoms have revealed the relevance of the T_{2g} mode and the E_g mode for the excess densities of states. These modes do not exist in the case of type-I clathrate compounds with on-center guest atoms. It is remarkable that the linewidths of these modes increase on cooling and the spectral energies shift lower; these are opposite behaviors to those expected for the usual crystalline materials. This key observation has been confirmed by INS experiments as well (Nakamura and Arai, 2010). These experiments and theoretical interpretation have been described in detail in Secs. VI and VII.

Furthermore, thermal conductivity measurements display glasslike behaviors characterized as follows: T^2 dependence at temperatures below 1 K, a plateau at temperatures of several K, and T-linear dependence above the plateau at around 10 K. Surprisingly enough, these temperature dependences as well as the magnitudes are identical to those of structural glasses in the whole temperature range. We described relevant experiments in Sec. V, emphasizing that off-center guest atoms play a key role for the emergence of glasslike thermal and dynamical properties.

Concerning the efficiency of the thermopower, type-I $Ba_8Ga_{16}Sn_{30}$ manifests low thermal conductivities in addition to high absolute values of the Seebeck coefficients S of 300 μV/K for both p-type and n-type crystals at 300 K. The electrical resistivity ρ at room temperature is in the range $(20–40)\times10^{-3}$ Ω cm, which is several times larger than that expected for efficient thermoelectric materials. This large ρ is caused by low carrier densities of 10^{19} cm^{-3} and low carrier mobilities 20–40 cm^2/V s. As a result, the dimensionless figure of merit $ZT = S^2T/\rho\kappa_{\rm tot}$ does not reach the desired value of 1.0, but exhibits maxima of 0.58 and 0.50 at around 450 K for the p-type and n-type samples, respectively. It is necessary to decrease the resistivity by doping carriers in order to realize the "electron-crystal" concept.

Type-VIII $Ba_8Ga_{16}Sn_{30}$ is a possible candidate for an efficient thermoelectric material. The Ba guest atoms in distorted dodecahedrons vibrate with the ADP 3 times larger than those of cage atoms. These anisotropic and anharmonic vibrations depress $\kappa_{\rm ph}$ at higher temperatures above 100 K. The actual values of $\kappa_{\rm ph}$ take the value 0.7 W/Km at above 100 K, as shown in Fig. 17. These values are higher than $\kappa_{\rm ph} = 0.4$ W/Km of β-BGS, but they are still lower than those of thermoelectric materials based on Bi-Te. The carrier density can be tuned by substituting various types of elements for the cage atoms Ga and Sn. For Cu substitution, ZT for p-type and n-type samples increases to 0.9 at 480 K and 1.45 at 520 K. These values exceed those of the Pb-Te-based materials at the same temperature. Therefore, type-VIII $Ba_8Ga_{16}Sn_{30}$ without toxic elements is regarded as a human-friendly thermoelectric material with operation temperatures around 400–600 K. At higher temperatures, Si- and Ge-based clathrates have better structural stability than Sn-based clathrates. Thermoelectric modules composed of similar clathrates based on Sn, Ge, and Si may have a conversion efficiency higher than 10% in a wide temperature range from 300 to 1200 K.

Finally, we emphasize that the theoretical understanding of glasslike behaviors of $\kappa_{\rm ph}$ in off-center clathrate compounds has benefited greatly from accumulated research on structural glasses. However, in structural glasses, it is difficult to identify relevant entities or elements due to their complex microscopic structures (Nakayama, 2002). This is the main reason why the arguments on the origin of the boson peak have continued for decades. This being said, it is clear that off-center guest atoms in type-I clathrate compounds are a key ingredient for emerging glasslike behavior. This has made it possible to provide clear theoretical interpretations of glasslike thermal and dynamic properties for these compounds.

To sum up, the subjects described in this review involve interesting phenomena not only for the physics itself but also for the exploration of renewable-energy materials. We hope that this review will serve as a basis for further development of clathrate-related efficient thermoelectric materials.

ACKNOWLEDGMENTS

We are most grateful to M. A. Avila, T. Kume, T. Mori, Y. Takasu, and N. Toyota for many valuable discussions and useful suggestions. We thank H. Fukuoka, T. Hasegawa, I. Ishii, C. H. Lee, T. Suzuki, K. Tanigaki, H. Tou, M. Udagawa, K. Umeo, J. Xu, and S. Yamanaka for fruitful discussions. We give special thanks to M. Nakamura and M. Arai for supplying the INS data on type-I clathrates prior to publication. We are grateful to O. B. Wright for a critical reading of the manuscript. T. N. acknowledges with gratitude the support and hospitality of Max-Planck Institute for the Physics of Complex Systems during his stay in 2012–2013. This work was partially supported by a NEDO Grant No. 09002139-0 and Grant-in-Aid for Scientific Research from the Ministry of Education, Culture, Sports, Science and Technology (MEXT) of Japan, Grants No. 18204032, No. 19051011, No. 20102004, No. 22013018, No. 22540404, and No. 22740225.

REFERENCES

Akai, K., T. Uemura, K. Kishimoto, T. Tanaka, H. Kurisu, S. Yamamoto, T. Koyanagi, K. Koga, H. Anno, and M. Matsuura, 2009, J. Electron. Mater. **38**, 1412.

Akai, K., G. Zhao, K. Koga, K. Oshiro, and M. Matsuura, 2005, in *Proceedings of the 24th International Conference on Thermoelectrics* (IEEE, New York), pp. 230–233.

Akhieser, A., 1939, J. Phys. USSR **1**, 277.

Alexander, S., O. Entin-Wohlman, and R. Orbach, 1986, Phys. Rev. B **34**, 2726.

Anderson, O. L., 1959, J. Phys. Chem. Solids **12**, 41.

Anderson, P. W., B. I. Halperin, and C. M. Varma, 1972, Philos. Mag. **25**, 1.

Anno, H., M. Hokazono, M. Kawamura, and K. Matsubara, 2003, in *Proceedings of the 22nd International Conference on Thermoelectrics* (IEEE, New York), pp. 121–126.

Anno, H., M. Hokazono, M. Kawamura, J. Nagao, and K. Matsubara, 2002, in *Proceedings of the 21st International Conference on Thermoelectrics* (IEEE, New York), pp. 77–80.

Anno, H., H. Yamada, T. Nakabayashi, M. Hokazono, and R. Shirataki, 2012, J. Solid State Chem. **193**, 94.

Arcon, D., A. Zorko, P. Jeglic, J. Xu, J. Tang, Y. Tanabe, S Hegri, and K. Tanigaki, 2013, J. Phys. Soc. Jpn. **82**, 014703.

Ashcroft, N. W. and N. D. Mermin, 1976, *Solid State Physics* (Thomson Learning, London), Chap. 16.

Avila, M. A., K. Suekuni, K. Umeo, H. Fukuoka, S. Yamanaka, and T. Takabatake, 2006, Phys. Rev. B **74**, 125109.

Avila, M. A., K. Suekuni, K. Umeo, H. Fukuoka, S. Yamanaka, and T. Takabatake, 2008, Appl. Phys. Lett. **92**, 041901.

Avila, M. A., K. Suekuni, K. Umeo, and T. Takabatake, 2006, Physica (Amsterdam) **383B**, 124.

Aydemir, U., C. Candolfi, A. Ormeci, Y. Oztan, M. Baitinger, N. Oeschler, F. Steglich, and Yu. Grin, 2011, Phys. Rev. B **84**, 195137.

Baumbach, R., F. Bridges, L. Downward, D. Cao, P. Chesler, and B. Sales, 2005, Phys. Rev. B **71**, 024202.

Baumert, J., C. Gutt, V. P. Shpakov, J. S. Tse, M. Krisch, M. Mueller, H. Requardt, D. D. Klug, S. Janssen, and W. Press, 2003, Phys. Rev. B **68**, 174301.

Beekman, M., and G. S. Nolas, 2008, J. Mater. Chem. **18**, 842.

Beekman, M., W. Schnelle, H. Borrmann, M. Baitinger, Y. Grin, and G. S. Nolas, 2010, Phys. Rev. Lett. **104**, 018301.

Bentien, A., M. Christensen, J. D. Bryan, A. Sanchez, S. Paschen, F. Steglich, G. D. Stucky, and B. B. Iversen, 2004, Phys. Rev. B **69**, 045107.

Bentien, A., B. B. Iversen, J. D. Bryan, G. D. Stucky, A. E. C. Palmqvist, A. j. Schlutz, and R. W. Henning, 2002, J. Appl. Phys. **91**, 5694.

Bentien, A., S. Johnsen, and Bo B. Iversen, 2006, Phys. Rev. B **73**, 094301.

Bentien, A., E. Nishibori, S. Paschen, and B. B. Iversen, 2005, Phys. Rev. B **71**, 144107.

Bentien, A., V. Pacheco, S. Paschen, Y. Grin, and F. Steglich, 2005, Phys. Rev. B **71**, 165206.

Bentien, A., A. E. C. Palmqvist, J. D. Bryan, S. Latturner, G. D. Stucky, L. Furenlid, and B. B. Iversen, 2000, Angew. Chem., Int. Ed. **39**, 3613.

Berman, R., 1949, Phys. Rev. **76**, 315.

Bernal, J. D., and R. H. Fowler, 1933, J. Chem. Phys. **1**, 515.

Bernasconi, A., T. Sleator, D. Posselt, J. K. Kjems, and H. R. Ott, 1992, Phys. Rev. B **45**, 10 363.

Blake, N. P., J. D. Bryan, S. Latturner, L. Møllnitz, G. D. Stucky, and H. Metiu, 2001, J. Chem. Phys. **114**, 10 063.

Blake, N. P., L. Møllnitz, G. Kresse, and H. Metiu, 1999, J. Chem. Phys. **111**, 3133.

Bobev, S., and S. C. Sevov, 2000, J. Solid State Chem. **153**, 92.

Bobev, S., and S. C. Sevov, 2001, J. Am. Chem. Soc. **123**, 3389.

Bridges, F., and L. Downward, 2004, Phys. Rev. B **70**, 140201(R).

Bryan, J. D., V. I. Srdanov, G. D. Stucky, and D. Schmidt, 1999, Phys. Rev. B **60**, 3064.

Buchenau, U., N. Nücker, and A. J. Dianoux, 1984, Phys. Rev. Lett. **53**, 2316.

Buchenau, U., M. Prager, N. Nücker, A. J. Dianoux, N. Ahmad, and W. A. Phillips, 1986, Phys. Rev. B **34**, 5665.

Bustarret, E., *et al.*, 2006, Nature (London) **444**, 465.

Cahill, D. G., and R. O. Pohl, 1987, Phys. Rev. B **35**, 4067.

Callen, H. B., 1948, Phys. Rev. **73**, 1349.

Callen, H. B., 1952, Phys. Rev. **85**, 16.

Carrillo-Cabrera, W., R. Cardoso Gil, V.-H. Tran, and Yu. Grin, 2002, Z. Kristallogr. New Cryst. Struct. **217**, 181.

Carrillo-Cabrera, W., J. Curda, H. G. von Schnering, S. Paschen, and Yu. Grin, 2000, Z. Kristallogr. New Cryst. Struct. **215**, 207.

Cederkrantz, D., A. Saramat, G. J. Snyder, and A. E. C. Palmqvist, 2009, J. Appl. Phys. **106**, 074509.

Chakoumakos, B. C., B. C. Sales, D. Mandrus, and V. Keppens, 1999, Acta Crystallogr. Sect. B **55**, 341.

Chakoumakos, B. C., B. C. Sales, and D. G. Mandrus, 2001, J. Alloys Compd. **322**, 127.

Chakoumakos, B. C., B. C. Sales, D. G. Mandrus, and G. S. Nolas, 2000, J. Alloys Compd. **296**, 80.

Chari, M. S. R., and M. V. N. Chari, 1989, Phys. Lett. A **136**, 149.

Chari, M. S. R., and M. V. N. Chari, 1990, J. Phys. Condens. Matter **2**, 631.

Chen, G., M. S. Dresselhaus, G. Dresselhaus, J. P. Fleurial, and T. Caillat, 2003, Int. Mater. Rev. **48**, 45.

Christensen, M., A. B. Abrahamsen, N. B. Christensen, F. Juranyi, N. H. Andersen, K. Lefmann, J. Andreasson, C. R. H. Bahl, and B. B. Iversen, 2008, Nat. Mater. **7**, 811.

Christensen, M., and B. B. Iversen, 2007, Chem. Mater. **19**, 4896.

Christensen, M., S. Johnsen, and B. B. Iversen, 2010, Dalton Trans. **39**, 978.

Christensen, M., S. Johnsen, F. Juranyi, and B. B. Iversen, 2009, J. Appl. Phys. **105**, 073508.

Christensen, M., F. Juranyi, and B. B. Iversen, 2006, Physica B (Amsterdam) **385–386**, 505.

Christensen, M., N. Lock, J. Overgaard, and B. B. Iversen, 2006, J. Am. Chem. Soc. **128**, 15 657.

Christensen, M., G. J. Snyder, and B. B. Iversen, 2006, in *Proceedings of the 25th International Conference on Thermoelectrics* (IEEE, New York), pp. 40–43.

Claussen, W. F., 1951a, J. Chem. Phys. **19**, 259.

Claussen, W. F., 1951b, J. Chem. Phys. **19**, 1425.

Claussen, W. F., 1951c, J. Chem. Phys. **19**, 662.

Cohen, M. H., and F. Keffer, 1955, Phys. Rev. **99**, 1128.

Cohen, R. W., B. Abeles, and G. S. Weisbarth, 1967, Phys. Rev. Lett. **18**, 336.

Cohn, J. L., G. S. Nolas, V. Fessatidis, T. H. Metcalf, and G. A. Slack, 1999, Phys. Rev. Lett. **82**, 779.

Condron, C. L., J. Martin, G. S. Nolas, P. M. B. Piccoli, A. J. Schultz, and S. M. Kauzlarich, 2006, Inorg. Chem. **45**, 9381.

Cutler, M., and N. F. Mott, 1969, Phys. Rev. **181**, 1336.

Davidson, D. W., 1973, in *A Water: A Comprehensive Treatise*, edited by F. Franks (Plenum Press, New York), Vol. 2.

Davy, H., 1811a, Phil. Trans. R. Soc. London **101**, 1.

Davy, H., 1811b, Phil. Trans. R. Soc. London **101**, 155.

De Yoreo, J. J., W. Knaak, M. Meissner, and R. O. Pohl, 1986, Phys. Rev. B **34**, 8828.

Dong, J., O. F. Sankey, and C. W. Myles, 2001, Phys. Rev. Lett. **86**, 2361.

Dresselhaus, M. S., G. Chen, M. Y. Tang, R. G. Yang, H. Lee, D. Z. Wang, Z. F. Ren, J.-P. Fleurial, and P. Gogna, 2007, Adv. Mater. **19**, 1043.

Dresselhaus, M. S., and I. L. Thomas, 2001, Nature (London) **414**, 332.

Eisenmann, B., H. Schäfer, and R. Zagler, 1986, J. Less-Common Met. **118**, 43.

Ekimov, E. A., V. A. Sidorov, E. D. Bauer, N. N. Mel'nik, N. J. Curro, J. D. Thompson, and S. M. Stishov, 2004, Nature (London) **428**, 542.

Englezos, P., 1993, Ind. Eng. Chem. Res. **32**, 1251.

English, N. J., P. D. Gorman, and J. M. D. MacElroy, 2012, J. Chem. Phys. **136**, 044501.

English, N. J., and J. S. Tse, 2009, Phys. Rev. Lett. **103**, 015901.

English, N. J., and J. S. Tse, 2010, Energiespectrum **3**, 1934.

English, N. J., and J. S. Tse, 2011, Phys. Rev. B **83**, 184114.

Ettingshausen, A. V., and W. Nernst, 1886, Ann. Phys. (Berlin) **265**, 343.

Euchner, H., S. Pailhés, L. T. K. Nguyen, W. Assmus, F. Ritter, A. Haghighirad, Y. Grin, S. Paschen, and M. de Boissieu, 2012, Phys. Rev. B **86**, 224303.

Falmbigl, M., and P. F. Rogl, 2012, in *Modules, Systems, and Applications in Thermoelectrics*, edited by D. M. Rowe (CRC Press, Taylor and Francis Group, Boca Raton, FL), Vol. 9, pp. 1–23.

Fano, U., 1960, Phys. Rev. **118**, 451.

Faraday, M., 1823, Quart. J. Sci. **15**, 71.

Flubacher, P., A. J. Leadbetter, J. A. Morrison, and B. P. Stoicheff, 1959, J. Phys. Chem. Solids **12**, 53.

Freeman, J. J., and A. C. Anderson, 1986, Phys. Rev. B **34**, 5684.

Fritzsche, H., 1971, Solid State Commun. **9**, 1813.

Fujita, I., K. Kishimoto., M. Sato, H. Anno, and T. Koyanagi, 2006, J. Appl. Phys. **99**, 093707.

Fujiwara, A., K. Sugimoto, C. H. Shih, H. Tanaka, J. Tang, Y. Tanabe, J. Xu, S. Heguri, K. Tanigaki, and M. Takata, 2012, Phys. Rev. B **85**, 144305.

Fukuoka, H., K. Iwai, S. Yamanaka, H. Abe, K. Yoza, and L. Häming, 2000, J. Solid State Chem. **151**, 117.

Gallmeier, J., H. Schäfer, and A. Weiss, 1969, Z. Naturforsch. B **24**, 665.

Gatti, C., L. Bertini, N. P. Blake, and Bo. B. Iversen, 2003, Chem. Eur. J. **9**, 4556.

Goldsmid, H. J., 2010, *Intorduction to Thermoelectricity* (Springer, Berlin).

Goldsmid, H. J, and R. W. Douglas, 1954, Br. J. Appl. Phys. **5**, 386.

Gonçalves, A. P., and C. Godart, 2013, in *New Materials for Thermoelectric Applications: Theory and Experiment*, edited by V. Zlatic, and A. Hewson (Springer, Dordrecht), pp. 1–24.

Gou, W., Y. Li, J. Chi, J. H. Ross, Jr., M. Beeckman, and G. S. Nolas, 2005, Phys. Rev. B **71**, 174307.

Graebner, J. E., B. Golding, and L. C. Allen, 1986, Phys. Rev. B **34**, 5696.

Grannan, E. R., M. Randeria, and J. P. Sethna, 1990a, Phys. Rev. B **41**, 7784.

Grannan, E. R., M. Randeria, and J. P. Sethna, 1990b, Phys. Rev. B **41**, 7799.

Gutt, C., J. Baumert, W. Press, J. S. Tse, and S. Janssen, 2002, J. Chem. Phys. **116**, 3795.

Hashimoto, D., and K. Shimizu, 2011, J. Opt. Soc. Am. B **28**, 2227.

Hayashi, M., K. Kishimoto, K. Kishio, K. Akai, H. Asada, and T. Koyanagi, 2010, Dalton Trans. **39**, 1113.

He, H., A. Zevalkink, Z. M. Gibbs, G. J. Snyder, and S. Bobev, 2012, Chem. Mater. **24**, 3596.

Helen, B., E. Courtens, R. Vacher, A. Yamanaka, M. Kataoka, and K. Inoue, 2000, Phys. Rev. Lett. **84**, 5355.

Hermann, R. P., F. Grandjean, and G. J. Long, 2005, Am. J. Phys. **73**, 110.

Hermann, R. P., V. Keppens, P. Bonville, G. S. Nolas, F. Grandjean, G. J. Long, H. M. Christen, B. C. Chakoumakos, B. C. Sales, and D. Mandrus, 2006, Phys. Rev. Lett. **97**, 017401.

Hermann, R. P., W. Schweika, O. Leupold, R. Rüffer, G. S. Nolas, F. Grandjean, and G. J. Long, 2005, Phys. Rev. B **72**, 174301.

Hester, K. C., and P. G. Brewer, 2009, Annu. Rev. Mar. Sci. **1**, 303.

Hou, X., Y. Zhou, L. Wang, W. Zhang, W. Zhang, and L. Chen, 2009, J. Alloys Compd. **482**, 544.

Hunklinger, S., and A. K. Raychaudhuri, 1986, *Progress in Low Temperature Physics* (North-Holland, Amsterdam), Vol. 9, pp. 265–344.

Huo, D, T. Sakata, T. Sasakawa, M. A. Avila, M. Tsubota, F. Iga, H. Fukuoka, S. Yamanaka, S. Aoyagi, and T. Takabatake, 2005, Phys. Rev. B **71**, 075113.

Inamura, Y., M. Arai, O. Yamamuro, A. Inabe, N. Kitamura, T. Otomo, T. Matsuo, S. M. Bennington, and A. C. Hannon, 1999, Physica (Amsterdam) B **263–264**, 299.

Inoue, R., H. Tanaka, and K. Nakanishi, 1996, J. Chem. Phys. **104**, 9569.

Ioffe, A. F., 1956, Izv. Akad. Nauk USSR, Ser. Fiz. **20**, 76.

Ioffe, A. F., 1958a, *Semiconductor Thermoelements and Thermoelectric Cooling* (Infosearch Ltd., London), pp. 1–183.

Ioffe, A. F., 1958b, Sci. Am. **199**, 31.

Ioffe, A. F., and A. R. Regel, 1960, in *Progress in Semiconductors*, edited by A. F. Gibson (FA Kroger and RE Burgess, London: Heywood), Vol. 4, pp. 237–291.

Ioffe, A. V., and A. F. Ioffe, 1954, Dokl. Akad. Nauk USSR **98**, 757.

Ioffe, A. V., and A. F. Ioffe, 1956, Izv. Akad. Nauk USSR, Ser. Fiz. **20**, 65.

Ishii, I., H. Higaki, S. Morita, M. A. Avila, T. Sakata, T. Takabatake, and T. Suzuki, 2006, Physica (Amsterdam) **383B**, 130.

Ishii, I., Y. Suetomi, T. K. Fujita, K. Suekuni, T. Tanaka, T. Takabatake, T. Suzuki, and M. A. Avila, 2012, Phys. Rev. B **85**, 085101.

Iversen, B. B., A. E. C. Palmqvist, D. E. Cox, G. S. Nolas, G. D. Stucky, N. P. Blake, and H. Metiu, 2000, J. Solid State Chem. **149**, 455.

Iwamoto, K., S. Kushibiki, H. Honda, S. Kajitani, T. Mori, H. Matsumoto, N. Toyota, K. Suekuni, M. A. Avila, and T. Takabatake, 2013, J. Phys. Soc. Jpn. **82**, 024601.

Jagannathan, A., R. Orbach, and O. Entin-Wohlman, 1989, Phys. Rev. B **39**, 13465.

Jeffrey, G. A., in *Inclusion Compounds*, edited by J. L. Atwood, J. E. D. Davies, and D. D. MacNicol (Academic Press, London, 1984), pp. 135–190.

Jiang, Y., F. Bridges, M. A. Avila, T. Takabatake, J. Guzman, and G. Kurczveil, 2008, Phys. Rev. B **78**, 014111.

Johnsen, S., A. Bentien, G. K. H. Madsen, M. Nygren, and B. B. Iversen, 2007, Phys. Rev. B **76**, 245126.

Johnsen, S., M. Christensen, B. Thomsen, G. K. H. Madsen, and B. B. Iversen, 2010, Phys. Rev. B **82**, 184303.

Kanatzidis, M. G., 2010, Chem. Mater. **22**, 648.

Kaneshita, E., and T. Nakayama, 2009, Europhys. Lett. **86**, 56 004.

Karttunen, A. J., T. F. Fässler, M. Linnolahti, and T. A. Pakkanen, 2011, Inorg. Chem. **50**, 1733.

Kasper, J. S, P. Hagenmuller, M. Pouchard, and C. Cros, 1965, Science **150**, 1713.

Kaye, G. W. C., and T. H. Laby, 1966, *Table of Physical and Chemical Constants* (Longmans Green, London).

Keppens, V., M. A. McGuire, A. Teklu, C. Laermans, B. C. Sales, D. Mandrus, and B. C. Chakoumakos, 2002, Physica (Amsterdam) B **316–317**, 95.

Keppens, V., B. C. Sales, D. Mandrus, B. C. Chakoumakos, and C. Laermans, 2000, Philos. Mag. Lett. **80**, 807.

Kim, J. H., N. L. Okamoto, K. Kishida, K. Tanaka, and H. Inui, 2007a, J. Appl. Phys. **102**, 034510.

Kim, J. H., N. L. Okamoto, K. Kishida, K. Tanaka, and H. Inui, 2007b, J. Appl. Phys. **102**, 094506.

Kim, S. J., S. Hu, C. Uher, T. Hogan, B. Huang, J. D. Corbett, and M. G. Kanatzidis, 2000, J. Solid State Chem. **153**, 321.

Kirchner, S., F. Zamani, and E. Muñoz, 2013, in *New Materials for Thermoelectric Applications: Theory and Experiment*, edited by V. Zlatic and A. Hewson (Springer, Dordrecht), pp. 129–168.

Kishimoto, K., S. Arimura, and T. Koyanagi, 2006, Appl. Phys. Lett. **88**, 222115.

Kishimoto, K., N. Ikeda, K. Akai, and T. Koyanagi, 2008, Appl. Phys. Express **1**, 031201.

Kishimoto, K., T. Koyanagi, K. Akai, and M. Matsuura, 2007, Jpn. J. Appl. Phys. **46**, L746.

Kittel, C., 2005, *Introduction to Solid State Physics* (John Wiley & Sons, NJ), Chap. 19, 8th ed.

Kleinke, H., 2010, Chem. Mater. **22**, 604.

Klug, D. D., J. S. Tse, J. Y. Zhao, W. Sturhahn, E. E. Alp, and C. A. Tulk, 2011, Phys. Rev. B **83**, 184116.

Kono, Y., N. Ohya, T. Taguchi, K. Suekuni, T. Takabatake, S. Yamamoto, and K. Akai, 2010, J. Appl. Phys. **107**, 123720.

Koumoto, K., I. Terasaki, and R. Funahashi, 2006, MRS Bull. **31**, 206.

Kovnir, K. A., and A. V. Shevelkov, 2004, Russ. Chem. Rev. **73**, 923.

Koza, M. M., M. R. Johnson, H. Mutka, M. Rotter, N. Nasir, A. Grysiv, and P. Rogl, 2010, Phys. Rev. B **82**, 214301.

Kozina, M., F. Bridges, Y. Jiang, M. A. Avila, K. Suekuni, and T. Takabatake, 2009, Phys. Rev. B **80**, 212101.

Krishnan, R. S., 1953, Proc. Indian Acad. Sci. A **37**, 377.

Krivchikov, A. I., V. G. Manzhelii, O. A. Korolyuk, B. Ya. Gorodilov, and O. O. Romantsova, 2005, Phys. Chem. Chem. Phys. **7**, 728.

Kröner, R., R. Nesper, and H. G. von Schnering, 1988, Z. Kristallogr. New Cryst. Struct. **182**, 164.

Kumar, G. S., G. Prasad, and R. O. Pohl, 1993, J. Mater. Sci. **28**, 4261.

Kume, T., S. Ohno, S. Sasaki, H. Shimizu, Y. Ohishi, N. L. Okamoto, K. Kishida, K. Tanaka, and H. Inui, 2010, J. Appl. Phys. **107**, 013517.

Kuznetsov, V. L., L. A. Kuznetsova, A. E. Kaliazin, and D. M. Rowe, 2000, J. Appl. Phys. **87**, 7871.

LaLonde, A. D., Y. Pei, H. Wang, and G. J. Snyder, 2011, Mater. Today **14**, 526.

Lasjaunias, J. C., A. Ravex, M. Vandorpe, and S. Hunklinger, 1975, Solid State Commun. **17**, 1045.

Lee, C. H., H. Yoshizawa, M. A. Avila, I. Hase, K. Kikou, and T. Takabatake, 2007, J. Phys. Conf. Ser. **92**, 012169.

Lee, C. H., H. Yoshizawa, M. A. Avila, I. Hase, K. Kihou, and T. Takabatake, 2008, J. Phys. Soc. Jpn. Suppl. A **77**, 260.

Leoni, S., W. Carrillo-Cabrera, and Yu. Grin, 2003, J. Alloys Compd. **350**, 113.

Li, D. C., L. Fang, S. K. Deng, K. Y. Kang, L. X. Shen, W. H. Wei, and H. B. Ruan, 2012, Physica (Amsterdam) **407B**, 1238.

Li, Y., and J. H. Ross, Jr., 2003, IEEE Trans. Appl. Supercond. **13**, 3047.

Li, Y., J. H. Ross, Jr., J. A. Larrea, and E. Baggio-Saitovitch, 2004, Physica (Amsterdam) C **408–410**, 869.

Liu, Y., L. M. Wu, L. H. Li, S. W. Du, J. D. Corbett, and L. Chen, 2009, Angew. Chem., Int. Ed. **48**, 5305.

Loidl, A., K. Knorr, J. M. Rowe, and G. J. McIntyre, 1988, Phys. Rev. B **37**, 389.

Lorenz, L., 1872, Ann. Phys. (Berlin) **223**, 429.

Lorenz, L., 1881a, Ann. Phys. (Berlin) **249**, 422.

Lorenz, L., 1881b, Ann. Phys. (Berlin) **249**, 582.

Lovesey, S. W., 1984, *Theory of Thermal Neutron Scattering from Condensed Matter* (Clarendon Press, Oxford).

Madsen, G. K. H., and G. Santi, 2005, Phys. Rev. B **72**, 220301(R).

Madsen, G. K. H., K. Schwarz, P. Blaha, and D. J. Singh, 2003, Phys. Rev. B **68**, 125212.

Mahan, G. D., 1998, in *Solid State Physics*, edited by H. Ehrenreich and F. Spaepen (Elsevier, New York), Vol. 51, pp. 81–157.

Mahan, G. D., B. Sales, and J. Sharp, 1997, Phys. Today **50**, No. 3, 42.

Mahan, G. D., and J. O. Sofo, 1996, Proc. Natl. Acad. Sci. U.S.A. **93**, 7436.

Mansour, A. N., J. Martin, W. Wong-Ng, and G. S. Nolas, 2012, J. Phys. Condens. Matter **24**, 485503.

Martin, J., S. Erickson, G. S. Nolas, P. Alboni, T. M. Tritt, and J. Yang, 2006, J. Appl. Phys. **99**, 044903.

Martin, J., S. Erickson, G. S. Nolas, H. Wang, and J. Yang, 2007, J. Appl. Phys. **102**, 103719.

Martin, J., H. Wang, and G. S. Nolas, 2008, Appl. Phys. Lett. **92**, 222110.

Matsumoto, H., T. Mori, K. Iwamoto, S. Goshima, S. Kushibiki, and N. Toyota, 2009, Phys. Rev. B **79**, 214306.

Melnychenko-Koblyuk, N., A. Grytsiv, P. Rogl, H. Schmid, and G. Giester, 2009, J. Solid State Chem. **182**, 1754.

Menke, H., and H. G. von Schnering, 1973, Z. Anorg. Allg. Chem. **395**, 223.

Morelli, D. T., G. P. Meisner, B. Chen, S. Hu, and C. Uher, 1997, Phys. Rev. B **56**, 7376.

Mori, T., K. Iwamoto, S. Kushibiki, H. Honda, H. Matsumoto, N. Toyota, M. A. Avila, K. Suekuni, and T. Takabataake, 2011, Phys. Rev. Lett. **106**, 015501.
Mori, T., *et al.*, 2009, Phys. Rev. B **79**, 212301.
Mott, N. F., and H. Jones, 1936, *The Theory of the Properties of Metals and Alloys* (Clarendon Press, Oxford), Chap. 7, Sec. 15.
Mudryk, Y., P. Rogl, C. Paul, S. Berger, E. Bauer, G. Hilscher, C. Godart, and H. Noël, 2002, J. Phys. Condens. Matter **14**, 7991.
Müller, H. R., and M. von Stackelberg, 1952, Naturwissenschaften **39**, 20.
Myles, C. W., K. Biswas, and E. Nenghabi, 2007, Physica (Amsterdam) B **401–402**, 695.
Myles, C. W., J. Dong, and O. F. Sankey, 2001, Phys. Rev. B **64**, 165202.
Nakamura, M., and M. Arai, 2010, unpublished.
Nakayama, T., 1998, Phys. Rev. Lett. **80**, 1244.
Nakayama, T., 2002, Rep. Prog. Phys. **65**, 1195.
Nakayama, T., 2009, Nucl. Instrum. Methods Phys. Res., Sect. A **600**, 266.
Nakayama, T., and E. Kaneshita, 2008, Europhys. Lett. **84**, 66 001.
Nakayama, T., and E. Kaneshita, 2011, J. Phys. Soc. Jpn. **80**, 104604.
Nakayama, T., and R. Orbach, 1999a, Physica (Amsterdam) **47B**, 468.
Nakayama, T., and R. Orbach, 1999b, Europhys. Lett. **47**, 468.
Nakayama, T., and N. Sato, 1998, J. Phys. Condens. Matter **10**, L41.
Nakayama, T., K. Yakubo, and R. Orbach, 1994, Rev. Mod. Phys. **66**, 381.
Narayanamurti, V., and R. O. Pohl, 1970, Rev. Mod. Phys. **42**, 201.
Nasir, N., A. Grytsiv, N. Melnychenko-Koblyuk, P. Rogl, I. Bednar, and E. Bauer, 2010, J. Solid State Chem. **183**, 2329.
Nathan, B. D, L. F. Lou, and R. H. Tait, 1976, Solid State Commun. **19**, 615.
Nenghabi, E. N., and C. W. Myles, 2008a, Phys. Rev. B **77**, 205203.
Nenghabi, E. N., and C. W. Myles, 2008b, J. Phys. Condens. Matter **20**, 415214.
Nguyen, L. T. K., *et al.*, 2010, Dalton Trans. **39**, 1071.
Nolas, G. S., 2003, in *Chemistry, Physics, and Materials Science of Thermoelectric Materials: Beyond Bismuth Telluride*, edited by M. G. Kanatzidis, S. D. Mahanti, and T. P. Hogan (Kluwer Academic/Plenum Publishers, New York), pp. 107–120.
Nolas, G. S., B. C. Chakoumakos, B. Mahieu, G. J. Long, and T. J. R. Weakley, 2000, Chem. Mater. **12**, 1947.
Nolas, G. S., J. L. Cohn, and G. A. Slack, 1998, Phys. Rev. B **58**, 164.
Nolas, G. S., J. L. Cohn, G. A. Slack, and S. B. Schujman, 1998, Appl. Phys. Lett. **73**, 178.
Nolas, G. S., and C. A. Kendziora, 2000, Phys. Rev. B **62**, 7157.
Nolas, G. S., J. Sharp, and H. J. Goldsmid, 2001, *Thermoelectrics: Basic Principle and New Materials Developments* (Springer, New York).
Nolas, G. S., G. A. Slack, J. L. Cohn, and S. B. Schujman, 1998, in *Proceedings of the 17th International Conference on Thermoelectrics* (IEEE, New York), p. 294.
Nolas, G. S., G. A. Slack, D. T. Morelli, T. M. Tritt, and A. C. Ehrlich, 1996, J. Appl. Phys. **79**, 4002.
Nolas, G. S., G. A. Slack, and S. B. Schujman, 2001, in *Recent Trends in Thermoelectric Materials Research I: Semiconductors and Semimetals*, edited by T. M. Tritt (Academic Press, San Diego), Vol. 69, pp. 255–300.
Nolas, G. S., G. A. Slack, T. M. Tritt, and D. T. Morelli, 1995, in *Proceedings of the 14th International Conference on Thermoelectrics*, edited by M. V. Vedernikov (A. F. Loffe Physical-Technical Institute, St. Petersburg, Russia), p. 236.
Nolas, G. S., T. J. R. Weakley, J. L. Cohn, and R. Sharma, 2000, Phys. Rev. B **61**, 3845.
O'Brien, B. J., and C. S. Wallace, 1958, J. Appl. Phys. **29**, 1010.
Onsager, L., 1931, Phys. Rev. **37**, 405.
Pacheco, V., A. Bentien, W. Carrillo-Cabrera, S. Paschen, F. Steglich, and Yu. Grin, 2005, Phys. Rev. B **71**, 165205.
Paschen, S., W. W. Carrillo-Cabrera, A. Bentien, V. H. Tran, M. Baenitz, Y. Grin, and F. Steglich, 2001, Phys. Rev. B **64**, 214404.
Paschen, S., V. Pacheco, A. Bentien, A. Sanchez, W. Carrillo-Cabrera, M. Baenitz, B. B. Iversen, Yu. Grin, and F. Steglich, 2003, Physica (Amsterdam) **328B**, 39.
Paschen, S., V. H. Tran, M. Baenitz, W. Carrillo-Cabrera, Yu. Grin, and F. Steglich, 2002, Phys. Rev. B **65**, 134435.
Pauling, L., 1948, *The Nature of the Chemical Bond* (Cornell University Press, Ithaca, NY).
Pauling, L., and R. E. Marsh, 1952, Proc. Natl. Acad. Sci. U.S.A. **38**, 112.
Peierls, R., 1929, Ann. Phys. (Berlin) **395**, 1055.
Peltier, J. C., 1834, Ann. Chim. Phys. **56**, 371.
Phillips, W. A., 1972, J. Low Temp. Phys. **7**, 351.
Phillips, W. A., 1987, Rep. Prog. Phys. **50**, 1657.
Pohl, R. O., 1981, in *Amorphous Solids: Low Temperature Properties*, edited by W. A. Phillips (Springer, Berlin), p. 27.
Qiu, L., I. P. Swainson, G. S. Nolas, and M. A. White, 2004, Phys. Rev. B **70**, 035208.
Rachi, T., *et al.*, 2005, Phys. Rev. B **72**, 144504.
Randeria, M., and J. P. Sethna, 1988, Phys. Rev. B **38**, 12 607.
Rodriguez, S. Y., L. Saribaev, and J. H. Ross, Jr., 2010, Phys. Rev. B **82**, 064111.
Rogl, P., 2006, in *Thermoelectrics Handbook: Macro to Nano*, edited by D. M. Rowe (CRC Press, Taylor and Francis Group, Boca Raton, FL), Vol. 32, pp. 1–24.
Roudebush, J. H., N. Tsujii, A. Hurtando, H. Hope, Y. Grin, and S. M. Kauzlarich, 2012, Inorg. Chem. **51**, 4161.
Rowe, D. M., 1995, in *CRC Handbook of Thermoelctrics*, edited by D. M. Rowe (CRC Press, Boca Raton, FL).
Rowe, D. M., 2003, in *Proceedings of the 22nd International Conference on Thermoelectrics* ((IEEA Catalog 03TH8726) (IEEE, Piscataway, NJ), pp. 1–12.
Safarik, D. J., A. Llobet, and J. C. Lashley, 2012, Phys. Rev. B **85**, 174105.
Sales, B. C., 1998, MRS Bull. **23**, 15.
Sales, B. C., 2002, Science **295**, 1248.
Sales, B. C., B. C. Chakoumakos, R Jin, J. R. Thompson, and D. Mandrus, 2001, Phys. Rev. B **63**, 245113.
Sales, B. C., B. C. Chakoumakos, D. Mandrus, and J. W. Sharp, 1999, J. Solid State Chem. **146**, 528.
Sales, B. C., D. Mandrus, B. C. Chakoumakos, V. Keppens, and J. R. Thompson, 1997, Phys. Rev. B **56**, 15081.
Sales, B. C., D. Mandrus, and R. K. Williams, 1996, Science **272**, 1325.
Saramat, A., G. Svensson, A. E. C. Palmqvist, C. Stiewe, E. Mueller, D. Platzek, S. G. K. Williams, D. M. Rowe, J. D. Bryan, and G. D. Stucky, 2006, J. Appl. Phys. **99**, 023708.
Sasaki, Y., K. Kishimoto, T. Koyanagi, H. Asada, and K. Akai, 2009, J. Appl. Phys. **105**, 073702.
Schujman, S. B., G. S. Nolas, R. A. Young, C. Lind, A. P. Wilkinson, G. A. Slack, R. Patschke, M. G. Kanatzidis, M. Ulutagay, and S.-J. Hwu, 2000, J. Appl. Phys. **87**, 1529.
Seebeck, T. J., 1822–1823, Abhandlungen der Deutscher Akademie der Wissenschaften zu Berlin, pp. 265–373.
Seebeck, T. J., 1826, Ann. Phys. (Berlin) **82**, 253.

Shevelkov, A. V., and K. Kovnir, 2011, in *Zintl Phases - Principles and Recent Developments*, edited by T. F. Fässler (Springer, Berlin/Heidelberg), pp. 97–142.
Shimizu, H., R. Oe, S. Ohno, T. Kume, S. Sasaki, K. Kishimoto, T. Koyanagi, and Y. Ohishi, 2009, J. Appl. Phys. **105**, 043522.
Shimizu, H., Y. Takeuchi, T. Kume, S. Sasaki, K. Kishimoto, N. Ikeda, and T. Koyanagi, 2009, J. Alloys Compd. **487**, 47.
Simons, S., 1964, Proc. Phys. Soc. London, **83**, 749.
Slack, G. A., 1995, in *CRC Handbook of Thermoelectrics*, edited by D. M. Rowe (CRC Press, Boca Raton, FL), pp. 407–440.
Snyder, G. J., and E. S. Toberer, 2008, Nat. Mater. **7**, 105.
Sommerfeld, A., 1927, Naturwissenschaften **15**, 825.
Sommerfeld, A., 1928, Naturwissenschaften **16**, 374.
Sootsman, J. R., D. Y. Chung, and M. G. Kanatzidis, 2009, Angew. Chem., Int. Ed. **48**, 8616.
Squires, G. L., 1978, *Introduction to the Theory of Thermal Neutron Scattering* (Cambridge University Press, London).
Stephens, R. B., 1973, Phys. Rev. B **8**, 2896.
Struzhkin, V. V., B. Militzer, W. L. Mao, H. K. Mao, and R. J. Hemley, 2007, Chem. Rev. **107**, 4133.
Suekuni, K., M. A. Avila, K. Umeo, H. Fukuoka, S. Yamanaka, T. Nakagawa, and T. Takabatake, 2008, Phys. Rev. B **77**, 235119.
Suekuni, K., M. A. Avila, K. Umeo, and T. Takabatake, 2007, Phys. Rev. B **75**, 195210.
Suekuni, K., Y. Takasu, T. Hasegawa, N. Ogita, M. Udagawa, M. A. Avila, and T. Takabatake, 2010, Phys. Rev. B **81**, 205207.
Suekuni, K., S. Yamamoto, M. A. Avila, and T. Takabatake, 2008, J. Phys. Soc. Jpn., Suppl. A **77**, 61.
Takabatake, T., E. Matsuoka, S. Narazu, K. Hayashi, S. Morimoto, T. Sasakawa, K. Umeo, and M. Sera, 2006, Physica (Amsterdam) **383B**, 93.
Takasu, Y., T. Hasegawa, N. Ogita, M. Udagawa, M. A. Avila, K. Suekuni, I. Ishii, T. Suzuki, and T. Takabatake, 2006, Phys. Rev. B **74**, 174303.
Takasu, Y., T. Hasegawa, N. Ogita, M. Udagawa, M. A. Avila, K. Suekuni, and T. Takabatake, 2008, Phys. Rev. Lett. **100**, 165503.
Takasu, Y., T. Hasegawa, N. Ogita, M. Udagawa, M. A. Avila, K. Suekuni, and T. Takabatake, 2010, Phys. Rev. B **82**, 134302.
Takasu, Y., T. Hasegawa, N. Ogita, M. Udagawa, K. Suekuni, M. A. Avila, and T. Takabatake, 2007, J. Phys. Conf. Ser. **92**, 012151.
Tanaka, T., T. Onimaru, K. Suekuni, S. Mano, H. Fukuoka, S. Yamanaka, and T. Takabatake, 2010, Phys. Rev. B **81**, 165110.
Tang, J., R. Kumashiro, J. Ju, Z. Li, M. A. Avila, K. Suekuni, T. Takabatake, F. Guo, K. Kobayashi, and K. Tanigaki, 2009, Chem. Phys. Lett. **472**, 60.
Tang, J., Z. Li, T. Nishiro, K. Sato, and K. Tanigaki, 2010, J. Phys. Chem. Solids **71**, 480.
Tang, J., J. T. Xu, S. Hegri, K. Akai, and K. Tanigaki, 2011, J. Electron. Mater. **40**, 769.
Tang, X. F., L. M. Zhang, R. Z. Yuan, L. D. Chen, T. Goto, T. Hirai, J. S. Dyck, W. Chen, and C. Uher, 2001, J. Mater. Res. **16**, 3343.
Toberer, E. S., M. Christensen, B. B. Iversen, and G. J. Snyder, 2008, Phys. Rev. B **77**, 075203.
Toberer, E. S., A. F. May, and G. J. Snyder, 2010, Chem. Mater. **22**, 624.
Topp, K. A., and R. O. Pohl, 2002, Phys. Rev. B **66**, 064204.
Tritt, T. M., 2001, in *Recent Trends in Thermoelectric Materials Research I, Semiconductors and Semimetals*, edited by T. M. Tritt (Academic Press, San Diego).
Tse, J. S., V. P. Shpakov, V. R. Belosludov, F. Trouw, Y. P. Handa, and W. Press, 2001, Europhys. Lett. **54**, 354.
Tse, J. S., V. P. Shpakov, V. V. Murashov, and V. R. Belosludov, 1997, J. Chem. Phys. **107**, 9271.
Uemura, T., K. Akai, K. Koga, T. Tanaka, H. Kurisu, S. Yamamoto, K. Kishimoto, T. Koyanagi, and M. Matsuura, 2008, J. Appl. Phys. **104**, 013702.
Uher, C., 2001, in *Recent Trends in Thermoelectric Materials Research I, Semiconductors and Semimetals*, edited by T. M. Tritt (Academic Press, San Diego), Vol. 69, pp. 139–252.
Uher, C., J. Yang, and S. Hu, 1998, Mater. Res. Soc. Symp. Proc. **545**, 247.
Umeo, K., M. A. Avila, T. Sakata, K. Suekuni, and T. Takabatake, 2005, J. Phys. Soc. Jpn. **74**, 2145.
Vedernikov, M. V., and E. K. Iordanishvili, 1998, in *Proceeding of the 17th International Conference on Thermoelectrics* (IEEE, Piscataway, NJ), p. 37.
von Schnering, H. G., W. Carrillo-Cabrera, R. Kröner, E.-M. Peters, K. Peters, and R. Nesper, 1998, Z. Kristallogr. New Cryst. Struct. **213**, 679.
von Stackelberg, M., and H. R. Müller, 1951a, J. Chem. Phys. **19**, 1319.
von Stackelberg, M., and H. R. Müller, 1951b, Naturwissenschaften **38**, 456.
Walton, D., H. A. Mook, and R. M. Nicklow, 1974, Phys. Rev. Lett. **33**, 412.
Wang, L., L-D. Chen, X-H. Chen, and W-B. Zhang, 2009, J. Phys. D **42**, 045113.
Wiedemann, G., and R. Franz, 1853, Ann. Phys. (Berlin) **165**, 497.
Winterlich, M., R. Böhmer, and A. Loidl, 1995, Phys. Rev. Lett. **75**, 1783.
Woods, G. T., J. Martin, M. Beekman, R. P. Hermann, F. Grandjean, V. Keppens, O. Leupold, G. J. Long, and G. S. Nolas, 2006, Phys. Rev. B **73**, 174403.
Xu, J., J. Tang, K. Sato, Y. Tanabe, S. Heguri, H. Miyasaka, M. Yamashita, and K. Tanigaki, 2011, J. Electron. Mater. **40**, 879.
Xu, J., J. Tang, K. Sato, Y. Tanabe, H. Miyasaka, M. Yamashita, S. Heguri, and K. Tanigaki, 2010, Phys. Rev. B **82**, 085206.
Xu, J., J. Wu, S. Heguri, G. Mu, Y. Tanabe, and K. Tanigaki, 2012, J. Electron. Mater. **41**, 1177.
Yamakage, A., and Y. Kuramoto, 2009, J. Phys. Soc. Jpn. **78**, 064602.
Yamanaka, S., E. Enishi, H. Fukuoka, and M. Yasukawa, 2000, Inorg. Chem. **39**, 56.
Yamanaka, S., H. Horie, H. Nakano, and M. Ishikawa, 1995, Fuller. Sci. Technol. **3**, 21.
Yang, J., 2004, in *Thermal Conductivity: Theory, Properties, and Applications*, edited by T. M. Tritt (Kluwer Academic/Plenum Publisher, New York), pp. 1–20.
Zaikina, J. V., K. A. Kovnir, F. Haarmann, W. Schnelle, U. Burkhardt, H. Borrmann, U. Schwarz, Yu. Grin, and A. V. Shevelkov, 2008, Chem. Eur. J. **14**, 5414.
Zaikina, J. V., T. Mori, K. Kovnir, D. Teschner, A. Senyshyn, U. Schwarz, Yu. Grin, and A. V. Shevelkov, 2010, Chem. Eur. J. **16**, 12582.
Zeller, R. C., and R. O. Pohl, 1971, Phys. Rev. B **4**, 2029.
Zerec, I., V. Keppens, M. A. McGuire, D. Mandrus, B. C. Sales, and P. Thalmeier, 2004, Phys. Rev. Lett. **92**, 185502.
Zhang, H., H. Borrmann, N. Oeschler, C. Candolfi, W. Schnelle, M. Schmidt, U. Burkhardt, M. Baitinger, J. T. Zhao, and Yu. Grin, 2011, Inorg. Chem. **50**, 1250.
Zhang, Y., P. L. Lee, G. S. Nolas, and A. P. Wilkinson, 2002, Appl. Phys. Lett. **80**, 2931.
Zheng, X., S. Y. Rodriguez, and J. H. Ross, Jr., 2011, Phys. Rev. B **84**, 024303.
Zheng, X., S. Y. Rodriguez, L. Saribaev, and J. H. Ross Jr., 2012, Phys. Rev. B **85**, 214304.